A newly developed 3D-printed porous titanium vertebral body implant for osteoporotic vertebral compression fractures: A proof of principle

Master Thesis Project

C.B.M.D. (Kirsten) Willemse

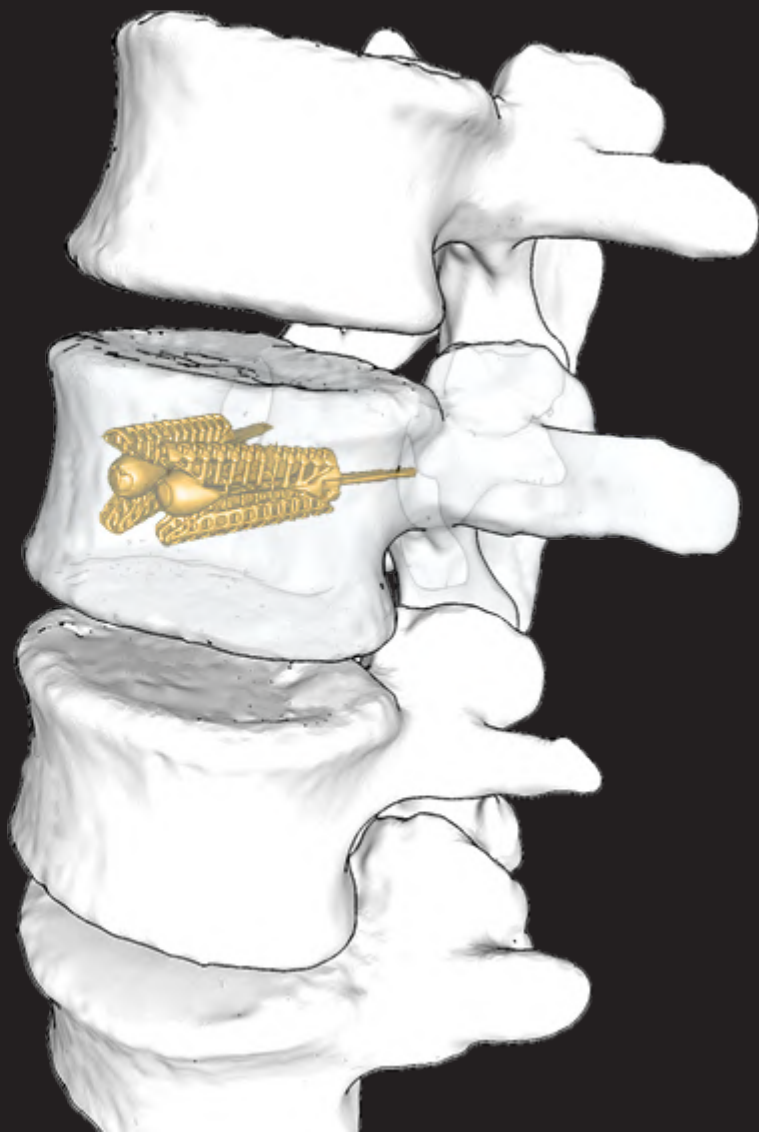

TU Delft

A newly developed 3D-printed porous titanium vertebral body implant for osteoporotic vertebral compression fractures: A proof of principle

Master Thesis Project

by

C.B.M.D. (Kirsten) Willemse

to obtain the degree of Master of Science
at the faculty of Mechanical, Maritime and Materials Engineering in Biomedical Engineering,
at the Delft University of Technology,
to be defended publicly on Thursday 5th of March, 2020 at 11:00 AM

Student number:	4322533	
Thesis committee:	Prof. dr. ir. H.H. Weinans,	TU Delft, supervisor
	Dr. ir. J. Zhou,	TU Delft
	Prof. dr. ir. J. Harlaar,	TU Delft
	Dr. ir. M. Ahmadi,	Amber Implants

This thesis is confidential and cannot be made public until March 5, 2022.

amber implants

TU Delft

Acknowledgements

This report reflects the personal development that I have made during the study period on the TU Delft, from my Bachelor in Civil Engineering to the last hurdle of the Master in Biomedical Engineering. This process would not have been achievable without the help and support of numerous people. Firstly, I would like to show my gratitude towards Dr. ir. Banafsheh Sajadi and Dr. ir. Mohammad Ahmadi from Amber Implants, for giving me the opportunity to perform these inspiring tests and having the trust in my capabilities to work with their newly developed implant. Besides, I would like to give a special thanks to ir. Pim Pellikaan, an employee of Amber Implants who served as my daily supervisor. His guidance, feedback and me picking his brain with the struggles that had to be encountered were invaluable for the success of my graduation process. Consecutively, I wish to express my sincere thanks to my supervisor, Prof. dr. ir. H. H. Weinans, who guided me through this process with his outstanding scientific knowledge.

Furthermore, various people helped me in the anatomy lab of the UMC during the specimen preparations. Especially, I would like to thank Prof. Bleys for allowing me to perform the tests inside his lab. Then, I would to like to thank the two prosectors of the anatomy lab, Simon Plomp and Marco Rondhuis for showing me around in the lab and for providing me tools and tricks for the segmentation. Furthermore, I would like to thank Naomi, Dennis and Arthur for their help during the dissections. Moreover, I wish to express my thanks to Dr. Paul van Urk, the orthopaedic surgeon who showed me how to dissect a spinal column and how to perform surgery on a vertebra. Besides, I'd like to thank Dr. Nicoline Korthagen for explaining the μCT process and Drs. Koen Willemsen for using the test machine.

Last but not least, I would like to thank my family and friends for their invaluable support throughout the process. Without them, all of this would not have been feasible.

Abstract

Background: The incidence of osteoporotic vertebral compression fractures (VCFs) is rapidly increasing, necessitating the identification of the most appropriate treatment method. The well-established first and second generation surgical procedures are not capable of giving optimal outcomes. Moreover, my literature study has shown little to no improvements for four of the most prevailing third generation procedures. As a consequence, the med-tech company Amber Implants B.V. developed a new 3D-printed porous titanium implant that has the potential to resolve difficulties and drawbacks that were identified for all former procedures. Nonetheless, the performance of this implant has never been tested before. Thus, the aim of this study was to pre-clinically evaluate the biomechanical properties regarding the spinal deformities for this implant. For the quantification, the prevention of spinal deformities was subdivided into the anterior height restoration and the kyphotic angle correction.

Methodology: The pre-clinical evaluation was conducted on isolated vertebrae originating from three human cadaver specimens. First, the most abundant type of all osteoporotic VCFs, a wedge fracture, was generated on the vertebrae with 40% anterior height decrease. Thereafter, vertebral restoration was performed with the implants. Besides, vertebral restoration with the second generation surgical procedure, the Balloon Kyphoplasty procedure (BKP), was performed likewise to serve as a comparative. After vertebral restoration, half of the implant group and the total BKP group were tested in a cyclic loading test that mimicked the activity during the first week after surgical VCF repair, i.e. 10.000 cycles with loads ranging from 100N to 600N. The other half of the implant group was tested under higher loading conditions, i.e. 10.000 cycles with loads ranging from 100N to 1000N. At each test stage the spinal deformities, which were subdivided into the anterior height and the kyphotic angle, were evaluated from micro-CT (μCT) data. Eventually, the μCT scans were compared in order to quantify the implant's performance.

Results: For the groups tested under the first loading condition, the mean anterior height after fracture generation was 59.8% for the implant group and 68.4% for the BKP group compared to the initial heights. After vertebral restoration, the heights increased to 98.0% and 89.2% respectively. Eventually, after cyclic loading the anterior heights were 72.5% and 86.5% respectively. The restored kyphotic angle for the implant group only deviated 0.5° from the initial angle, while for the BKP procedure it was 2.4°. Yet, after cyclic loading deviations of 4.2° and 3.1° were found respectively. For the implant group tested under the higher loading condition, anterior heights of 64.2%, 92.1% and 68.9% were found after fracture generation, vertebral restoration and cyclic loading respectively. Furthermore, the kyphotic angle deviated 1.4° and 8.7° after vertebral restoration and cyclic loading compared to the initial angle. The decrease in outcomes for both implant groups was primarily related to the plastic deformation in the trabecular bone inferior to the implant, which was induced by high local stresses as a result of the minimal contact area between the implant and the trabecular bone. Complementary, the rotation of the implant was observed to effect the implant's performance.

Conclusion: Ultimately, it was concluded that the implant in its current design could not compete with the BKP procedure, neither with the third generation surgical repair procedures for an osteoporotic VCF such as Vertebral Body Stenting (VBS) and SpineJack. Nevertheless, the outcomes after vertebral restoration were promising. Therefore, it was assumed that the implant has a decent chance of succeeding after implementing some adjustments on the implant's geometry and the corresponding surgical tools.

Contents

List of Figures

List of Tables

Nomenclature

BKP	*Balloon Kyphoplasty*
BMD	*Bone Mineral Density*
FU	*Follow-up*
µCT	*Micro Computed Tomography*
PMMA	*Polymethyl methacrylate*
PLA	*Polylactic Acid*
POM	*Polyoxymethylene*
Postop	*Postoperative*
Preop	*Preoperative*
VCF	*Vertebral Compression Fracture*
VB	*Vertebral Body*
VP	*Vertebroplasty*

Chapter 1

Introduction

The increased risks of mortality and morbidity can be seen as the most hazardous effects of an osteoporotic vertebral compression fracture (VCF) (Kado et al., 2003; Silverman, 1992). Not only is this a result of the chronic pain that patients encounter, the spinal deformities can lead to these detrimental circumstances likewise. As worldwide approximately 1.4 million osteoporotic VCFs were reported in 2000 and as numbers are still continuing to increase (Johnell & Kanis, 2006), identifying the appropriate treatment option is of utter importance.

Conservative treatment has been the standard treatment method in the past, but preferences have been shifting over the past decades towards surgical repair procedures. Currently, vertebroplasty (VP) and balloon kyphoplasty (BKP) are two established minimal invasive procedures for VCFs, while multiple third generation procedures have recently started entering the market.

My literature study revealed three main outcome parameters to compare multiple VCF procedures. These were considered to be spinal deformities, pain relief and PMMA pitfalls. Despite the attempts of the third generation procedures to improve the clinical outcomes for a repaired VCF compared to the established procedures, in my literature study it was concluded that none of the third generation procedures led to optimal results for all parameters. However, it was suggested that the surgical tooling and guiding techniques, the geometry of the implant and the volume of injected PMMA all had severe influences.

At Amber Implants B.V., a medical technology company located in Delft, The Netherlands, a new 3D-printed porous titanium implant was developed and manufactured. Based on the influential factors to obtain optimal results described above, this implant has the potential to resolve the difficulties that have been identified for all former procedures. Nonetheless, none of the outcome parameters of this implant have been examined so far.

The aim of this master thesis is to quantify the clinical feasibility for the titanium implant with pre-clinical testing. Therefore, the first outcome parameter, spinal deformities, will be studied. The outcomes for pain relief should be addressed at a later stage during clinical tests. As the implant could be inserted and fixated without PMMA, there is no need to encounter PMMA pitfalls. The short-term outcomes for spinal deformities will be observed in a biomechanical test with cadaveric specimens. Additionally, during the tests the fixation of the implant under spinal loading will be tested to evaluate the potential stability of an implant without the use of PMMA. In order to verify the outcomes of the implant, the tests will be performed with the BKP procedure simultaneously.

1.1 Document Structure

In the coming chapter, chapter 2, the theoretical background will be deliberated on more specifically by encountering the occurrence and consequences of osteoporotic VCFs and their current surgical repair procedures. Thereafter, a more thorough description of the titanium implant will be presented in chapter 3. In chapter 4 research questions will be drawn to determine the clinical feasibility of the implant. The methods to address the biomechanical tests will be exploited in chapter 5. Subsequently, the results of the tests are given in chapter 6. Finally, the discussion will bring the research questions together and conclusions will be drawn. Ultimately, recommendations for future developments and studies will be presented.

Chapter 2

Theoretical Background

This chapter provides a brief introduction to the subject of this master thesis. A more extended version of this introductory chapter can be found in Appendix A, where the anatomy and physiology, the pathology, the occurrence, the consequences coherent to VCFs and finally the surgical repair procedures are discussed more thoroughly. In the coming sections of this chapter, the occurrence of osteoporotic VCFs, the consequences and the current surgical repair procedures will be discussed concisely.

2.1 The Occurrence of an Osteoporotic VCF

According to the US Department of Health and Human Services (2004), vertebral fractures are among the most common osteoporotic fracture types accounting for approximately half of all osteoporotic-related fractures. Most osteoporotic VCFs occur at the thoracolumbar spine, which is located at the angle transition from the kyphotic to the lordotic region. As a result of the transition, the load distribution at this location is more complex and vertebrae are subjected to higher loads (Wilson et al., 2012). As the spinal loads are predominantly carried by vertebral bodies, which are mostly composed of trabecular bone, the majority of osteoporotic VCFs presents itself here.

Osteoporotic VCFs can occur spontaneously or after a minor activity or traumatic event such as sneezing, stepping down or falling from a minimal height (Ombrect, 2013). Different types of VCFs can be categorized according to the Magerl AO classification system. The most abundantly diagnosed type of osteoporotic VCFs are classified as a type A1.2 fracture, also referred to as the wedge compression fracture (Viera, Santos, & Henriques, 2018). A wedge compression fracture is characterized by an intact posterior wall, while the anterior column is fractured, see figure 2.1. Furthermore, only a single endplate is allowed to fracture and none of the components of the vertebral arch are affected. As a result of the fracture, the anterior height of the vertebral body is often reduced. This could eventually lead to an increase in kyphotic or lordotic angle of the spine, depending on the vertebra in question.

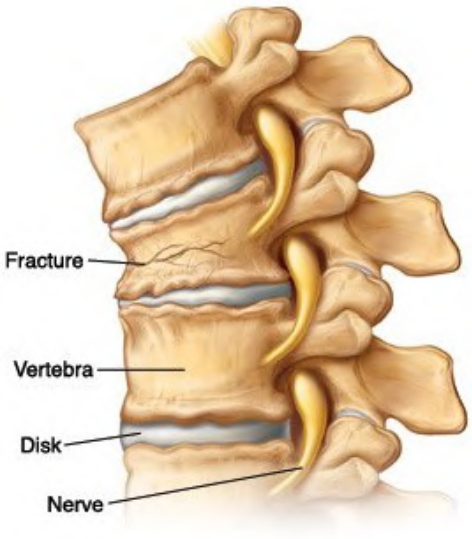

Figure 2.1: A vertebral wedge compression fracture (Fairview, 2018)

2.2 The Consequences of an Osteoporotic VCF

Symptomatic osteoporotic VCFs repeatedly result in chronic back pain, causing patients to prefer bed rest. However, in the long-term bed rest can lead to several adverse events such as muscle fatigue, loss of strength and immobility (Silverman, 1992). Consequently, the degradation of the emotional and mental health is correlated to reduced physical activity. Not surprisingly, patients with an osteoporotic VCF regularly are appointed to experience side effects as isolation and depression.

Moreover, the increase in kyphotic or lordotic angle that has been briefly discussed above, can result in hazardous health conditions simultaneously. The angle deformities can have influences to the extent of a decreased thoracic or abdominal cavity, introducing a restricted lung volume or a protuberant abdomen respectively. A reduced physical tolerance and weight loss due to early satiety are symptomatic consequences that are perceived intermittently. Furthermore, spinal deformities can give rise to neurological compressions of the spinal cord, which in turn can initiate numbness or loss of sensation and reflexes (Sabo, Hatgis, Granville, & Jacobson, 2017). Besides, the load distribution in the spine is likely to be adjusted due to spinal deformities, which enhances the risk for iterative fractures and enduring pain. Visually, patients with spinal deformities can present themselves with a stooped posture, which not only increases the risk of fall (Premat et al., 2018), but often affects ones self-esteem supplementary to the physical consequences (Silverman, 1992). The difference between a normal and stooped posture can be evaluated in figure 2.2.

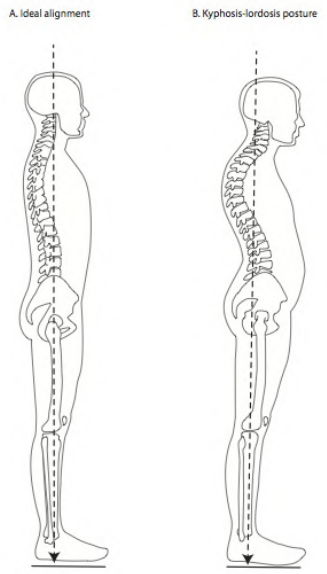

Figure 2.2: A visual representation of a normal (left) and stooped (right) posture (Wyss, 2013)

All things considered, both chronic pain and spinal deformities can initiate several hazardous complications on both physical and mental domain. Ultimately, former studies have shown that the risks of mortality and morbidity can both be increased due to an osteoporotic VCF (Kado et al., 2003; Silverman, 1992). Therefore, the repair techniques for this fracture type should try to prevent chronic pain and spinal deformities at any cost.

2.3 Current Surgical Procedures

The conservative treatment method for osteoporotic patients encompasses analgesics, external fixation, rehabilitation and, most remarkably, bed rest. As has been described in the previous section, bed rest can initiate a set of undesirable complications. Presumably, these findings have contributed to the shift from conservative towards surgical treatment over the past decades.

Fixation with screws and rods in the spine is referred to as external fixation. This surgical method has regularly failed for osteoporotic patients in the past, as proper fixation was disabled by the poor quality of the bone in the vertebral bodies (Hsieh, Chen, & Chen, 2013). Therefore, currently minimal invasive surgical procedures are performed internally in the vertebral bodies in hospitals worldwide. The first and second generation procedures, the vertebroplasty (VP) and balloon kyphoplasty (BKP) respectively, are mainly based on the injection of bone cement or polymethyl methacrylate (PMMA).

Numerous former studies, among which was the KAVIAR trial, have concluded that both the VP and BKP procedures did not result in the most optimal outcomes (Dohm, Black, Dacre, Tillman, & Fueredi, 2014). Therefore, multiple third generation procedures have been developed over the past years. All those procedures are based on the insertion of a remaining implant in the VB. Vertebral Body Stenting (VBS), Spine Jack, Osseofix and KIVA could be seen as four of the most commonly known and studied third generation surgical procedures. The performances of the former studies have been compared in my literature review, which led to some conclusions that will be briefly discussed.

As pain relief is an important measure to score the effectiveness of a VCF repair procedure, the improvement of the Visual Analogue Scale (VAS) score was compared at two time intervals, postoperative and at last follow-up (FU). It was concluded that all third generation procedures could adequately decrease the VAS-scores for patients. While VBS did show remarkably lower VAS-score improvements at post-op, making a fair distinction between the other procedures was inaccessible as equivalent satisfying outcomes were found.

The prevention of spinal deformities has proven to be more complicated. Determining the effectiveness per procedure, the prevention of spinal deformities were evaluated based on three characteristics; the anterior height restoration, the kyphotic angle correction and the Cobb angle correction. Regarding all three characteristics, none of the third generation procedures managed to result in optimal outcomes at both time intervals. Reasonably, this was partly caused by the maldeployments and misplacements of the implants, as was mentioned by a fair amount of studies that were included. Nonetheless, the geometric design of the implants themselves was assumed to have a considerable influence simultaneously. Therefore, both the surgical tooling and guiding techniques as the geometry of the implants were propositioned to affect the biomechanical outcomes for all VCF procedures.

Additionally, the injection of PMMA has shown to bring along several risks and complications. Firstly, the high stiffness of the PMMA is likely to alter the load distribution in the VB, which could eventually lead to fractures in adjacent vertebrae. Besides, PMMA leakage can result in harmful conditions such as pulmonary embolisms or neurological deficits. Lastly, no osseointegration is feasible as PMMA is non-absorbable. From the studies that have investigated third generation procedures, it was concluded that a high volume of injected PMMA is more likely to result in complications. Not surprisingly, solely implementing the PMMA for fixation purposes has shown the least amount of PMMA pitfalls. Though, a procedure without necessitating PMMA injection is preferred even more.

Chapter 3

Description of the Implant

Thus, there is room for improvement regarding the surgical repair procedures for osteoporotic VCFs. In particular, the outcomes regarding the spinal deformities and PMMA pitfalls should be tackled. At Amber Implants B.V., a med-tech company located in Delft, The Netherlands, a new porous titanium implant has been manufactured with the use of additive manufacturing (AM). In figure 3.1, this newly designed third generation implant is demonstrated.

Figure 3.1: The vertebral implant designed and manufactured by Amber Implants in compact (left) and expanded state (middle and right)

The implants consist of two porous endplates, that open in craniocaudal direction. The endplates are connected to each other with a thin frame and a screw, which allows expansion of the implants. Lastly, on the anterior and posterior end of the screw, two wedges are placed that can move over the screw. The inner part of the posterior one is threaded, while it is smooth for the anterior wedge. Thus, by rotating the screw counterclockwise, the wedges are moving towards each other and thereby push the endplates in the correct direction. On the posterior wedge, two recesses are visible which allow the implant inserter to hold the implant in position. Through the inner part of the inserter, the screw driver can be placed on the implant's screw. The inserter and screw driver can be seen in figure 3.2.

Figure 3.2: The tools developed for the implant; the implant inserter (left) and the screw driver (right)

The principle of this implant is most comparable to Spine Jack, as it expands in craniocaudal direction in the VB likewise. As can be seen in figure 3.1, the implant can open either with both endplates parallel to each other or angular. The pressure on the implant's posterior end will determine the opening mechanism of this design. During the procedure, two implants would be inserted transpedicular inside the VBs. For this prototype, two implant sizes have been manufactured. The dimensions for the bigger implant, primarily intended for the inferior thoracic and lumbar vertebrae, in compact state are 34mm, 6mm and 6mm respectively for the length,

width and height. In expanded position, the anterior height can increase up to 15.0mm, which would ideally provide endplate-to-endplate fixation in the craniocaudal direction. Simultaneously, the length of the implant in the expanded position can decrease to 26.7mm and both expanded parts can make a maximum angle of 19.1° with the implant's body. The length, width and height for the compact smaller implant, intended for the superior thoracic vertebrae, are 28.2mm, 5.0mm and 5.0mm respectively. As a result of the decrease in compact length, the maximum expansion was reduced to 12.5mm, the expanded length to 22.2mm and an identical maximum angle. In table 3.1 the most important dimensions of both implants are given.

Implants	Initial implant length [mm]	Initial implant diameter [mm]	Maximum implant expansion [mm]
Big implant	34.0	6.0	15.0
Small implant	28.2	5.0	12.5

Table 3.1: The dimensions of the implant

However, in contrast to Spine Jack, this implant is made out of a porous titanium structure which would enable bone ingrowth. Potentially, this would lead to faster osseointegration and eventually earlier patient mobilization (Amber Implants, n.d.). On its turn this would enhance the working mechanism between the trabecular bone and the implant. Conceivably, hereby the adjustments to the biomechanical properties can be diminished or impeded over time. The titanium alloy that is used for this implant is Ti6Al4V, which is widely used for a variety of human body implants.

Moreover, due to the osseointegration and the expansion a natural fixation of the implant is feasible, which would obviate the need for PMMA insertion. Thus, this implant seems to have the potential to address the points of improvement that were stated before. However, the implant's performance without the use of PMMA and the feasibility of the procedure still need to be evaluated. In the next chapter, the research questions to address this evaluation are elaborated on.

Chapter 4

Problem Statement

Potentially, the implementation of the porous titanium implant could resolve difficulties or optimize outcomes that were shown for the current surgical procedures for an osteoporotic VCF. Notwithstanding, this implant has never been tested before. In order to verify its potentials, pre-clinical, biomechanical tests need to be conducted before this product can be introduced in clinical trials. As the second outcome parameter from my literature study, pain relief, can not be addressed with pre-clinical tests and as PMMA will not be implemented in the implant's procedure, only the outcomes regarding spinal deformities will be encountered. Ultimately, these tests are in the concept of a proof of principle. Thus the aim of this master thesis can be stated as follows:

The pre-clinical evaluation of the biomechanical properties for a 3D-printed titanium porous vertebral body implant for osteoporotic vertebral compression fractures.

This problem statement has been formulated as one question, which has been subdivided into three research questions that will be addressed in this master thesis report;

1. Can the implant adequately prevent spinal deformities to occur?

    1.1 Can the implant restore the anterior height of the vertebral body?

    1.2 Can the implant correct the kyphotic angle of the vertebral body?

    1.3 Can the implant withstand higher loading conditions?

Biomechanical tests with human cadaveric specimens will be conducted to answer the above stated research questions. The second generation procedure, balloon kyphoplasty (BKP), will be tested simultaneously in order to verify and compare the outcomes for the first and second research question. These questions will be answered by mimicking physiological conditions during the first week after surgery. In the third research question, it will be evaluated if the implant would be able to withstand higher loading. As bone regeneration after VCF repair encompasses several months, this was expected to be relevant. Hypothetically, some additional decrease for the anterior height restoration and the kyphotic angle correction would be expected after loading. The methodology for these tests will be discussed in the coming chapter, chapter 5.

Chapter 5

Biomechanical Methodology

This chapter provides a description of the methodology that is used for the biomechanical tests of the implant in human cadaveric specimens. First, the test requirements will be considered. Thereafter, the main study characteristics will be evaluated and finally the data processing will be discussed.

5.1 Test Requirements

The aim of the biomechanical tests were bilateral; the spinal deformities of the vertebral body after VCF repair with the implant needed to be quantified as well as the interaction between the implant and the internal trabecular structures of the vertebral body. Thus mimicking the clinical conditions from the occurrence of a wedge compression fracture until the mobilization of the treated spine with the implant was suggested to give answer to all research questions.

For the first two research questions, the vertebrae were tested under normal loading conditions. In other to verify the obtained results, an extra test group was implemented. The vertebrae of this latter group were restored with the established BKP procedure. Furthermore, the quantification of the spinal deformities could be answered by evaluating the questions that focused on the restoration of the anterior height and the correction of the kyphotic angle of the fractured VB. As the implementation of the analysis on the Cobb angle restoration would require tests with more variability, which were suggested undesirable for this proof of principle, this outcome value was not appraised. Additionally, the third research question would give a better understanding of the behaviour of the restored vertebrae under higher loading. As this kind of testing is not regularly described in other studies, no comparison group was implemented to answer this question. Therefore, this question should rather be seen as a gain of information that could be used for the further improvement of the implant.

For all research questions, biomechanical tests needed to take place in order to test the vertebrae under loading. Moreover, multiple micro-CT scans (μCT) at various stages of the biomechanical tests were made to obtain information on the internal structure of the vertebral body with the inserted materials. Besides, the potential translation and rotation of the implants could be evaluated using the μCT scans.

5.1.1 Specimen preparation

As this study could be seen as a proof of principle for the implant, minimizing the variability of the specimens was desired. Thus, isolated vertebrae were assumed to be the appropriate specimen type. As much as feasible the soft tissue around the vertebrae was dissected and a substantial amount of the vertebral arches were cut away. The laminae, spinous processes, inferior articular processes and the upper part of the superior articular processes were removed. Thus, the remaining vertebrae consisted of the vertebral bodies, pedicles, transverse processes and the lower part of the superior articular processes. As the surgical fracture repair of all VCF procedures is normally performed transpedicular, it was crucial to keep them intact.

Since most VCFs occur at the thoracolumbar region in the spine, 27 vertebrae from three cadaveric spines from T8 until L4 were included in this study. The isolated vertebrae were then embedded in an epoxy resin

(Technovit® 3040, Heraeus Kulzer, Wehrheim, Germany) to fixate them and place them in a mechanical set-up. The moulds were composed of two 3D-printed plastic PLA components and were manufactured for the embedding of the vertebrae; a ring that remained on each vertebra after embedding and a bottom plate that was removed when the epoxy resin had hardened. The embedding protocol can be found in Appendix B. As will be explained in the coming subsection, loading the VBs at their centers was important. Thus, the centers of the VBs were aligned in the moulds with a digital caliper (0.2mm accuracy) as far as practically feasible. In figure 5.1 six potted and isolated vertebrae are visible. In order to obtain information on the internal structures and the dimensions of the vertebrae, μCT scans were made after embedding.

Figure 5.1: Potted and isolated vertebrae (cadaveric specimen 3; T8 till L1)

5.1.2 Mechanical set-up

For the fracture generation and the cyclic loading after vertebral restoration, applying an axial compressive load on the vertebral body was required. The universal test machine that was used to exert this load was the LRX5 material testing machine from AMETEK (Lloyd Instruments Ltd, Bognor Regis, UK). As the vertebrae were loaded on different positions during fracture generation and cyclic loading, a variable vertebral positioning was required in the mechanical set-up. Therefore, the part visible in figure 5.2 was manufactured. This part only allowed a displacement of the vertebra in anterior-posterior direction, while constraining the medial-lateral direction. To ensure the location of the vertebra on this bottom disc, two M6 screws were tightened to fixate the vertebra in anterior-posterior direction. More detailed information on the fracture generation and the cyclic loading are given in subsection 5.2.1 and 5.2.3.

Furthermore, pure axial loading was necessary to prevent shear forces that could potentially influence the results and lead to more variability among outcomes. Thus, during the cyclic loading a spinal follower load was resembled by axial compressive loading on the center of each vertebral body. To ensure pure axial loading during the tests, a ball and socket joint was manufactured. Besides, the plate superior to the isolated vertebrae was ribbed in order to prevent slipping. Eventually, the ball and socket joint was connected to a rod, which on its turn was connected to the testing machine. An overview of all the parts of the mechanical set-up is visible in figure 5.3. In Appendix C the technical drawings of all parts can be evaluated.

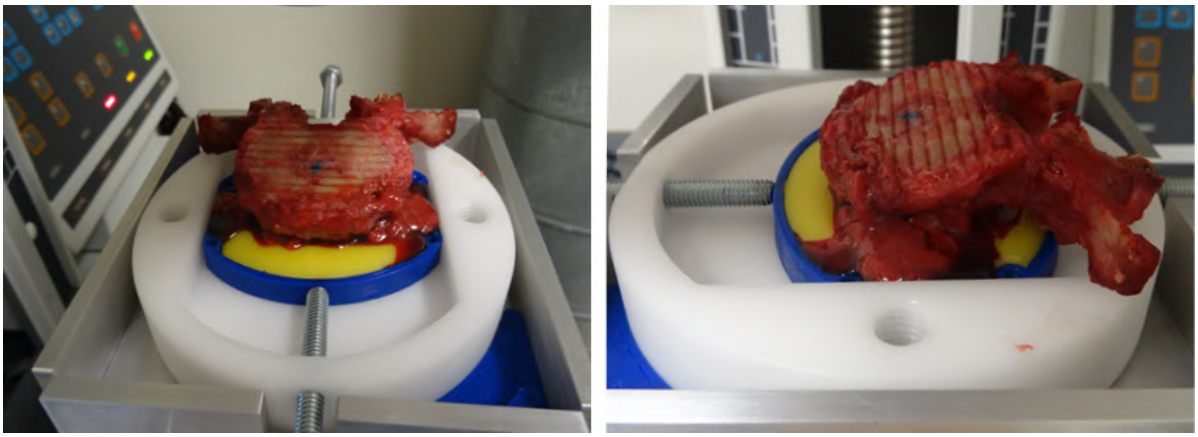

Figure 5.2: The bottom disc of the mechanical set-up enabling axial compressive loading for each vertebra

In order to gain information on the internal structure of the VBs, μCT scans were made after different test stages; after specimen preparation, after fracture generation, after vertebral restoration and after cyclic loading. To establish a stable translocation from the mechanical test machine to the Quantum FX Caliper^{TM} μCT (PerkinElmer, Caliper Life Sciences, Hopkinton, MA, USA), nylon threads and nuts were used to fixate the set-up. In subsection 5.3 the analysis of the μCT data is discussed further. As metal parts would have distorted the μCT image, the parts of the set-up close to the vertebra were made of polyoxymethylene (POM, Delrin®) whenever possible. POM is regularly used to replace metals as it has a high strength, stiffness and hardness in combination with a low friction coefficient and high wear resistance. The metal parts of the set-up were made out of an aluminium alloy, aluminium 6061-T6. All parts were manufactured with CNC (Computer Numerical Control) machining.

Figure 5.3: An overview of the mechanical set-up

5.2 Study Design

Before deliberating on the study design for the tests, it has to be stressed that no standard guidelines are developed for in vitro studies on spinal implants. In contrast to in vitro studies on intervertebral implants, a wide variety of study designs have been implemented in former studies. As my literature study suggested, this is one of the main reasons why the current third generation procedures cannot be compared one to one. Nonetheless, an evaluation on former studies was required in order to create an appropriate study design. An overview of the most important characteristics of the cadaver studies that were included in my literature study is given in Appendix D. The main study design characteristics were assumed to be the fracture generation, the vertebral restoration and lastly the cyclic loading conditions. In the coming subsections each of these characteristics are discussed and declared. For all research questions, the test stages fracture generation and vertebral restoration are identical. The differences in the cyclic loading stage are discussed in subsection 5.2.3. In Appendix E the test protocols for the biomechanical tests can be evaluated.

5.2.1 Fracture generation

A wedge fracture, Magerl AO type A1.2, is the most abundant fracture type that osteoporotic patients suffer from. In chapter 2 the anatomical meaning of this fracture type has already been discussed. Thus, during the fracture generation an anterior height decrease should be realised without fracturing the posterior wall of the VB. Therefore, the axial compressive load exerted by the universal test machine LRX 5K (AMETEK, Lloyd Instruments Ltd, Bognor Regis, UK; 5kN load cell, accuracy 0.5%) was placed on the anterior fourth of the vertebral body. The stopping criterion for the fracture generation was formulated as a reduction in anterior height of 40%. To accomplish that, the load cell was compressing the vertebra with a speed of 2mm/min until the 40% height reduction was reached. According to the Genant grading system, 40% anterior reduction resembles a severe fracture, also referred to as Genant grade 3. While some of the former studies only implemented fractures up to 25% height reduction, classified as moderate fractures, it was assumed that severe fractures would give a better and more honest impression of the implant's capability. To prevent the reexpansion of the fractured vertebra, the load at fracture was maintained for 15 minutes after fracture generation. Thereafter, the vertebra was placed in a 3D-printed holder that was tightened with nylon threads and nuts. The holder was compressed by 50N to standardize tightness. Thereafter, vertebral body heights were redetermined by a μCT scan.

5.2.2 Vertebral restoration

Apart from the screw driver and implant inserter shown in chapter 3 no specific surgical tools were developed for the implant, as the concept of the implant first needed to be proved. Thus, equipment from the balloon kyphoplasty procedure and equipment that was present at the anatomy lab of the UMC were used. First, the vertebral body needed to be accessed through the pedicles. Hereby, the approach was similar to the current, minimally invasive, repair procedures. In order to access, two puncture devices, one with a trocar and one with a diamond shaped tip, were inserted to make a path that ended just before the anterior wall was reached. Thereafter, a bone drill was inserted to remove any remaining bone tissue. Then, the porous implants were inserted and pushed to the anterior wall as much as feasible. When both implants were in the right position, the implants were expanded with a specially designed screw driver. The amplification was continued until the anterior height of the vertebral body was visibly restored or until the implants were at their maximum expansion.

For the BKP procedure, the Kyphon® Balloon Kyphoplasty (Medtronic Inc., Minneapolis, MN, USA) was used. The standard protocol for this procedure was followed during these tests. Both procedures were first performed with the assistance of orthopaedic surgeon Dr. Paul van Urk. After vertebral restoration, the vertebrae were placed back in the 3D-printer holder and a compressive load of 50N was again exerted. Consequently, μCT scans were made to obtain the initial position and expansion of the implants.

5.2.3 Cyclic loading

To test whether the restoration of the anterior height and correction of the kyphotic angle would remain, the vertebrae were tested under cyclic loading. A cyclic loading with 10.000 cycles approximately corresponded to the activity during the first week after the VCF repair for elderly patients. The study from Wilke et al. (2006) was used as a reference to determine the characteristics for this cyclic loading test. This study has formed the basis for multiple former studies in the same field of research. Nevertheless, in Wilke et al. (2006) 100.000 cycles were implemented, resembling the activity of several months after fracture repair. As this would take a considerable amount of time per vertebra, various recent studies have implemented 10.000 cycles only (Krüger et al., 2013; Rotter et al., 2010; Rotter et al., 2015; Wang et al., 2018). During the cyclic test under normal loading, i.e. research questions 1 and 2, the loading gradually increased from 100N to 600N, representing activities from lying supine to walking (Wilke et al., 2006). These values were determined through intradiscal pressure measurements by Wilke, Neef, Caimi, Hoogland, and Claes (1999). Since it was not expected that patients who would undergo this kind of procedure would execute physically demanding activities soon after surgery, outcomes at higher compressive loads were not evaluated for these research questions. As the testing machine showed an inaccuracy at higher testing speeds, for the first and second research question a frequency of 0.5Hz was implemented.

For the third research question higher loads were applied; the loads ranged between 100N and 1000N. Thereby, more physically demanding activities were resembled such as holding a weight of 20kg close to the body or bending forward (Wilke et al., 2006). Since the bone regeneration would take several months after VCF repair, these kind of activities should not cause any problem. Furthermore as the outcomes for this question were not compared to other studies and as the total study time had to be taken into account, the frequency for the third research question was 1 Hz. When any of the cyclic loading tests were finished, the vertebrae were placed back in the 3D-printer holder and a compressive load of 50N was again exerted on them. Finally, μCT scans were made in order to evaluate the spinal deformities and internal vertebral structures.

5.3 Statistical Analysis

The data from the LRX5 material testing machine was recorded and analysed in Nexygen^{TM} Software, Nexygen version 4.5 and Ondio version 4.5 (Lloyd LRX, Fareham, UK). The data points were exported to Matlab version R2018a (The MathWorks Inc, Natick, MA, USA) in order to see whether uncommon or remarkable events happened during the fracture generation or cyclic loading. The data from the μCT was analysed in ImageJ, an image processing program. Furthermore, the changes of the internal vertebral structure were evaluated in this program. The data obtained from the μCT scans was analyzed using IBM SPSS Statistics version 25 (SPSS Inc, Chicago, Illinois, USA). For visualisation purposes, the imaging processing and visualization softwares MeVisLab version 3.0.1. (MeVis Medical Solutions AG, Bremen, Germany) and 3DSlicer version 4.10.2 (The Brigham and Women's Hospital, Inc. Boston, USA) were used.

Chapter 6

Results

As mentioned before, three human cadaveric specimens were used for the tests. The source of the donors was anatomic donation, whereby no medical history was available other than gender and age. Unfortunately, the age of specimen two and three were unknown. In table 6.1 the study characteristics can be evaluated. All specimens were fresh frozen until testing. During the preparation of the second specimen spondylitus in the thoracic region was discovered. Therefore, it was unable to segment these vertebrae. So, only the lumbar vertebrae were included in the tests. The fifth lumbar vertebra, L5, of the second specimen was segmented and prepared additionally in order to obtain extra data points for this specimen and thereby minimize the effect of potential outliers. Nonetheless, it should be noted that VCFs regularly do not occur at this site.

Study Characteristics

	Specimen 1	Specimen 2	Specimen 3
Gender	Female	Male	Female
Age (yr)	77	Age Unknown	Age Unknown
Included vertebrae	T8 - L4	L1 - L5	T8 - L4
Remarks	-	Spondylitis in thoracic vertebrae	Scoliosis in lumbar region

Table 6.1: Study Characteristics

Furthermore, scoliosis was present in the lumbar region of the third specimen. However, this was not seen as a reason to exclude these vertebrae as VCFs can occur in patients with scoliosis as well. A visible representation of the scoliotic region is given in figure 6.1.

Figure 6.1: Scoliosis visible in the lumbar region of the third specimen

Eventually, the vertebrae were distributed into three test groups; the group restored with the implant and tested in a cyclic test under normal loading, the group restored with the BKP procedure and tested in a cyclic test under normal loading and the group restored with the implant and tested in a cyclic test under high loading. The specimen distribution can be found in table 6.2. Between brackets the size of the inserted implants is given. For all vertebrae in the BKP group, size 20/3 of the Kyphon Expander Inflatable Bone Tamp was used. In the remaining part of this report the vertebrae are coded according to their specimen number, followed by their spinal position. Thus, T8 of specimen 1 is referred to as S1T8.

Specimen Distribution

	Specimen 1	Specimen 2	Specimen 3
Implant_Normal Loading	T8 (5) T9 (5) T11 (5) T12 (5)	-	T9 (6) T10 (6) T12 (6) L1 (6)
BKP_Normal Loading	T10 L1	L2 L5	T8 T11 L3
Implant_High Loading	L2 (6) L3 (6) L4 (6)	L1 (6) L3 (6) L4 (6)	L2 (6) L4 (6)

Table 6.2: Specimen Distribution. The numbers in brackets indicate the size of the implants that were inserted.

The initial dimensions of all vertebrae can be found in Appendix F. The heights are measured at the anterior, central and posterior site of the vertebrae while the width and depth are measured at the superior, central and inferior sites. The kyphotic angle was measured as the angle at the intersection of both endplates. In figure 6.2 the measurement diagram is given.

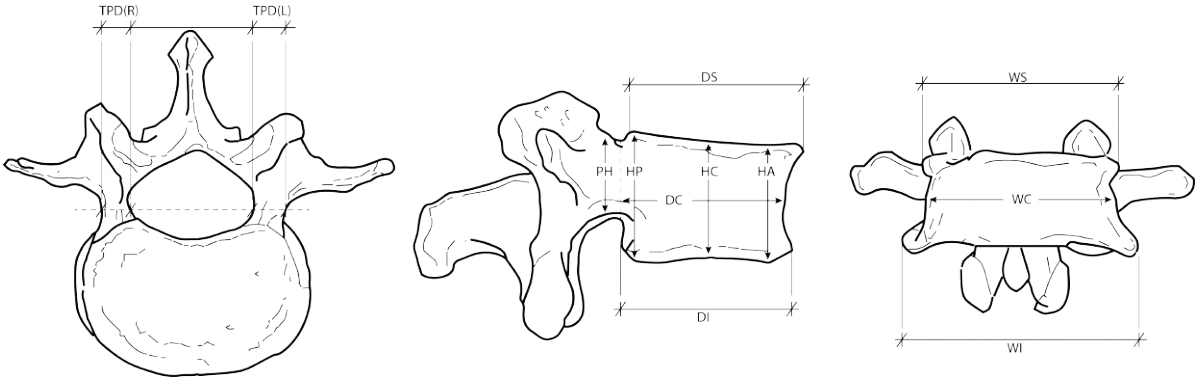

Figure 6.2: The measurement diagram for the vertebral dimensions. HA, HC and HP; height anterior, central and posterior. WS, WC and WI; width superior, central and inferior. DS, DC and DI; depth superior, central and inferior. PH; pedicle height. TPD (R) and TPD (L); transverse pedicle diameter right and left.

Before deliberating further on the results it should be noted that seven vertebrae were excluded from the results as they failed somewhere along the testing process. In Appendix G these seven vertebrae (S1T8, S1T11, S1L2, S2L2, S2L4, S3T12 and S3L4) and their failures are discussed. In the remaining of this report, the implant group tested under normal loading, the BKP group tested under normal loading and the implant group tested under high loading consisted of five, six and five vertebrae respectively.

6.0.1 Fracture generation

In figure 6.3 the load-displacement curves for all vertebrae are given. As one can evaluate, the stiffnesses of most vertebrae were comparable. The average fracture load approximated 1949N, which is in accordance with fracture loads in osteoporotic patients shown in former studies (Haidekker, Andresen, & Werner, 1999; Wang et al., 2018). Furthermore, the average stiffness was 637 N/mm. Some curves clearly showed a displacement before the linear part of the load-displacement curve took off. Presumably, these vertebrae had a substantial initial kyphotic angle or had a severe concavity in the superior endplate. Thereby, the posterior parts of these vertebrae first encountered some deformation before the axial compressive load was applied at the anterior fourth. The initial dimensions of the vertebrae, visible in table F.1, F.2 and F.3 confirmed this suggestion.

In figure 6.4, figure 6.5 and figure 6.6 the mean load-displacements curves are given per specimen, spinal region and test procedure respectively. In table 6.3 the stiffnesses (N/mm) for the fracture generation are given as a mean for all vertebrae and for the vertebrae grouped per specimen, spinal region and test procedure in order to observe potential variabilities.

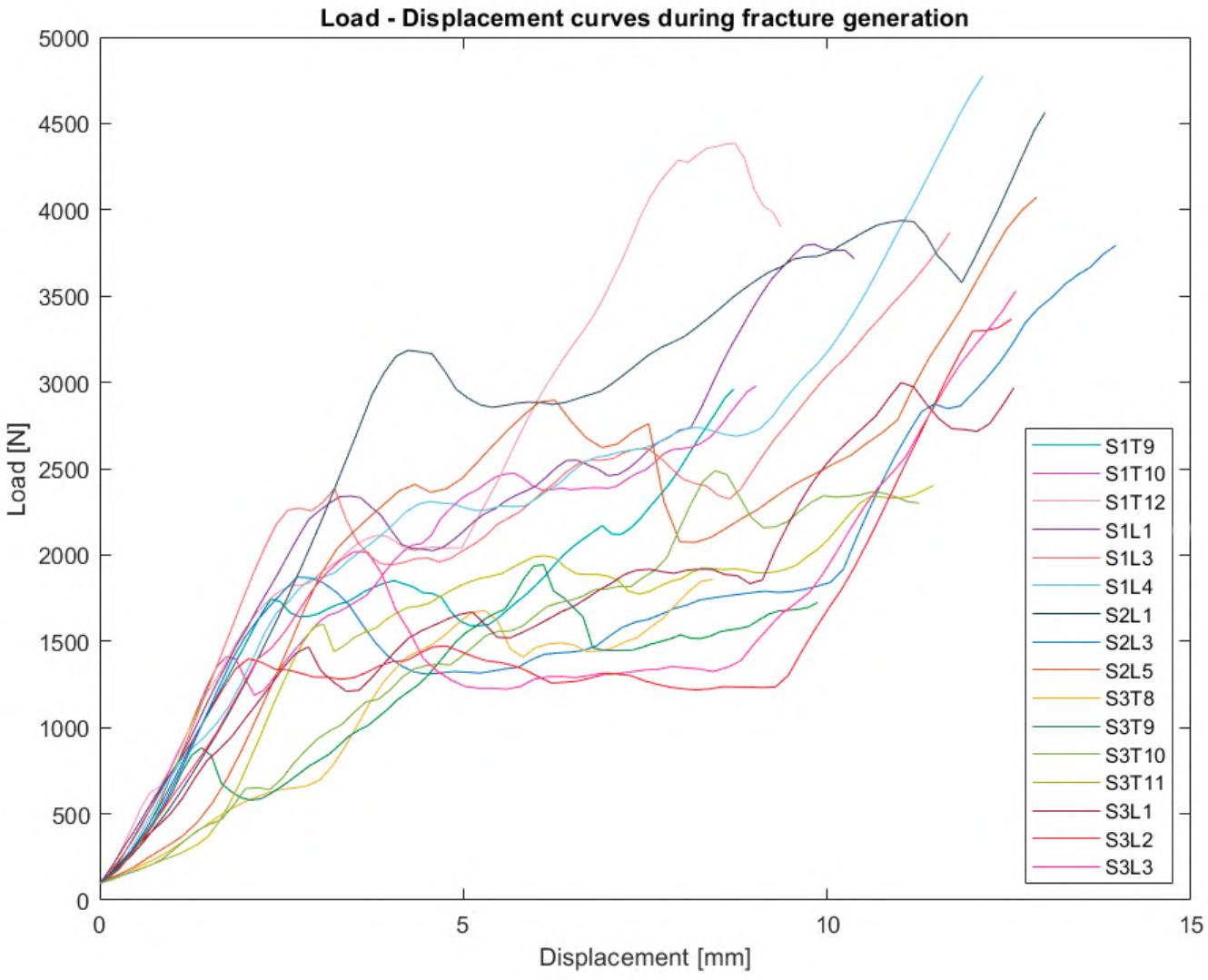

Figure 6.3: The load-displacement curves during fracture generation for all vertebrae

Overview of the stiffnesses observed during fracture generation

Vertebral group	Stiffness (N/mm)
All	637
Per specimen	
Specimen 1	674
Specimen 2	674
Specimen 3	589
Per spinal region	
Thoracic	591
Lumbar	665
Per procedure	
Implant	520
BKP	658
Implant_high loading	698

Table 6.3: The stiffnesses observed during fracture generation for all vertebrae, per specimen, per spinal region and per test procedure

In figure 6.4 it can be seen that specimen 1 and 2 showed identical stiffnesses. Furthermore, specimen 3 clearly showed a lower stiffness as could be obtained from table 6.3 simultaneously.

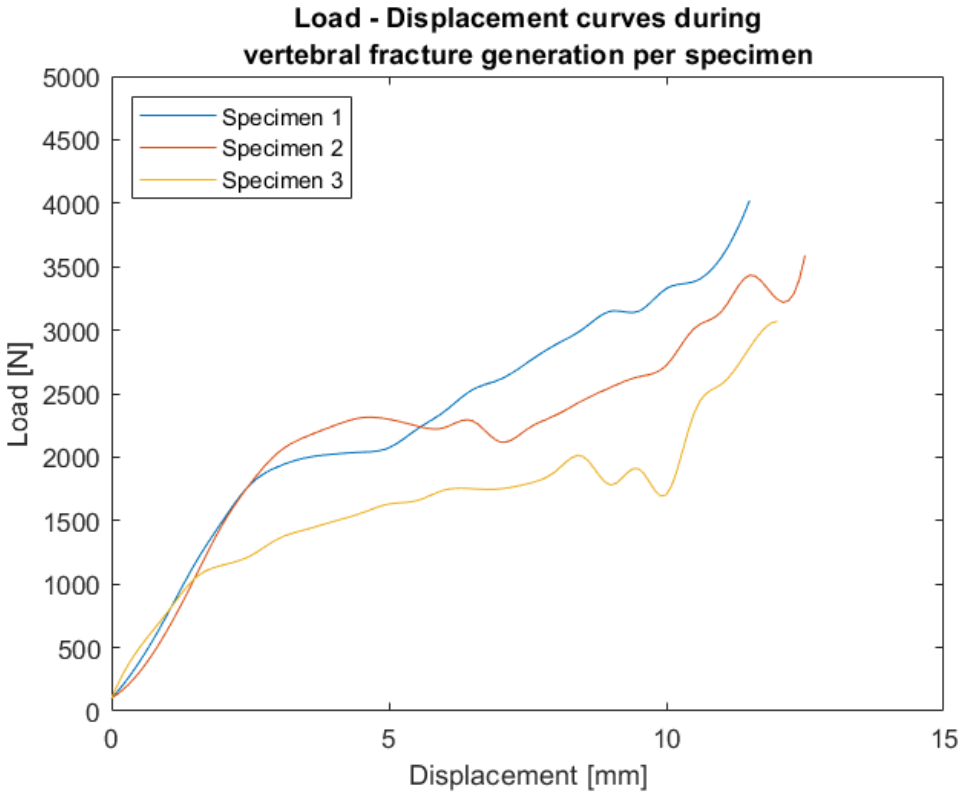

Figure 6.4: The mean load-displacement curves during fracture generation per specimen

From figure 6.5 it could be concluded that the lumbar vertebrae had higher stiffnesses compared to the thoracic vertebrae. As specimen 3 consisted out of four thoracic vertebrae and three lumbar vertebrae, this partially declared the lower stiffness observed for this specimen. Moreover, the first test group, implants tested under normal loading, encompassed the most thoracic vertebrae. Therefore, a lower stiffness was observed for this group in figure 6.6. Additionally, as more lumbar vertebrae were included in the third test group, the implants tested under high loading, a slightly higher stiffness was observed in figure 6.6. Furthermore, no remarkable outcomes were found during fracture generation.

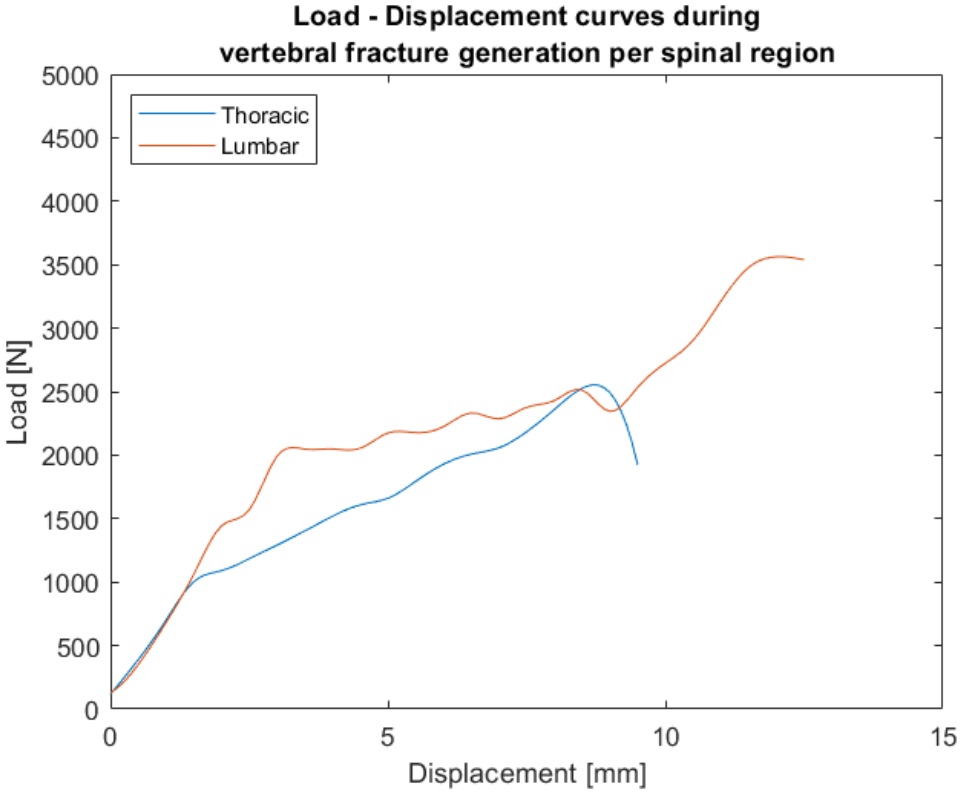

Figure 6.5: The mean load-displacement curves during fracture generation per spinal region

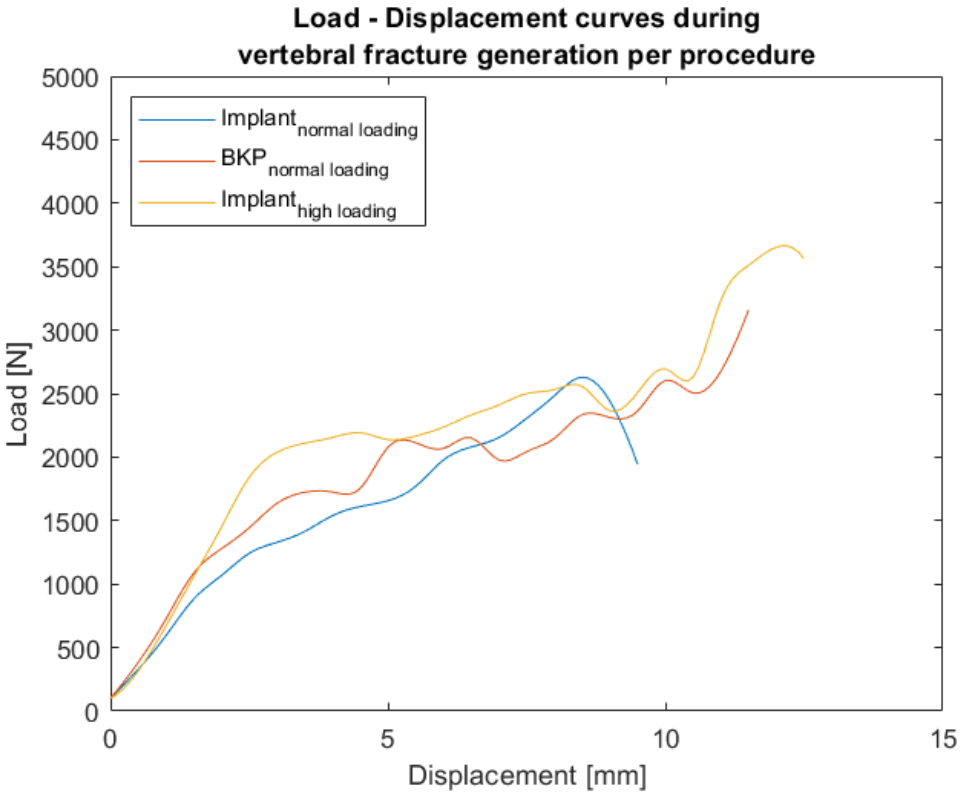

Figure 6.6: The mean load-displacement curves during fracture generation per procedure

6.1 Can the implant adequately prevent spinal deformities to occur?

After the fracture generation, the vertebrae were restored with either the implant or the BKP procedure. Thereafter, they were all tested in a cyclic loading test. First, the two groups that were cyclic tested under normal loading are discussed. The results are subdivided into the restoration of the anterior height and the correction of the kyphotic angle in order to quantify the prevention of spinal deformities.

In section 6.1.3, the results for the vertebrae restored with the implant that were cyclic tested under higher loading are given. Again, both the anterior height restoration and the kyphotic angle correction are discussed.

6.1.1 Can the implant restore the anterior height of the vertebral body?

In figure 6.7 and figure 6.8 the deformations of the vertebrae can be observed during cyclic loading. By evaluating figure 6.7 and 6.8 it could be concluded that a decrease in height during cyclic loading was observed for both test groups. The height decrease was given as a percentage of the **restored height**. In both graphs, an initial height decrease is visible at the start of the test. Thus, for both groups the vertebrae deformed due to the static preload of 100N before the cyclic loading started. The bright lines in both graphs represent the development of the lower limits of the percentual height decrease that was observed over the number of test cycles. The remaining dynamic deformation, shown by the more transparent fluctuating curves, was assumed to be elastic deformation.

For the vertebrae restored with BKP a mean static height decrease of 9.0% was evaluated, as well as a mean cyclic height decrease of 9.4% during the test. The mean static height decrease for the implant group was in a similar range, while a more significant mean cyclic height decrease was detected. From figure 6.7 it could be concluded that the means were 8.7% and 25.2% respectively.

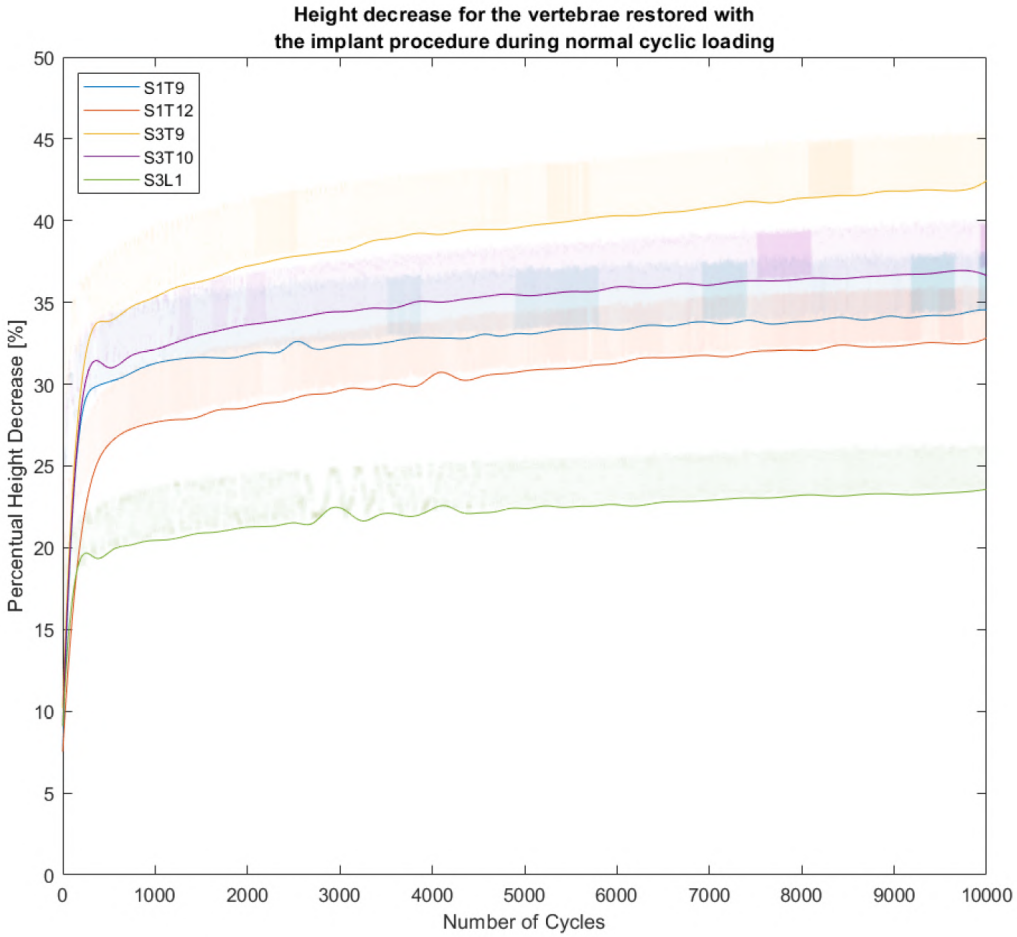

Figure 6.7: The percentual decrease of the restored height during the cyclic loading for the vertebrae restored with the implant. The brightly coloured lines represent the development of the lower limits of the percentual height decrease over the number of test cycles for all vertebrae, while the more transparent fluctuating curves represents the dynamic height decrease during the tests.

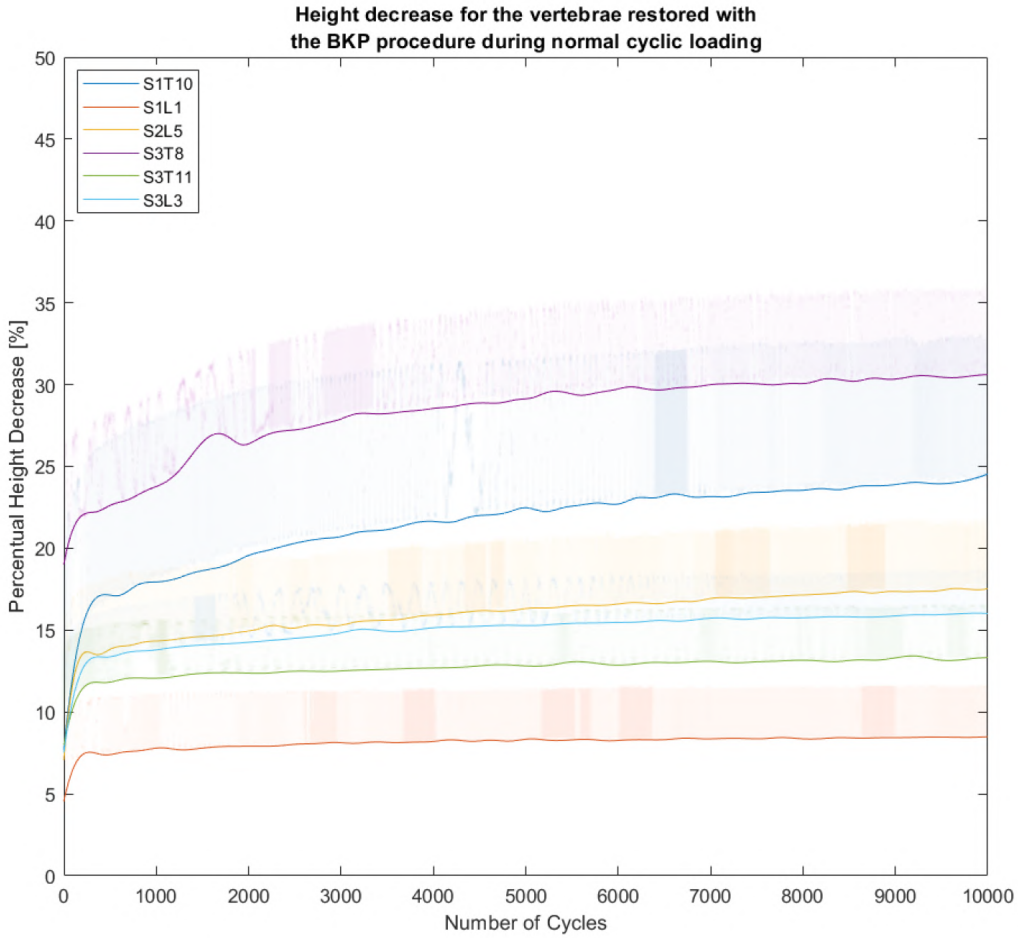

Figure 6.8: The percentual decrease of the restored height during the cyclic loading for the vertebrae restored with BKP. The brightly coloured lines represent the development of the lower limits of the percentual height decrease over the number of test cycles for all vertebrae, while the more transparent fluctuating curves represents the dynamic height decrease during the tests.

However, these outcomes were only observed at the center of the vertebrae where the compressive load was applied. In table 6.4, the vertebral heights at the anterior, central and posterior sites are given, which were obtained from the μCT scans. All outcomes are presented as percentages, relative to the **initial heights**. The observed differences for the central restored height and the central cyclic height in table 6.4 lead back to the two figures described above, figure 6.7 and 6.8.

For the BKP group only a minor central height decrease of 2.5% between these test stages was observed in table 6.4. Thereby, it could be concluded that the static and cyclic height decrease, presented in figure 6.8, were predominantly elastic deformation that restored itself after unloading. For the implant group, the outcomes of table 6.4 showed considerably more height decrease. As table 6.4 showed a central height decrease of 25.5% when comparing the restored and cyclic outcomes, it was suggested that most of the static and cyclic height decrease observed in figure 6.7 were a result of plastic deformation. For the implant group, 70.6% of the deformations shown in figure 6.7 were plastic, while only 14.3% of the deformations observed in figure 6.8 were found to be plastic deformation. This phenomenon of plastic deformation is further deliberated on after discussing the height restoration outcomes presented in table 6.4.

Overview of the results for height restoration (the initial height equals 100%)

	Implant		BKP	
	Mean	SD	Mean	SD
Fractured height (%)				
Anterior	59.8	13.3	68.4	8.5
Central	74.3	6.7	80.6	8.5
Posterior	79.5	10.9	90.1	4.8
Restored height (%)				
Anterior	98.0	6.5	89.2	10.2
Central	106.5	4.2	95.3	8.5
Posterior	100.3	1.3	96.5	7.0
Cyclic height (%)				
Anterior	72.5	5.5	86.5	7.5
Central	81.0	2.4	92.8	6.3
Posterior	83.4	3.2	92.6	6.0

Table 6.4: An overview of the vertebral heights per test stage

In figure 6.9 and 6.10 a visible representation of the data in table 6.4 is given. Not surprisingly, the anterior height decreased most during the fracture generation. Nonetheless, an exact height reduction of 40% was not evaluated for the BKP group. Presumably, the higher stiffness that was shown in figure 6.6 might have caused this observation to some extent.

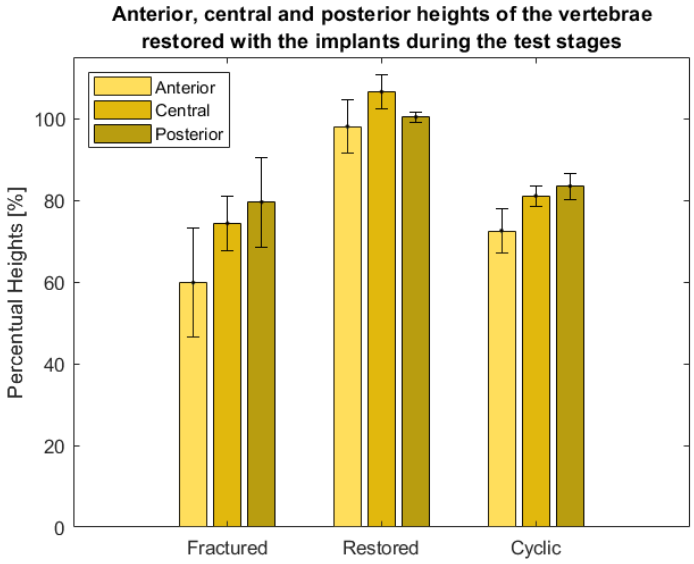

Figure 6.9: An overview of the vertebral heights per test stage for the implant group. Errorbars represent the standard deviation.

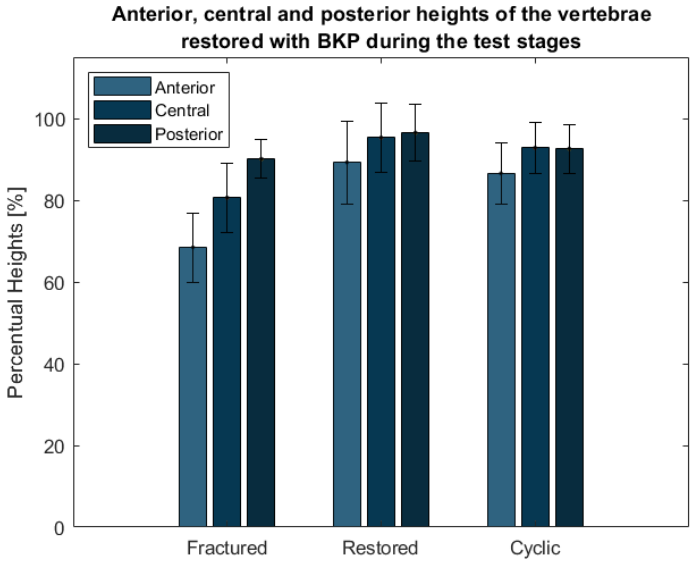

Figure 6.10: An overview of the vertebral heights per test stage for the BKP group. Errorbars represent the standard deviation.

From the restored data in table 6.4, it could be concluded that the implant group showed more impressive outcomes for the anterior, central and posterior height restoration in comparison to the BKP group. A statistical significant difference ($p<0.05$) was found between the implant and BKP group when comparing the fractured and restored data. On the most important site, i.e. the anterior site, a height restoration of nearly 40% was realised. In comparison to the BKP group, an additional 17.4% of the height was thereby restored. Thus, the potential of the implant to restore vertebral height was demonstrated. The central restored height even exceeded the initial value and thereby slightly decreased the concavity of the endplates. However, as it only exceeded the initial value by 6.5% on average, this was not expected to be harmful. In conclusion, it had to be stressed that the implant group was the only group that succeeded to fully restore the heights on all sites.

Nonetheless, the cyclic loading seemed to have had less impact on the BKP group, as the cyclic height outcomes for this group positively exceeded the outcomes of the implant group. The percentual decrease of the height after cyclic loading compared to the restored height was approximately 3% for all three sites in the BKP group. However, for the implant group more decrease was evaluated anteriorly and centrally in comparison to the posterior site. Although, all sites experienced substantial height losses, 25.5%, 25.5% and 16.9% respectively. Notwithstanding, when comparing the **fractured and cyclic heights** no statistical significant differences (p>0.05) were found between both test groups.

As the anterior height was assumed to be the most important site to restore after a VCF, figure 6.11 showed the anterior height development over the test stages for both test groups. Here, one can even better evaluate the potential of the implant to restore the fractured height in comparison to the BKP. However, it clearly shows its pitfalls too when looking at the height difference after the cyclic loading.

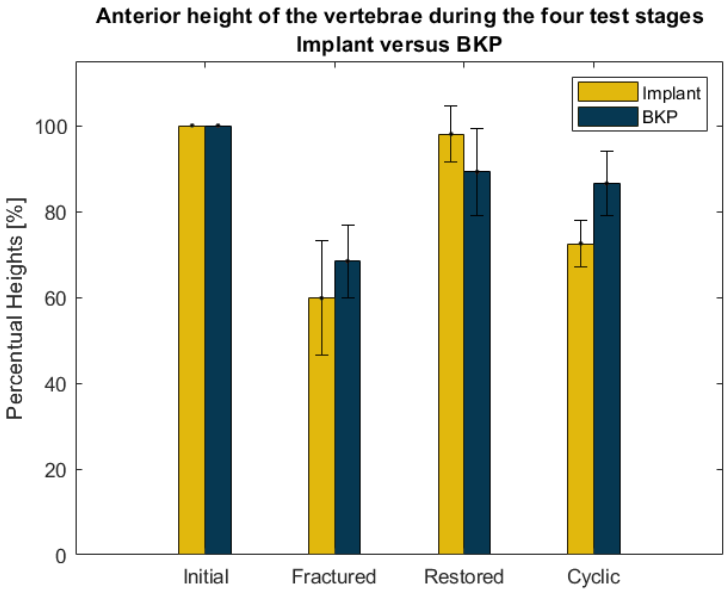

Figure 6.11: The development of the anterior height over the test stages. Errorbars represent the standard deviation.

Hereby the question arose: Where did the anterior height decrease and the plastic deformation come from in the implant group? To answer this question, the distribution between the implant and the adjacent bone structures of the vertebrae was examined more closely. This was performed for the BKP group likewise to serve as a comparison. As the implants and the PMMA were not exactly positioned at the anterior wall, the heights were rather measured at the anterior end of the inserted materials. For all vertebrae, this led to a variation of height measurements between the anterior and central line. Therefore, the initial and fractured heights at these positions were remeasured.

In figure 6.12 one can evaluate the outcomes for the implant group. Obviously, the height of the bone inferior to the implant decreased most after cyclic loading with 16.9%. However, a 2.0% decrease in height for the superior bone structures was evaluated simultaneously. Additionally, even a small decrease in the implant's height was observed.

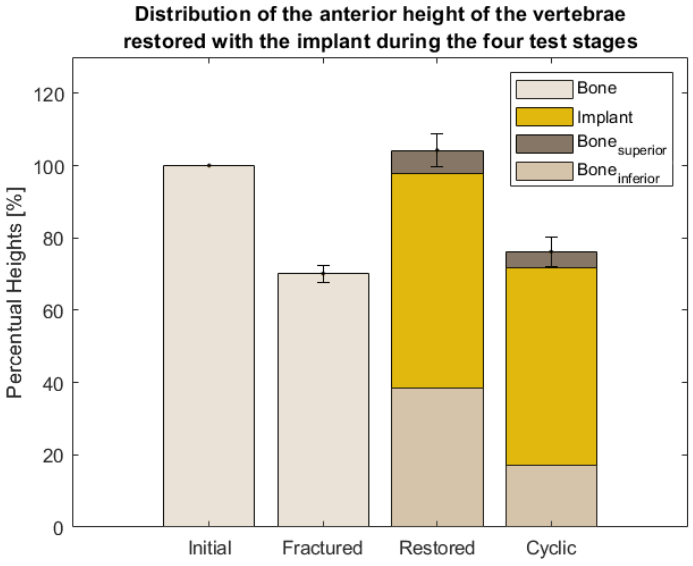

Figure 6.12: Distribution of the vertebral height for the implant group. Errorbars represent the standard deviation.

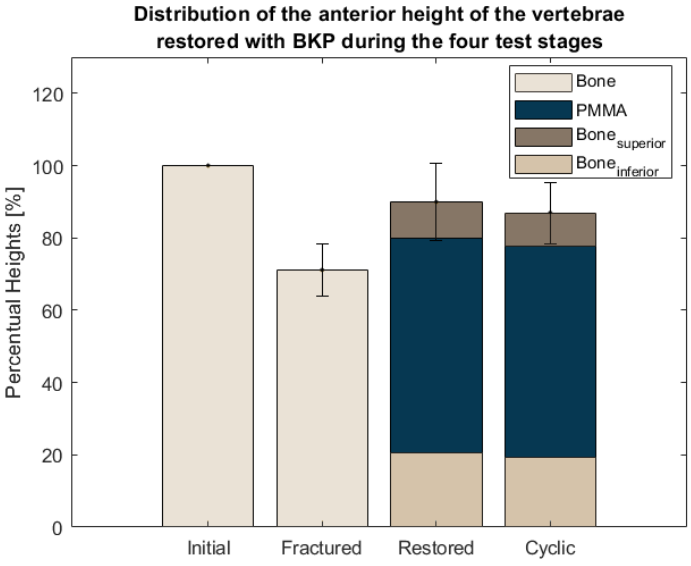

Figure 6.13: Distribution of the vertebral height for the BKP group. Errorbars represent the standard deviation.

In the BKP group, the decrease in heights were considerably lower. Only a minor height decrease was seen for the superior and inferior bone structures, 0.8% and 1.3% respectively. Furthermore, practically no change in height was observed for the PMMA. In table 6.5 the outcomes are given numerically, relative to the initial heights. The height of the PMMA decreased by 0.9%, which could be either explained by a slight indent of the outer surface of the PMMA or by a result of measurement errors. For the implant the difference was 4.9%. Although this could have been a result of measurement errors, question marks raised as the titanium alloy was not supposed to deform under the cyclic loading. Therefore, the vertebrae with the implants were once more investigated thoroughly.

Overview of the material distribution

	Implant		BKP	
	Mean	SD	Mean	SD
Restored height (%)	104.2	4.6	89.9	10.6
Bone superior	6.3		9.9	
Implant/PMMA	59.5		59.4	
Bone inferior	38.4		20.6	
Cyclic height(%)	76.1	4.1	86.9	8.5
Bone superior	4.3		9.1	
Implant/PMMA	54.6		58.5	
Bone inferior	21.5		19.3	

Table 6.5: The numerical distribution of the heights for the implant and the BKP group

As mentioned before, the materials of the implants were supposed to withstand loads far above those that were applied during the cyclic test, i.e. 600N. Thus, it was assumed that the positioning of the implants was a more critical factor to address. Therefore, the initial rotation of the implant (after restoration of the vertebrae) and the rotation after cyclic loading were evaluated along with the heights of the implants during both stages in the coronal plane. The outcomes are given in table 6.6 and shown in figure 6.14.

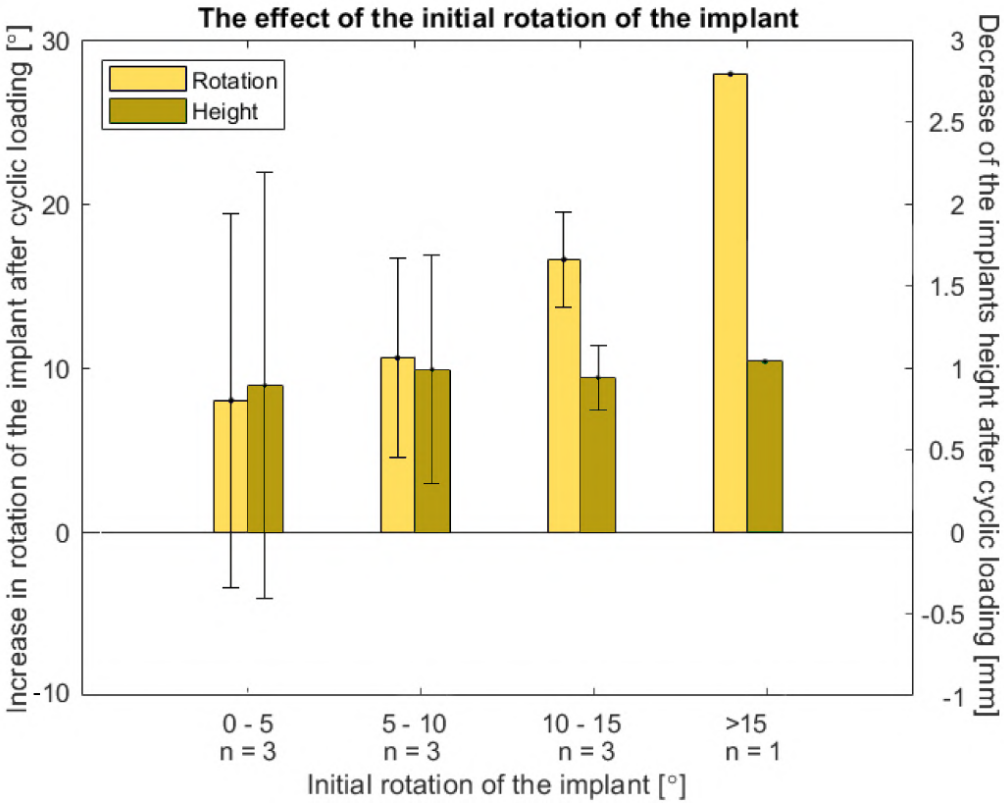

Figure 6.14: A graphical representation of the influence of the initial implant rotation on the rotational increase and height decrease. Errorbars represent the standard deviation. The number of included implants is given as n.

For the evaluation, the implants were subdivided according to their initial rotation. Both figure 6.14 and table 6.6 indicate that a higher initial rotation increases the change of rotation under loading. In other words, an implant with a higher initial rotation is more likely to rotate when load is applied to the vertebrae. Moreover, the height decrease seemed to slightly increase with the initial rotation. Although this correlation could not be confirmed from this data. When the initial rotation was over 15°, severe influences on the rotation during cyclic loading could be observed. Thus, it could be concluded that the initial rotation is of utmost importance for the functionality of the implant.

The mean initial height for the implant group in figure 6.12 was 20.7mm and the mean height decrease observed in figure 6.14 was 0.95mm. Thus, the percentual decrease of the implant's height in respect to the initial height was 4.6%. This is in accordance with the implant's height decrease of figure 6.12, which was 4.9%. Hereby, it was presumed that the height decrease of the implant that was evaluated is declared.

Overview of the results for implant rotation

Initial implant rotation (°)	Increase in implant rotation (°)		Decrease in implant height (mm)	
	Mean	SD	Mean	SD
0 - 5 (n = 3)	8.0	11.4	0.89	1.3
5 - 10 (n = 3)	10.6	6.1	0.99	0.7
10 - 15 (n = 3)	16.6	2.9	0.94	0.2
>15 (n = 1)	27.9	-	1.04	-

Table 6.6: The influence of the initial implant rotation on the rotational increase and height decrease. The number of included implants per group is indicated by n.

6.1.2 Can the implant correct the kyphotic angle of the vertebral body?

In addition to the anterior height restoration, the correction of the kyphotic angle was observed. In table 6.7 the mean kyphotic angles for both test groups are given per test stage. As one can evaluate, the initial kyphotic angles for both groups were comparable. Only a slight difference of 0.6° was observed. After fracture generation, the difference between both groups increased to some extent.

Overview of the results for kyphotic angle correction

	Implant		BKP	
	Mean	SD	Mean	SD
Initial kyphotic angle (°)	4.4	1.2	3.8	6.6
Fractured kyphotic angle (°)	11.9	2.8	14.0	2.4
Restored kyphotic angle (°)	4.9	2.8	6.2	8.3
Cyclic kyphotic angle (°)	8.6	3.0	6.9	5.6

Table 6.7: The correction of the kyphotic angle over all test stages for the implant and BKP group

The results for the restored correction of the kyphotic angle showed similar results compared to the height restoration; the implant group showed more favourable outcomes as the restored kyphotic angle only deviated 0.5° from the initial angle. For the BKP group the deviation between both angles was 2.4°. Nonetheless, for the outcomes after cyclic loading the tendency described for the height restoration repeated itself. A severe decrease for the kyphotic angle correction was observed for the implant group, i.e. 3.7°. On the other hand, for the BKP group only a decrease of 0.7° was detected. Overall, no statistical significant differences ($p<0.05$) were observed between both test groups.

Equally to the investigation on the implant's rotation in the coronal plane in respect to the decrease of height, the insertion angle of the implants in the sagittal plane was compared to the decrease of kyphotic angle here. However, no tendencies could be described based on the initial insertion angle in this plane. It was seen that the implant's angle changed corresponding to the change of the kyphotic angle. Logically, this could be explained by the fact that the implant subsided in the inferior trabecular bone by the load applied on the superior endplate, as has been concluded in subsection 6.1.1.

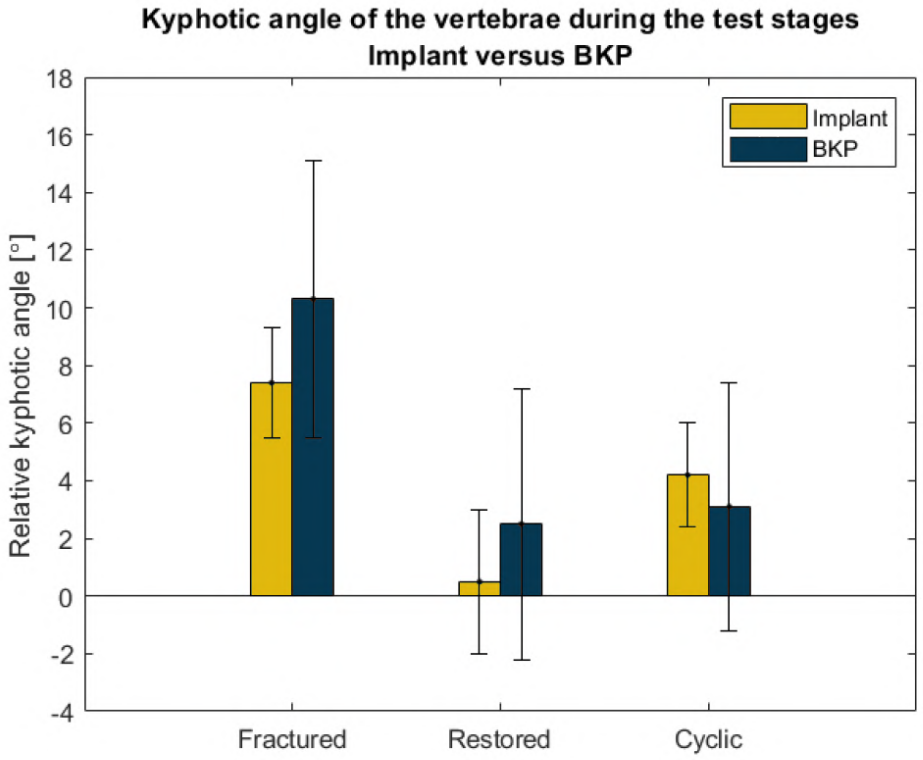

Figure 6.15: The graphical representation of the relative correction of the kyphotic angle over all test stages for both groups. All outcomes are given relative to the initial kyphotic angle. Errorbars represent the standard deviation.

6.1.3 Can the implant withstand higher loading conditions?

Now that the comparisons between the implant group and BKP group under normal loading are made, the results of the implant group under high loading can be discussed.

Can the implant restore the anterior height of the vertebral body?

In figure 6.16 the percentual decrease in height during the cyclic loading for this group is given. As one can evaluate, the central height reached a static mean decrease of 9.5%. During the test, the height decrease developed further to a mean total of 29.0% at the end of the cyclic testing. In comparison to figure 6.7 and 6.8, the cyclic height decrease during the test was, contrary to the hypothesis, slightly lower compared to the implant group tested under normal loading i.e. 19.5% vs. 25.5%, but still much higher compared to the BKP group, i.e. 9.4%. Similarly to section 6.1.1, an overview presenting the anterior, central and posterior heights during the test stages is given in table 6.8 and figure 6.17.

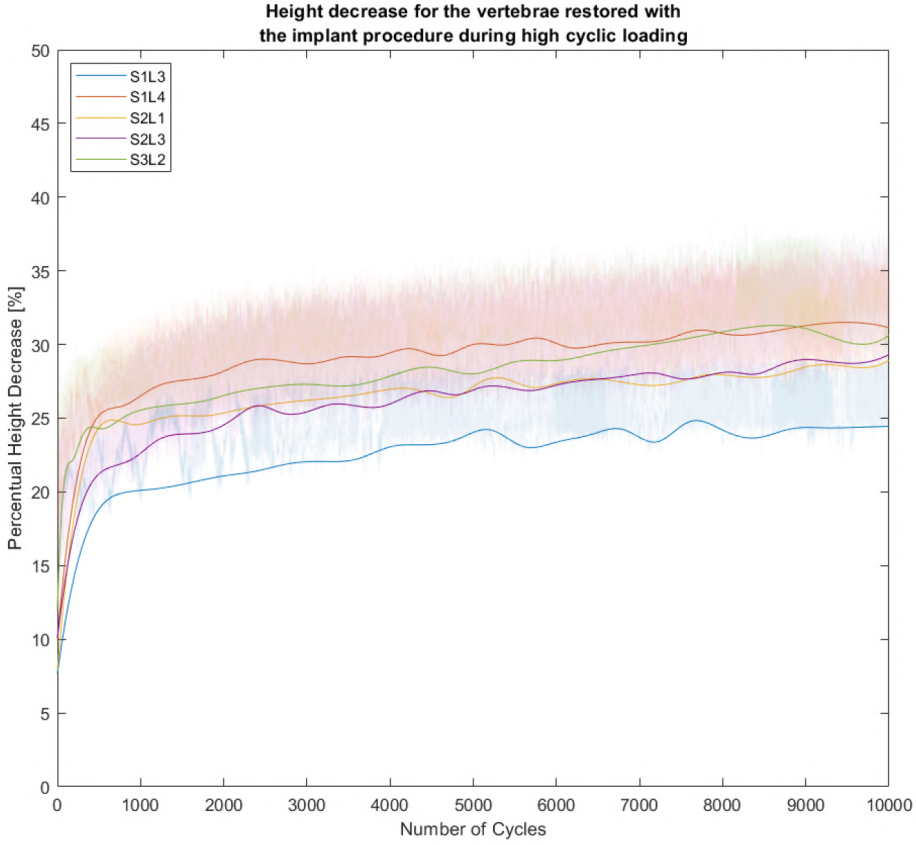

Figure 6.16: The percentual decrease of the restored height during the cyclic loading for the vertebrae restored with the implant tested under high loading. The brightly coloured lines represent the development of the lower limits of the percentual height decrease over the number of test cycles for all vertebrae, while the more transparent fluctuating curves represents the dynamic height decrease during the tests.

Again, satisfying height restorations for all three sites in the vertebrae were observed. The anterior height was restored by nearly 28% which proved the capability of the implant once more. However, as the vertebrae in this group were all part of the lumbar spinal region, the size of the implants to the vertebrae were proportionally smaller. Therefore, the anterior height restoration observed in this group was lower compared to the implant group tested under normal loading. Still, the difference in height restoration, compared to the fractured state, was even statically significantly higher ($p<0.05$) for the central and posterior sites between this implant group and the BKP group.

Repeatedly, the results after cyclic loading were less promising. As one can observe in figure 6.17, the anterior height after cyclic loading decreased by 23.2% and the central height by 19.8%. Again, 67.5% of the height decrease observed in figure 6.16 was a result of plastic deformation which was in accordance to the 70.6% found for the implant group in section 6.1.1. The difference in anterior, central and posterior height decrease between the implant groups was assumed to be a result of the difference in stiffnesses between the groups shown in table 6.3 and figure 6.6. In order to confirm the proposition of plastic deformation, a closer look at the distribution between the bone structures and implant after restoration and cyclic loading was taken.

Overview of the results for height restoration (the initial height equals 100%)

	Implant	
	Mean	SD
Fractured height (%)		
Anterior	64.2	3.5
Central	78.0	6.5
Posterior	91.1	3.1
Restored height (%)		
Anterior	92.1	5.1
Central	101.2	7.5
Posterior	97.9	3.2
Cyclic height (%)		
Anterior	68.9	6.9
Central	81.4	8.3
Posterior	86.8	3.4

Table 6.8: An overview of the vertebral heights per test stage for the implant group tested under high loading

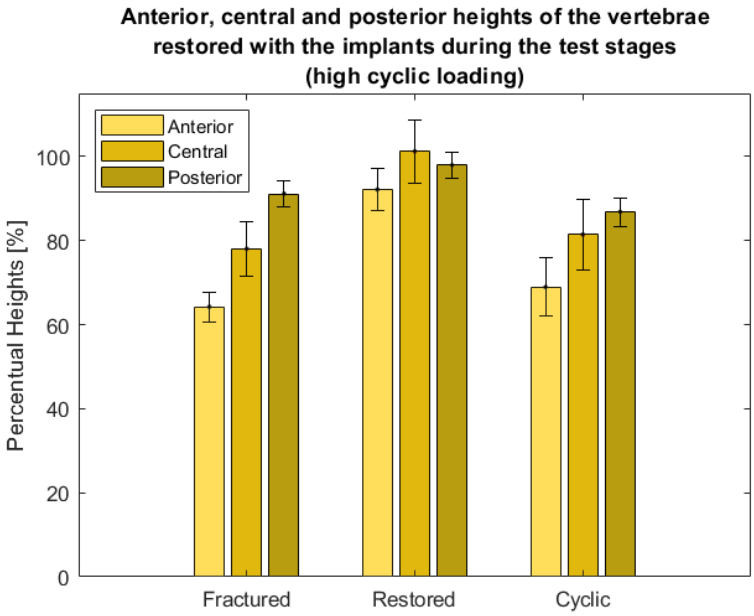

Figure 6.17: An overview of the vertebral heights per test stage for the implant group tested under high loading. Errorbars represent the standard deviation.

From both table 6.9 as figure 6.18 it could be quickly concluded that the trabecular bone structures indeed decreased in height after cyclic loading. The superior bone decreased by 6.2%, whereas the inferior bone decreased by 17.7%. Furthermore, the implant's height decreased by 0.9%. Apparently, the decrease of the implant's height was lower in this group compared to the one in section 6.1, which presumably is caused by the proportional size of the implants once more.

Overview of the material distribution

	Implant	
	Mean	SD
Restored height (%)	98.7	7.7
Bone superior	14.6	
Implant/BKP	51.9	
Bone inferior	32.2	
Cyclic height(%)	74.0	10.0
Bone superior	8.4	
Implant/BKP	51.1	
Bone inferior	14.5	

Table 6.9: Distribution of the height for the implant group tested under high loading

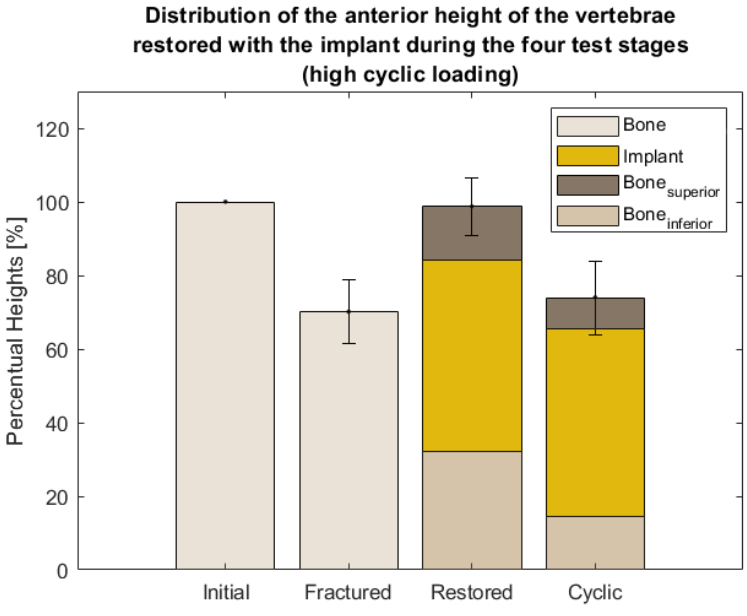

Figure 6.18: Distribution of the vertebral height for the implant group tested under high loading. Errorbars represent the standard deviation.

The outcomes for the increase in rotation and the decrease in height for this test group are shown in figure 6.19 and given in table 6.10.

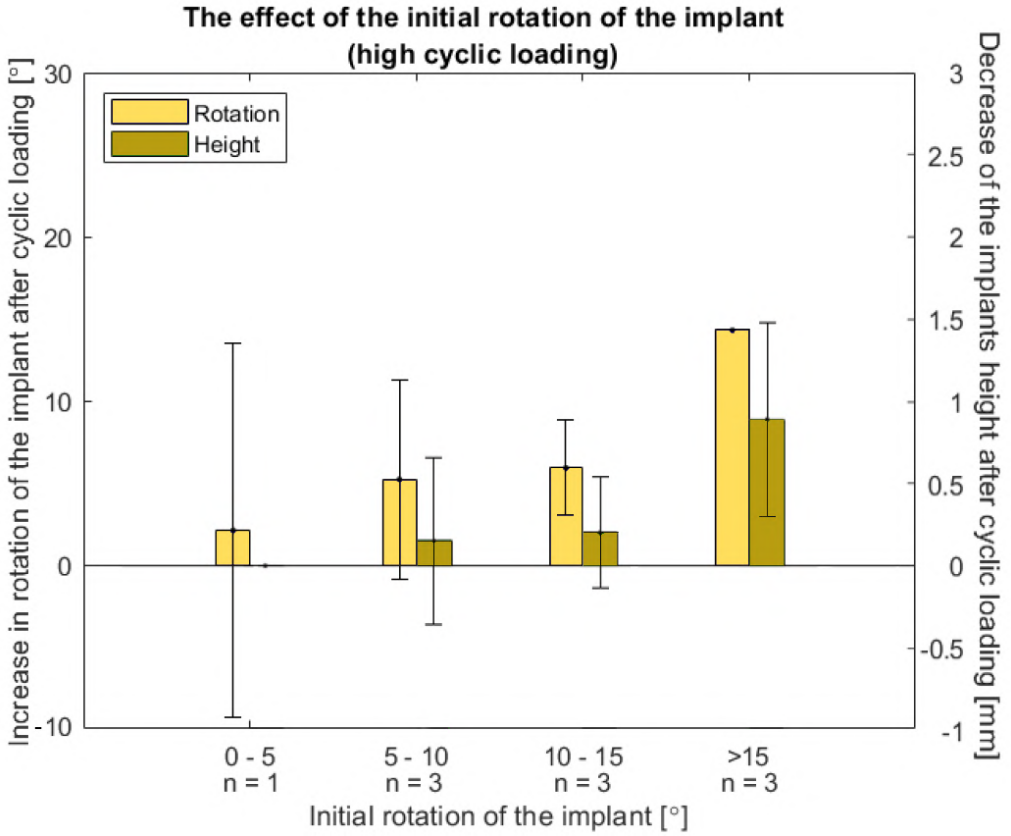

Figure 6.19: A graphical representation of the influence of the initial implant rotation on the rotational increase and height decrease for the implant group tested under high loading. Errorbars represent the standard deviation.

Both figure 6.19 and table 6.10 indicate that a higher initial rotation increases the risk for rotation under loading. It could be concluded once more that the initial rotation is of utmost importance as both the implant's rotation and the height decrease seemed to be affected according to the initial implant's rotation. In this group, a more obvious correlation between the initial implant rotation and the height decrease is visible, as was already suggested in the previous section.

Overview of the results for implant rotation

Initial implant rotation (°)	Increase in implant rotation (°)		Decrease in implant height (mm)	
	Mean	SD	Mean	SD
0 - 5 (n = 1)	2.1	-	0.00	-
5 - 10 (n = 3)	5.2	5.1	0.15	0.51
10 - 15 (n = 3)	5.9	7.2	0.20	0.34
>15 (n = 3)	14.3	6.3	0.89	0.59

Table 6.10: The influence of the initial implant rotation on the rotational increase and height decrease for the implant group tested under high loading. The number of included implants per group is indicated by n.

Can the implant correct the kyphotic angle of the vertebral body?

Finally, the kyphotic angle correction and the influence of the high cyclic loading was evaluated. In table 6.11 the mean kyphotic angle for the implants tested under high loading is given. As one can see, the initial kyphotic angle for the implant group was negative, indicating a lordotic angle. Since this test group consisted of solely lumbar vertebrae, this was no abnormal value.

Overview of the results for the kyphotic angle correction

	Implant	
	Mean	SD
Initial kyphotic angle (°)	-0.4	2.8
Fractured kyphotic angle (°)	12.9	1.0
Restored kyphotic angle (°)	1.0	4.2
Cyclic kyphotic angle (°)	8.3	3.5

Table 6.11: The correction of the kyphotic angle over all test stages for the implant group tested under high loading

The mean correction of the kyphotic angle was 11.9° compared to the fractured data, which again showed a successful correction of the initial kyphotic angle. Then, after the cyclic loading, an increase in the kyphotic angle was observed repeatedly. From table 6.11 it could be concluded that this increase was equal to 7.3°. Thereby, the remaining correction of the kyphotic angle after cyclic loading was only 4.6°. This led to a statistical significant difference ($p<0.05$) between the two implant groups when comparing the outcomes for the initial and cyclic kyphotic angles. Presumably, this could be traced back to the proportional implant size.

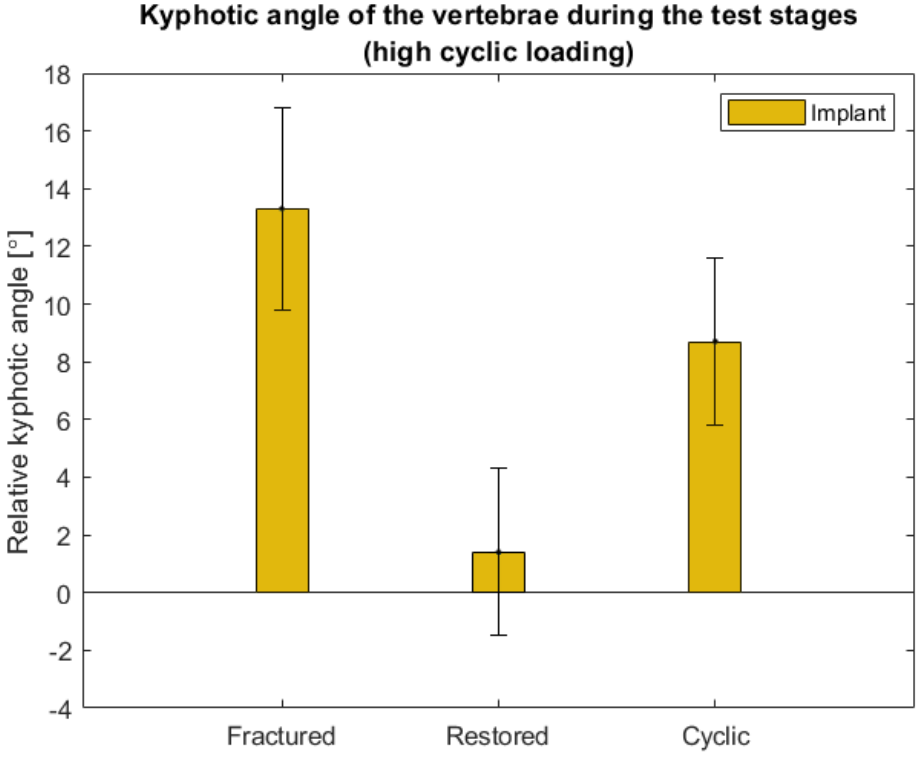

Figure 6.20: The correction of the kyphotic angle over all test stages for the implant group tested under high loading. Errorbars represent the standard deviation.

Chapter 7

Discussion

In this thesis the feasibility for a newly developed vertebral implant for vertebral compression fractures has been investigated. As former studies have shown multiple risks for complications regarding PMMA injection, the implant procedure was evaluated without the use of PMMA augmentation. The established Balloon Kyphoplasty procedure (BKP) was used as a comparative to verify the outcomes. As this pre-clinical study was conducted with human cadaveric specimens, spinal deformities were supposed to be the most important outcome parameter to address. The outcomes on spinal deformities were subdivided into the anterior height restoration and the kyphotic angle correction. The most important outcomes are discussed below, followed by some general comments on the test observations.

It was hypothesized that a distinction in outcomes would be detectable between the two implant test groups as different loading conditions were applied, i.e. 100N-600N at 0.5Hz and 100N-1000N at 1Hz. However, unexpected drawbacks for the implant procedure were observed, which are discussed below. Consequently, no noticeable distinctions between both implant groups could be made. Therefore, the outcomes for both groups were combined and collectively used in the evaluation on the spinal deformities, unless differences between groups were noteworthy.

7.1 Anterior Height Restoration

A variance in the outcomes for fracture generation was seen between the implant group tested under normal loading and the other two test groups. Presumably, the geometry of the vertebrae, the initial stiffnesses and the size of the test groups resulted in this variation. For the BKP group and the implant group tested under high loading, an exact anterior height reduction of 40% was not reached. Although the fracture load was maintained for 15 minutes after fracture generation, some reexpansion due to viscoelasticity was detected. In Krüger et al. (2015), a similar fracture protocol was used and identical outcomes were presented. The effect of the maintenance of the fracture load was demonstrated by the outcomes shown by Krüger et al. (2013) and Rotter et al. (2013), as their fractured anterior heights approximately decreased only 20% compared to the initial heights.

Promising height restorations on the anterior, central and posterior site of the vertebral bodies were evaluated after implant insertion and expansion. For the implant group tested under normal loading, the initial heights were all satisfactory restored. The outcomes for the implants tested under high loading confirmed the capability of the implant to restore the vertebral heights after experiencing a VCF. Nevertheless, this group showed slightly lower restoration percentages. The size of the included vertebrae for each of the test groups was determined to be the cause for this variation. As the vertebrae of the implant group tested under normal loading were smaller, proportionally the implants could restore more of their heights and thereby led to even higher restoration percentages. By comparing the mean restored outcomes for the implant groups to the vertebrae restored with the BKP procedure, the superiority of the implants was once more confirmed. On average the implant groups resulted in 33.1% anterior, 27.7% central and 13.8% posterior height restoration. In contrast, the BKP procedure demonstrated 20.8%, 14.7% and 6.4% height restoration respectively. In conclusion, the implant accomplished an additional restoration of 12.3%, 13.0% and 7.4% for the anterior, central and posterior heights of the fractured vertebral bodies. Thereby statistical significant differences

($p<0.05$) were observed for the central and posterior height restoration between the implant groups and the BKP group. Furthermore, the anterior height restoration in the implant group tested under normal loading was significantly higher than the restoration shown in the BKP group. The inferiority of the BKP was primarily a result of the height loss after balloon deflation that was discussed in various former studies.

The percentual height restoration between the fractured and restored test stage observed for both procedures in this report exceeded the outcomes that were found in Krüger et al. (2013), Rotter et al. (2010) and Rotter el al. (2015). Partially, the outcomes in this study were higher as the loading experienced in prone position was not applied. Although, the restored height for the BKP evaluated in this report and observed by Krüger et al. (2013) did match. In the former studies, they concluded that the VBS procedure and the SpineJack procedure could slightly outperform the BKP procedure. Looking back at the restoration outcomes observed for the implant in this report, it could be suggested that this implant could even outperform those procedures regarding height restoration.

Nonetheless, a severe decrease of the restored height was seen after cyclic loading in the implant groups compared to the BKP group. For the BKP group only minor height losses were evaluated, corresponding to the outcomes of Krüger et al. (2013). Notably, this study was the only study with a corresponding study design to report the heights after cyclic loading. For both implant groups much plastic deformation was observed after cyclic loading leading to severe height decreases. The anterior, central and posterior height decrease observed between vertebral restoration and cyclic loading were significantly higher for both implant groups ($p<0.05$). Although, it should be noted that the implant group tested under high loading showed slightly better results. Presumably, these were a result of the initial stiffness of this test group.

When solely comparing the fractured and cyclic heights, the restoration for the BKP procedure outperformed the implant group by 12.3% anteriorly, 13.0% centrally and 7.4% posteriorly. As these outcomes already showed their inferiority to the second generation BKP procedure, a comparison with third generation procedures was expected to be redundant. Thereby it was concluded that the implants could not adequately restore any of the vertebral heights. While it was hypothesized that the anterior height restoration was the most important parameter to address, all vertebral sites showed severe height decreases. Therefore, it was decided to report all outcomes. Notwithstanding, the absolute values for the anterior heights after cyclic loading were the lowest. Reasonably, this was a result of the fracture generation on the anterior fourth of the vertebrae. As this would induce spinal deformities to occur, the plastic deformation observed anteriorly was evaluated more thoroughly.

7.1.1 Material Distribution

The reason for the height decrease and the plastic deformation in the implant groups was found by looking at the material distribution of the vertebrae at each test stage. Here it was found that the trabecular bone inferior to the implants severely decreased in height after cyclic loading. Presumably, the trabecular bone directly inferior to the implant was prone to high local stresses as a result of a minimal contact area. The outcomes for the BKP procedure, which distributed the vertebral loads on a bigger surface area, has confirmed this suggestion as only minor decreases were observed for that procedure. Furthermore, Krüger et al. (2013) already concluded that the trabecular bone in osteoporotic patients is the least stable part of the vertebral body. Thus, this component would sooner fail under compressive loads in comparison to cement and implants. Besides, they concluded that for the SpineJack procedure the more cement inserted, the bigger the surface area and thus the smaller pressure per surface area on the trabecular bone (Krüger, 2013). Therefore, a bigger surface area would result in better height maintenance after loading. This contributed to the assumption that the minimal surface area of the implants resulted in high local stresses and thereby induced the plastic deformation of the inferior trabecular bone and the subsidence of the implant. In the trabecular bone superior to the implant height decreases were observed likewise, although these were less severe. For the implant group tested under normal loading only 2.0% decrease was evaluated while 6.3% was observed for the implant group tested under normal loading. Supposedly, the size of the vertebrae in the latter group resulted in more distance between the implant and the superior vertebral endplate. Thereby, the chance for plastic deformation to occur was enhanced.

7.1.2 Initial Implant Rotation

Furthermore, decreases of 4.9% and 0.8% of the implant's height were evaluated for both implant groups simultaneously. The rotation of the implants in the coronal plane showed to be responsible for this phenomenon. Besides, it was detected that the initial rotation angle of the implant can have serious consequences for the fixation of the implants and the height decrease. Therefore, it was concluded that an initial rotation over 15° must be impeded. Moreover, two of the excluded vertebrae that were deliberated on in Appendix G showed failures when the initial rotation was over 20°. Furthermore, by comparing the outcomes for the implant groups tested under normal and high loading, a lot of deviation was shown for the increase in rotation as well as the decrease in height. A follow-up study with an extended number of vertebrae should be performed to confirm these suggestions regarding initial angle rotation.

As the implants did not have a locking mechanism to ensure their expansion, the implant's height decrease that was observed after cyclic loading could also have been a result of the backward movement of the posterior wedge on the implant's screw. However, from the μCT data it was determined that this phenomenon was not detected.

Moreover, while 14 of the 20 implants that were inserted expanded with symmetrical endplates, for the other six implants a different phenomenon was observed after vertebral restoration. For two of them, the endplates showed nonsymmetric expansion while the frame holding the endplates together remained intact. For the last four implants, this frame was not attached to one of the endplates anymore, leading to loosening and severe rotation of that endplate. In figure 7.1 the three different expansion types can be observed. Besides, for five implants a deformation in one of the endplates was observed. Out of those five endplates, one seemed to be broken while the other four only revealed deformations to a lesser extent. In figure 7.2, both cases are demonstrated. Probably, this was caused during the insertion of the implants as a suitable locking mechanism on the implants was missing as well as the appropriate surgical tools to create an insertion canal.

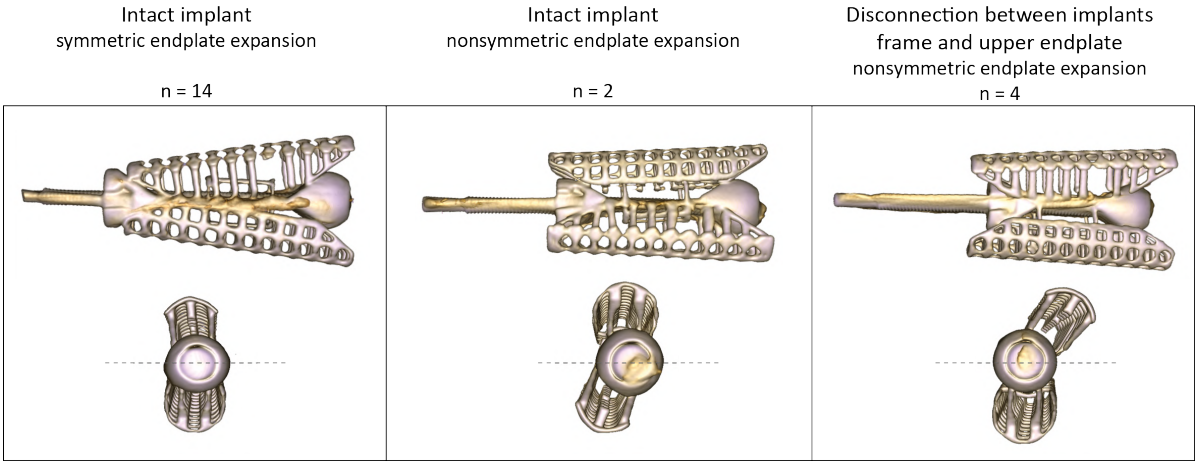

Figure 7.1: The three different expansion types that were observed for the implants during the tests. The number of included implants per type are given as n.

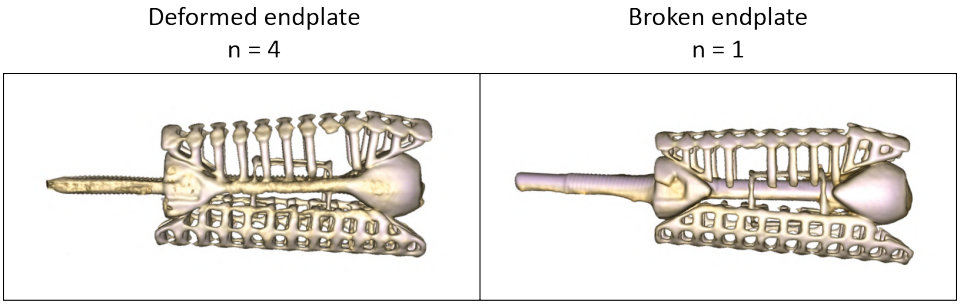

Figure 7.2: The deformed and broken implant endplates. The number of deformed or broken endplates in the included implants are given as n.

7.2 Kyphotic Angle Correction

Considering the kyphotic angle correction, an identical tendency was observed compared to the outcomes for anterior height restoration. The implant groups were feasible to adequately correct the fractured kyphotic angles. The observed difference between the initial and corrected angles were 0.5° and 1.4° respectively for the vertebrae with implants tested under normal and high loading. Presumably, due to the proportion of the implant size to the vertebrae, the former group showed better results. For the BKP procedure the difference remained 2.4°, while the mean vertebral size was smaller than the latter implant group. In comparison to Krüger et al. (2015) both procedures in this report showed better angle corrections. As other studies did not present the initial kyphotic angles, no comparison could be made with these outcomes.

Nonetheless, as for the height restoration, a decrease of the kyphotic angle correction was observed for the implant groups after cyclic loading, while the BKP procedure showed only little reduction of the angle correction. The decrease in correction for the BKP test group observed in this study was in accordance to the outcomes found by Disch et al. (2014). Repeatedly, this was the only study to report kyphotic angle correction after cyclic loading. Unmistakably, the decrease for the correction in the implant groups was a result of the subsidence of the implant. Accordingly, it was determined that the implants were unable to correct the kyphotic angles.

7.3 Other Test Observations

Overall, the BKP procedure showed better result after cyclic loading regarding the prevention of spinal deformities. Although, it should be noted that various leakages of the PMMA were observed during the vertebral restoration. As mentioned before in my literature study, PMMA leakage can result in harmful conditions such as pulmonary embolisms or neurological deficits. Besides, an adverse event regarding the stiffness adjustment was observed. The restored stiffnesses were extracted from the first cycle of the cyclic loading test and compared to the initial stiffnesses observed during fracture generation. Out of that comparison, is was concluded that the mean restored stiffness for the BKP group only deviated 29N/mm from the mean initial stiffness. This was in accordance with Belkoff et al. (2001), that found no statistical significant difference between the two stiffnesses likewise. Thereby, it could have been concluded that the PMMA did not alter the kinematics. Nonetheless, by having a closer look at the individual vertebrae, the data showed differences in stiffness ranging between -364N/mm and +223N/mm. This showed the variability and unreliability of the BKP procedure once more. Moreover, the altered vertebral stiffness can easily induce adjacent fractures to occur.

Regarding the test execution, no technical complications were observed during the fracture generation or cyclic loading with 10.000 cycles (100N-600N at 0.5Hz and 100N-1000N at 1Hz). However, during the vertebral restoration multiple difficulties were observed and were tried to be overcome. The seven excluded vertebrae, that were deliberated on in Appendix G, are illustrative for these difficulties. Six vertebrae that underwent restoration with the implants needed to be excluded, mostly due to the lack of appropriate surgical tools and guiding techniques. One vertebrae restored with the BKP procedure was excluded as a result of the researchers inexperience and the lack of visual guidance.

As was concluded before, the initial rotation of the implant was important for the implant's performance. However, it was impossible to change the rotation of the implant after the transpedicular insertion. Furthermore, craniocaudal repositioning was impeded after implant insertion, as well as the anterior-posterior repositioning after expansion. Normally, good pre-operative planning and fluoroscopic guidance are crucial for satisfactory fracture repair and could resolve the difficulties described above. However, as no visual guidance nor feedback by the surgical tools was provided, a variety of failures were evaluated.

Lastly, some remarks on the tests groups must be given. Firstly, the groups were considerably small whereby conclusions were hard to be drawn and correlations hard to be detected. Besides, as the ages for specimen two and three were unknown and as the μCT data could not elucidate some aspects on the bone quality, no clarification was given on the included vertebral properties. Thereby, it could not be ensured that all tested specimens would be classified as osteoporotic. While most of the human bodies were donated by elderly whose bone quality has probably decreased, outliers could have been present.

Chapter 8

Conclusions

In this report the pre-clinical evaluation of the biomechanical properties for a newly developed 3D-printed titanium porous vertebral body implant for osteoporotic vertebral compression fractures (VCF) was conducted. According to the potential complications of an osteoporotic VCF and the outcomes of my literature study, the prevention of spinal deformities was seen as the most important outcome parameter to determine the feasibility of the implants in a pre-clinical test setting. The appraisal of the spinal deformities was subdivided into the vertebral height restoration, specifically at the anterior site, and the kyphotic angle correction. These outcome parameters were tested after vertebral restoration as well as after cyclic loading that mimicked physiological loading conditions.

In total three test groups were evaluated; the implant group that was tested under normal loading, i.e. ranging between 100N and 600N, the BKP group that was tested under normal loading conditions which served as a comparative procedure and the implant group that was tested under high loading, i.e. ranging between 100N and 1000N. For both implant groups, excellent anterior height restoration and kyphotic angle correction were observed after vertebral restoration, which exceeded the outcomes of the BKP procedure. Nevertheless, after cyclic loading severe decreases for those outcome parameters were detected for the implant groups, while the BKP showed more favourable results with only minor decreases. After a thorough evaluation of the μCT scans, it was concluded that the bone inferior to the implants was most responsible for these decreases. Presumably, the minimal contact area between the implants and the surrounding bone resulted in high local stresses that could not be distributed by the trabecular bone without experiencing plastic deformation, inducing the subsidence of the implants. Moreover, the initial rotation of the implants contributed considerably to their performances.

Ultimately, it was concluded that the implant could not compete with the current surgical repair procedures for an osteoporotic VCF as it was unable to sufficiently prevent spinal deformities to occur. Not only did the tests reveal a handful of drawbacks for the implants themselves, the importance of the surgical tools was stressed simultaneously. Additionally to the outcomes discussed above, the failures deliberated on in Appendix G gave rise to the most important issues that should be tackled. In the next chapter, Recommendations, some suggestions for the implants and the surgical tools are contemplated. Besides, some improvements regarding the study design for future studies are given.

Chapter 9

Recommendations

In the last chapter of this study, recommendations for the future development of the implant and the surgical tools are given, as well as some remarks on and recommendations for the study design for future studies.

9.1 Implant Improvements

As was concluded in the previous chapters, the plastic deformation in the trabecular bone inferior to the implants was seemingly a result of the minimal surface area between the two materials, which on its turn led to high local stresses and the subsidence of the implants. The observed plastic deformation resulted in an insufficient restoration of the anterior height and an unsatisfactory correction of the kyphotic angle. Thus, some adjustments to the implant's design should be made to improve its performance. In this section, four suggestions are made for the current design which will be discussed consecutively. Thereafter, some additional considerations on the current design will be given.

9.1.1 PMMA insertion

Evidently, the insertion of PMMA would be the most straightforward solution to prevent spinal deformities to occur after vertebral restoration. As the BKP procedure in this study has shown, the PMMA resulted in good fixation of the fractured vertebrae and demonstrated only minor deformations after cyclic loading. This phenomenon has been proved by several other studies. Obviously, there is a reason why all third generation surgical repair procedures still use PMMA insertion. Thus, by the use of PMMA in addition to the current implant, outstanding height restorations could potentially be achieved that would remain after cyclic loading. A visual representation of this suggestion is given in figure 9.1. Nonetheless, PMMA have shown to bring along a handful of severe complications. Therefore, the development of a surgical repair procedure without PMMA insertion would be unique, create added value and provide a unique selling point. Thus, preferably the insertion of PMMA should be inhibited.

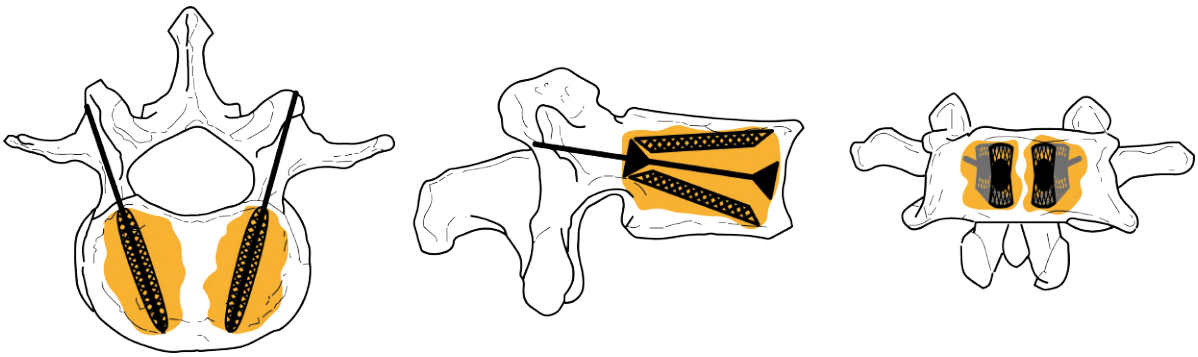

Figure 9.1: Implant suggestion; PMMA Insertion. The vertebra is shown in axial, sagittal and coronal view from left to right.

9.1.2 Endplate-to-endplate fixation

It was proved that the trabecular bone was incapable of distributing spinal loads without deforming. However, the compressive strength of the cortical shell is much higher, especially when comparing to osteoporotic trabecular bone (Keaveny & Hayes, 1993). Thereby, a new solution to prevent spinal deformities arose. In this solution, the implant would reach endplate-to-endplate fixation, since the endplates purely consist of cortical bone. As a result, most of the spinal loads would be distributed from the superior endplate, along the implant, towards the inferior endplate. Consequently, the trabecular bone would not be exposed to high compressive loads and little to no plastic deformation would be expected for the total vertebral body. For this suggestion, the implant would need to open with parallel endplates unlike the angular opening in the current design. In figure 9.2 this suggestion can be evaluated. Nevertheless, the unloading of the trabecular bone could result in stress shielding. Besides, the shift in load distribution could potentially impair the normal load distribution along the cortical shell and could thereby generate higher local stresses on specific points in the intervertebral disc. Since severe adjustments to the biomechanical behaviour of the vertebral body and the adjacent structures are not desired, other solutions should be evaluated.

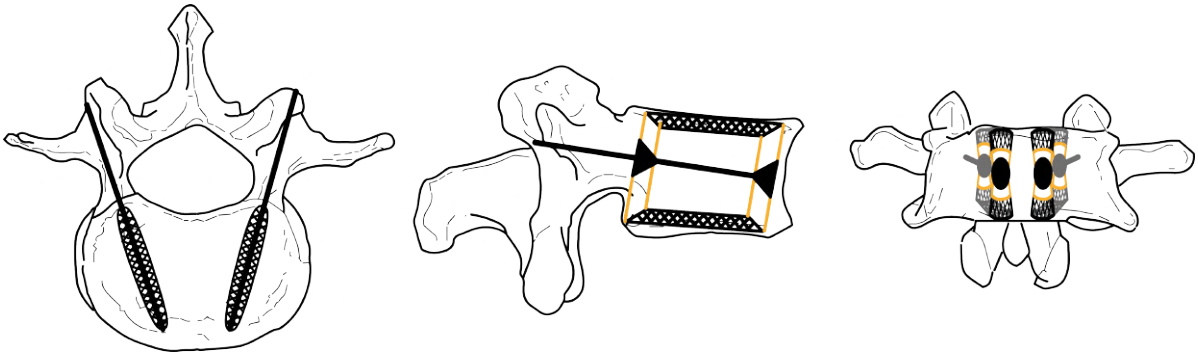

Figure 9.2: Implant suggestion; Endplate-to-Endplate Fixation. The vertebra is shown in axial, sagittal and coronal view from left to right.

9.1.3 Increased implant surface

A third suggestion focused on the surface area of the implants. In the current design, the implant's endplates only have small surface areas. Thereby, the stress concentration on the surrounding trabecular bone exceeds its compressive strength. An increased contact area would better distribute the stresses in the trabecular bone. In order to achieve that, the implant's endplates would need more support in medial-lateral and anterior-posterior directions. In figure 9.3 a suggestion for the new implant's geometry is shown. As one can evaluate, the endplates now have an elliptical shape. Thereby, most of the space is utilized while the interference of the two implants is prevented. This design would allow a surface area for the implant's endplates that is approximately 3-4 times the current size of the endplates.

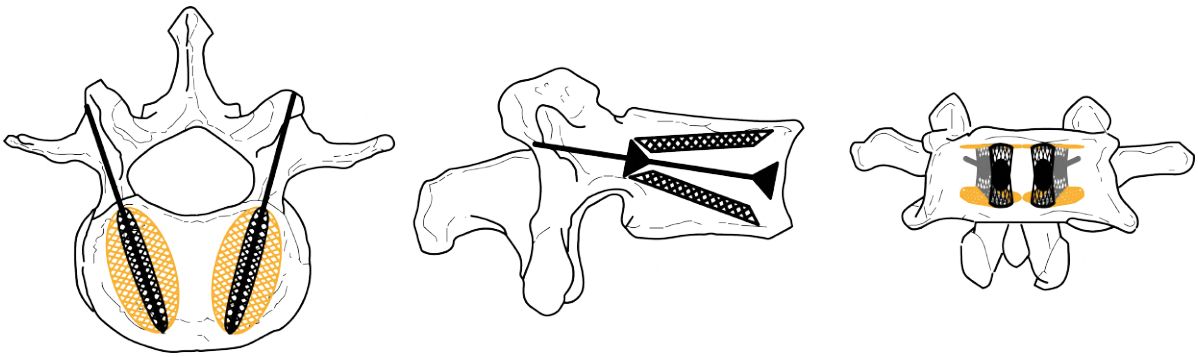

Figure 9.3: Implant suggestion; Increased Implant Surface. The vertebra is shown in axial, sagittal and coronal view from left to right.

9.1.4 Pedicle fixation

As the previous suggestion would bring along severe changes to the implant's design, a fourth and last suggestion is elaborated on here. The external fixation of other spinal implants have given rise to this solution; pedicle fixation. In this suggestion, the implant's design remains unchanged and solely the fixation of the implant is enhanced. By additional fixation of the implant inside the pedicle, where more cortical bone is present, the implant would not immediately subside in the trabecular bone, but rather distribute the forces in posterior direction. Additionally, the pedicle rods could be connected to adjacent vertebrae in order to unload the fractured vertebral body. Notwithstanding, as there is a high risk for fracturing the pedicles during vertebral restoration, the practicality of this suggestion should be further evaluated. Besides, the torque that would be experienced by the pedicles should be quantified. In figure 9.4 one can evaluate this fourth suggestion.

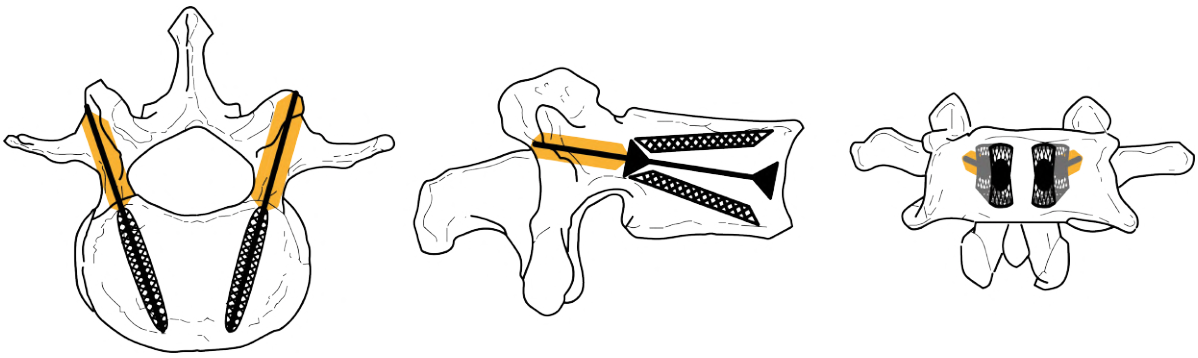

Figure 9.4: Implant suggestion; Pedicle Fixation. The vertebra is shown in axial, sagittal and coronal view from left to right

9.1.5 Additional considerations

In addition to the above stated suggestions, some considerations for the current implant design are given. These considerations result from practical failures or difficulties observed during the tests.

Firstly, a locking mechanism should be added to the design. Currently, the insertion of the implant was complicated as the implants tried to expand when they were inserted transpedicular. Thereby, a considerable amount of force was exerted on the implants in order to push them through the pedicles. Presumably, this caused the endplates to deform in five implants as was mentioned in the discussion. Besides, by creating an appropriate insertion canal, which will be discussed in the coming subsection, the deformation of the endplates could be prevented additionally. Furthermore, a second locking mechanism should be present to secure symmetric expansion of the endplates and the angular expansion of the implants.

Supplementary, during the expansion the implants should all open similarly. In the current design, the implants can open either with parallel endplates or angular, depending on the internal vertebral forces exerted on the implants during expansion. As the implants were mainly developed to restore vertebral wedge fractures with severe anterior height decreases, angular opening would be preferred.

Besides, it was not determined which endplate should be placed in which direction, though the endplates were not symmetrical identical. For the superior-inferior direction as well as the anterior-posterior direction, it should be evaluated if differences between outcomes would be expected. If so, a guideline should be made on how to correctly insert and expand the implants. Besides, this should be clearly, visually marked on the implants to prevent confusion during surgery.

Lastly, the implant sizes should be carefully reevaluated. As mentioned before, two implant sizes have been implemented in this study. However, even the small implants with a 5mm diameter resulted in fractured pedicles after vertebral restoration. Thus, a smaller size would be preferred for vertebrae with small transverse pedicle diameters. The devices of the third generation procedures SpineJack and Osseofix are produced in three diameter sizes; 4.2mm, 5.0mm and 5.8mm and 4.5mm, 5.5mm and 7.0mm respectively. As the 6mm implant in this study showed no necessity for a bigger implant, the sizes of the SpineJack procedure are considered most favourable.

Additionally, the implant lengths should be analyzed. In the current study, the choice for the implant size was made based on two aspects; the transverse pedicle diameter ánd the vertebral depth. The initial length of the bigger sized implant was 34mm, which was observed to be too long for a considerable amount of the vertebral depths. Therefore, the smaller implants were used while these resulted in less implant expansion and thus less height restoration. In consideration of this, it is proposed to reduce the implant lengths. For SpineJack the initial lengths of the devices were 20mm, 25mm and 28mm. As one can see, the length of the biggest SpineJack device was smaller than the length of the smallest implant in this study, i.e. 28.2mm. Moreover, the device of the VBS procedure was produced with the initial lengths of 22mm, 27mm and 31mm. Thereby, it could be concluded that the lengths of the current implants are considerably big and should be adjusted to better fit inside the vertebral bodies.

9.2 Tool Improvements

Not only were difficulties observed for the implants themselves, some were observed for the surgical tools likewise. Definitely, these were largely attributable to the underdevelopment of the current tools as first the feasibility of the implants needed to be proved. Nevertheless, some improvements for the tools are given below. Before further elaborating on them, it should be noted that visual guidance with fluoroscopy, which is frequently used in spinal surgeries, would improve outcomes drastically.

As stated before, during the transpedicular insertion of the implants some difficulties were observed as the implant had no locking mechanism. Besides, no appropriate bone drills were designed for the implants whereby a suitable insertion canal could not be manufactured. Preferably, this canal is created in a step-by-step process. First, a bone introducer and a Yamshidi needle should be inserted transpedicular until the anterior wall is reached. Then the bone introducer and Yamshidi needle should be replaced with a K-wire and a drill with a small diameter should be placed over it. After rotating this drill, a new drill with a bigger diameter should be placed over the K-wire and should increase the size of the canal. The replacement of the drills with larger variants should be done carefully to ensure the direction of the canal and should be performed until the diameter of the implant is reached. By virtue of the fluoroscopy, the three dimensional direction of the canal could be additionally monitored and adjusted if necessary.

Subsequently, the feedback on the surgical tools must be discussed. The current implant inserter barely showed the initial rotation of the implant, which has proved to be important for the implant's performance. Besides, when the implant was inserted inside the pedicle the rotation could not be adjusted. While this problem could be partially resolved by an appropriate insertion canal and a locking mechanism of the implant, having feedback on the rotation of the implant during insertion would not be redundant.

Furthermore, with the current surgical tools no feedback is given on the development of the expansion while screwing. Thereby, the height restoration could only be evaluated visually and the maximum expansion was not consistently reached. Besides, in one vertebrae the implant broke and flipped over during expansion as the screwing was continued after maximum expansion was reached. Furthermore, for four implants the frame holding the endplates of the implant together failed. Probably, the frame and one of the endplates disconnected as a result of screwing after maximum expansion was reached simultaneously. While fluoroscopy would improve the estimation for maximum expansion, a feedback on the tools must be implemented likewise.

9.3 Future Studies

Furthermore, for future studies studies some recommendations could be given. First of all, outcome variations between test groups could be minimized by more evenly distributed test groups, taking into account the different specimens as well as the spinal regions. Besides, an extended amount of test objects would minimize variations. Thereby, observed statistical significant differences in outcomes could be considered more meaningful and conclusions on outcomes would be easier to be drawn.

Regarding the test machine and the test set-up, the stiffness in all directions should be checked and potentially increased. During the performed tests, some deflection of the load cell was observed. As a result, not only pure axial loading might have been applied to the vertebrae but rather a torque and shear forces could have been present simultaneously. Since pure axial loading is preferred in order to mimic physiological spinal loading conditions, for future studies the stiffnesses should be reevaluated. Additionally, the load cell that was used in the current study was a 5kN load cell. While this was necessary for the fracture generation, for the cyclic loading a smaller load cell could have been used so that the accuracy would increase. Lastly, the test machine was displacement driven and thereby a test frequency could not be given as direct input in the test script. For future studies, it would be beneficial if the frequencies could be promptly implemented.

Subsequently, some suggestions could be made to further develop the current study design. By implementing spinal segments in contrast to the isolated vertebrae, physiological spinal conditions would be easier to mimic and the influences of the adjacent vertebrae and vertebral discs could be better observed. Besides, during vertebral restoration a load of 100N could be exerted on the vertebrae, thereby mimicking the loads that are normally applied in surgery when a patient is placed in prone position. This is based on the spinal load in prone position evaluated by Sato et al. (1999) to simulate the compressive forces that act on the vertebrae. In the current study, this was infeasible as a result of the lack of surgical tools. Moreover, during all test stages the vertebrae should be sprayed with a saline solution to prevent vertebral dehydration. The dehydration of the vertebrae could result in higher stiffnesses and more brittleness. Lastly, to better observe the pressure distribution of the vertebrae, pressure mapping sensors could be placed inferior to the vertebrae. As a result, the pressure distribution on the cortical endplate for the initial and restored vertebrae could be evaluated and the effect of the implants regarding this aspect could be observed.

All things considered, it was concluded that improvements for the implant procedure were found for the implant's geometry and the implant's surgical tools. As a result, the drawbacks found in this study could presumably be minimized or impeded. Accordingly, the implant could have a decent chance of succeeding when encountering and competing with the current treatment options for an osteoporotic VCF. Besides, some recommendations were given on the study design to enhance the quality of future study outcomes.

Bibliography

[1] Amber Implants. Future implant technology delivered today, n.d. Retrieved on October 22th 2019 from https://amberimplants.com/.

[2] Benvenue Medical. Media kit., 2019. Retrieved on July 29th 2019 from https://benvenuemedical.com/mediakit/.

[3] U Berlemann, SJ Ferguson, L-P Nolte, and PF Heini. Adjacent vertebral failure after vertebroplasty: a biomechanical investigation. *The Journal of bone and joint surgery. British volume*, 84(5):748–752, 2002.

[4] Dangol Bijendra, Xiaotao Wu, Zanli Jiang, Lei Zhu, Maharjan Promish, and Singh Ratish. Adjacent level vertebral fractures in patients operated with percutaneous vertebroplasty. *Open Journal of Orthopedics*, 8(3):116–126, 2018.

[5] Ann Cranney, Sophie A Jamal, James F Tsang, Robert G Josse, and William D Leslie. Low bone mineral density and fracture burden in postmenopausal women. *Cmaj*, 177(6):575–580, 2007.

[6] Alexander C Disch and Werner Schmoelz. Cement augmentation in a thoracolumbar fracture model: reduction and stability after balloon kyphoplasty versus vertebral body stenting. *Spine*, 39(19):E1147–E1153, 2014.

[7] M Dohm, CM Black, A Dacre, JB Tillman, and G Fueredi. A randomized trial comparing balloon kyphoplasty and vertebroplasty for vertebral compression fractures due to osteoporosis. *American Journal of Neuroradiology*, 35(12):2227–2236, 2014.

[8] Fairview. Vertebral compression fracture, 2018. Retrieved on July 29th 2019 from https://www.fairview.org/patient-education/115884EN.

[9] P Galibert, H Deramond, P Rosat, and D Gars Le. Preliminary note on the treatment of vertebral angioma by percutaneous acrylic vertebroplasty. *Neuro-chirurgie*, 33(2):166–168, 1987.

[10] Hossein Ghofrani, Thomas Nunn, Claire Robertson, Andrew Mahar, Yupo Lee, and Steven Garfin. An evaluation of fracture stabilization comparing kyphoplasty and titanium mesh repair techniques for vertebral compression fractures: is bone cement necessary? *Spine*, 35(16):E768–E773, 2010.

[11] MA Haidekker, R Andresen, and HJ Werner. Relationship between structural parameters, bone mineral density and fracture load in lumbar vertebrae, based on high-resolution computed tomography, quantitative computed tomography and compression tests. *Osteoporosis international*, 9(5):433–440, 1999.

[12] K-R Han, C Kim, J-S Eun, and Y-S Chung. Extrapedicular approach of percutaneous vertebroplasty in the treatment of upper and mid-thoracic vertebral compression fracture. *Acta Radiologica*, 46(3):280–287, 2005.

[13] Ming-Kai Hsieh, Lih-Huei Chen, Wen-Jer Chen, et al. Current concepts of percutaneous balloon kyphoplasty for the treatment of osteoporotic vertebral compression fractures: evidence-based review. *Biomed J*, 36(4):154–161, 2013.

[14] Olof Johnell and JA Kanis. An estimate of the worldwide prevalence and disability associated with osteoporotic fractures. *Osteoporosis international*, 17(12):1726–1733, 2006.

[15] Deborah M Kado, T Duong, KL Stone, Kristine E Ensrud, MC Nevitt, GA Greendale, SR Cummings, Study of Osteoporotic Fractures Research Group, et al. Incident vertebral fractures and mortality in older women: a prospective study. *Osteoporosis international*, 14(7):589–594, 2003.

[16] Tony M Keaveny, Wilson C Hayes, et al. Mechanical properties of cortical and trabecular bone. *Bone*, 7: 285–344, 1993.

[17] Choll Kim, Andrew Mahar, Andrew Perry, Jennifer Massie, Lichun Lu, Brad Currier, and Michael J Yaszemski. Biomechanical evaluation of an injectable radiopaque polypropylene fumarate cement for kyphoplasty in a cadaveric osteoporotic vertebral compression fracture model. *Clinical Spine Surgery*, 20(8):604–609, 2007.

[18] Antonio Krüger, Gamal Baroud, David Noriega, Jens Figiel, Christine Dorschel, Steffen Ruchholtz, and Ludwig Oberkircher. Height restoration and maintenance after treating unstable osteoporotic vertebral compression fractures by cement augmentation is dependent on the cement volume used. *Clinical Biomechanics*, 28(7):725–730, 2013.

[19] Antonio Krüger, Ludwig Oberkircher, Jens Figiel, Felix Floßdorf, Florent Bolzinger, David C Noriega, and Steffen Ruchholtz. Height restoration of osteoporotic vertebral compression fractures using different intravertebral reduction devices: a cadaveric study. *The Spine Journal*, 15(5):1092–1098, 2015.

[20] Le Pape, S. . Vertébroplastie & cimentoplastie., n.d. Retrieved on July 29th 2019 from https://www.lepape-rachis.fr/chirurgies/chirurgie-des-tassements-vert%C3%A9braux/.

[21] Jongseok Lee, Sungwha Lee, Sungok Jang, and Ohk Hyun Ryu. Age-related changes in the prevalence of osteoporosis according to gender and skeletal site: the korea national health and nutrition examination survey 2008-2010. *Endocrinology and Metabolism*, 28(3):180–191, 2013.

[22] F Magerl, M Aebi, SD Gertzbein, J Harms, and S Nazarian. A comprehensive classification of thoracic and lumbar injuries. *European Spine Journal*, 3(4):184–201, 1994.

[23] Medtronic. Bone access tools, n.d. Retrieved on August 29th 2019 from https://www.medtronic.com/us-en/healthcare-professionals/products/spinal-orthopaedic/balloon-kyphoplasty/kyphon-balloon-kyphoplasty/bone-access-tools.html.

[24] L Ombrect. Disorders of the thoracic spine: pathology and treatment. *A system of orthopedic medicine. 3rd ed., Elsevier, Churchill Livingstone*, pages E169–84, 2013.

[25] Kévin Premat, Saskia Vande Perre, Évelyne Cormier, Eimad Shotar, Vincent Degos, Laetitia Morardet, Catherine Fargeot, Frédéric Clarençon, and Jacques Chiras. Vertebral augmentation with the spinejack® in chronic vertebral compression fractures with major kyphosis. *European radiology*, 28(12):4985–4991, 2018.

[26] Robert Rotter, Heiner Martin, Sebastian Fuerderer, Michael Gabl, Christoph Roeder, Paul Heini, and Thomas Mittlmeier. Vertebral body stenting: a new method for vertebral augmentation versus kyphoplasty. *European spine journal*, 19(6):916–923, 2010.

[27] Robert Rotter, Lena Schmitt, Philip Gierer, Klaus-Peter Schmitz, David Noriega, Thomas Mittlmeier, Peter-J Meeder, and Heiner Martin. Minimum cement volume required in vertebral body augmentation—a biomechanical study comparing the permanent spinejack device and balloon kyphoplasty in traumatic fracture. *Clinical Biomechanics*, 30(7):720–725, 2015.

[28] Alex Sabo, Jesse Hatgis, Michelle Granville, and Robert E Jacobson. Multilevel contiguous osteoporotic lumbar compression fractures: The relationship of scoliosis to the development of cascading fractures. *Cureus*, 9(12), 2017.

[29] Katsuhiko Sato, Shinichi Kikuchi, and Takumi Yonezawa. In vivo intradiscal pressure measurement in healthy individuals and in patients with ongoing back problems. *Spine*, 24(23):2468, 1999.

[30] SL Silverman. The clinical consequences of vertebral compression fracture. *Bone*, 13:S27–S31, 1992.

[31] Southern Oregon Neurosurgical & Spine Associates (SONSA). Spine anatomy; regions of the spine, n.d. Retrieved on September 29th 2019 from https://www.sonsa.org/spine-surgery/spine-anatomy/the-regions-of-the-spine/.

[32] Vidyadhar V Upasani, Claire Robertson, Deborah Lee, Tucker Tomlinson, and Andrew T Mahar. Biomechanical comparison of kyphoplasty versus a titanium mesh implant with cement for stabilization of vertebral compression fractures. *Spine*, 35(19):1783–1788, 2010.

[33] DHHS US. Bone health and osteoporosis: a report of the surgeon general. *http://www. surgeongeneral. gov/library/bonehealth/content. html*, 2004.

[34] Daniele Vanni, Renato Galzio, Anna Kazakova, Andrea Pantalone, Giovanni Grillea, Marcello Bartolo, Vincenzo Salini, and Vincenzo Magliani. Third-generation percutaneous vertebral augmentation systems. *Journal of Spine Surgery*, 2(1):13, 2016.

[35] André Luiz Pagotto Vieira, Juliano Rodrigues dos Santos, and Guilherme Galito Henriques. Comparative analysis of two classification systems of thoracolumbar spine fractures. *Coluna/Columna*, 17(1):35–38, 2018.

[36] Dalin Wang, Shengnai Zheng, An Liu, Jie Xu, Xiaotao Du, Yijin Wang, and Liming Wang. The role of minimally invasive vertebral body stent on reduction of the deflation effect after kyphoplasty. *Spine*, 43 (6):E341–E347, 2018.

[37] L Warming, C Hassager, and C Christiansen. Changes in bone mineral density with age in men and women: a longitudinal study. *Osteoporosis International*, 13(2):105–112, 2002.

[38] Hans-Joachim Wilke, Peter Neef, Marco Caimi, Thomas Hoogland, and Lutz E Claes. New in vivo measurements of pressures in the intervertebral disc in daily life. *Spine*, 24(8):755–762, 1999.

[39] Hans-Joachim Wilke, Ulrich Mehnert, Lutz E Claes, Michael M Bierschneider, Hans Jaksche, and Bronek M Boszczyk. Biomechanical evaluation of vertebroplasty and kyphoplasty with polymethyl methacrylate or calcium phosphate cement under cyclic loading. *Spine*, 31(25):2934–2941, 2006.

[40] Derek C Wilson, Ryan J Connolly, Qingan Zhu, Jeff L Emery, Stephen P Kingwell, Scott Kitchel, Peter A Cripton, and David R Wilson. An ex vivo biomechanical comparison of a novel vertebral compression fracture treatment system to kyphoplasty. *Clinical Biomechanics*, 27(4):346–353, 2012.

[41] World Health Organization. WHO scientific group on the assessment of osteoporosis at primary health care level. In *Summary meeting report*, pages 5–7, 2004.

[42] Wyss. The hazards of a misaligned spine, 2013. Retrieved on September 13th 2019 from https://womensvoicesforchange.org/dr-pat-consults-the-hazards-of-a-misaligned-spine.htm.

[43] Y. Yimin, Z. Zhi, R. ZhiWei, M. Wei, and R. K. Jha. Applications of memory alloy stent in vertebral fractures. *Med Sci Monit Basic Res*, 20:76–81, 2014. ISSN 2325-4394. doi: 10.12659/msmbr.890835.

Appendix A

Extended version of the theoretical background

In addition to chapter 2, the theoretical background will be deliberated on more extensive in this appendix. Firstly, the anatomy and physiology of the spine and vertebrae will be described. Thereafter, the pathology of an osteoporotic vertebral compression fracture (VCF) will be discussed. Subsequently, the current surgical procedures will be briefly evaluated.

A.1 Anatomy & Physiology

The human spine is composed of four main regions and the coccyx. Starting superior, these are referred to as the cervical, thoracic, lumbar and sacral region and show a natural S-shaped curve in the sagittal plane. In the left image of figure A.1 all spinal regions are visible. The convex areas that are seen in the thoracic and sacral regions are termed kyphotic, whilst the concave areas in the cervical and lumbar regions are specified as lordotic. The transition from the kyphotic angle to the lordotic angle at the thoracolumbar region is mostly responsible for the high occurrence of a VCF at this particular location. As a result of the transition, the load distribution at this location is more complex and vertebrae are subjected to higher loads (Wilson et al., 2012).

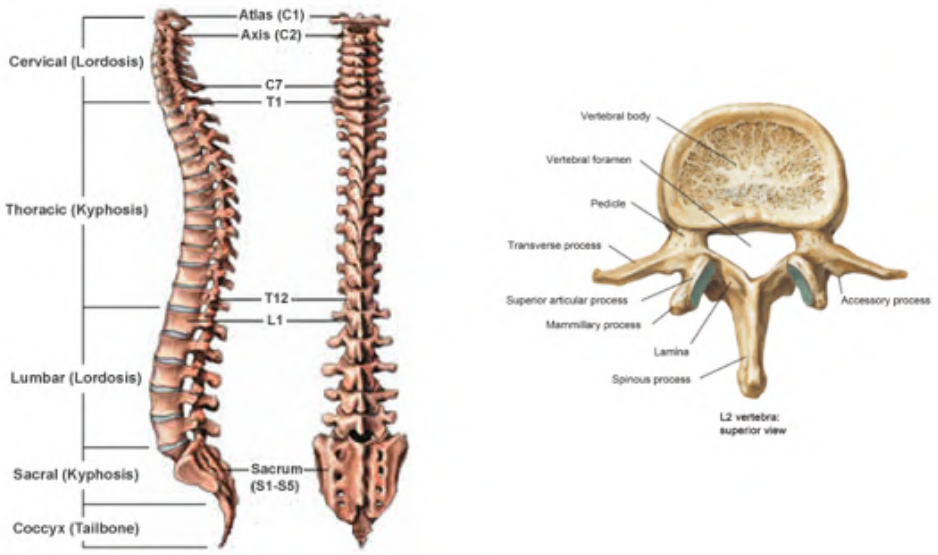

Figure A.1: Anatomical overview of the spinal regions left (Southern Oregon Neurosurgical & Spine Associates (SONSA), n.d.) and the individual vertebra right (Bijendra et al., 2018)

Under normal conditions, the weight of the upper body determines the compressive loads in the spine. These loads are predominantly carried by the vertebral bodies (VBs), which form the anterior part of a vertebra, see the right image of figure A.1. Together, the compressive loads in the spine result in a follower path that minimizes shear forces and bending moments and thereby ensures a safe and stable load distribution.

Basically, a VB consists of three components; the superior and inferior endplates, the cortical shell and the trabecular core. The first two components both have a thickness of less than a millimeter, but have a high compressive strength. However, the most substantial part of the vertebral body contains trabecular bone which is significantly weaker. Not surprisingly, this is the part where most VCFs occur.

A.2 Pathology

Thus, instead of ensuring safe and stable load distribution throughout the spine, osteoporotic vertebrae have a tendency to fracture due to the compressive loads. Stated differently, this implies that osteoporosis induces the trabecular bone of the vertebral bodies to weaken. Predictably, a low, clinically measured bone mineral density (BMD) and microarchitectural deterioration of bone tissue characterize osteoporosis. In order to classify osteoporosis and its severity, the World Health Organization (WHO) has developed standardized T-scores. The threshold for osteoporosis is a T-score of at least -2.5 (World Health Organization, 2004). This T-score represents the decrease of BMD compared to a healthy, young individual in a specific bone. So, a T-score of -2.5 indicates that 25% reduction of BMD has been observed. A T-score ranging between -1.0 and -2.5 indicates osteopenic bone. The relationship between the T-scores and vertebral fracture in the lumbar spine has been investigated by Cranney, Jamal, Tsang, Josse, and Leslie (2007). The results of this study clearly show the coherence, as can be seen in figure A.2.

The occurrence of osteoporosis is closely correlated to age and gender. Former studies have shown that postmenopausal women are, beyond question, the most susceptible group for osteoporotic VCFs (Lee, Lee, Jang, & Ryu, 2013; Warming, Hassager, & Christiansen, 2002).

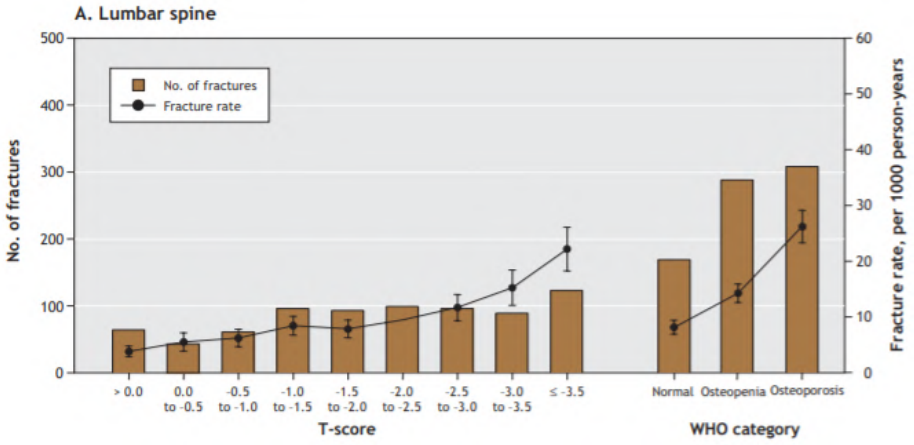

Figure A.2: The relationship between T-scores and number of fractures in the lumbar spine (Cranney et al., 2007)

As stated in chapter 2, an osteoporotic VCF can occur unexpectedly. But how does such a fracture present itself?

Regarding the visual representation, most abundantly the anterior column of the VB is fractured while the posterior wall remains intact. This type of fracture is classified as a type A1.2 fracture, also known as a wedge compression fracture, according to the Magerl AO classification system. To give some more insights in this classification system, it will be briefly discussed below.

The classification system can be subdivided into three main categories; type A, B and C. Axial compression injuries particularly resulting in fractures in the vertebral body are described by type A, injuries with transverse disruptions by type B and injuries resulting from axial torque by type C (Magerl, Aebi, Gertzbein,

Harms, & Nazarian, 1994). In osteoporotic people the bone strength in the vertebrae has decreased substantially. Thereby, the resistance of the bony structures, largely existing of the vertebral body, to compressive forces is minimized and fracture type A is most likely to occur. Besides, type A was found to be the most abundant type among all patient groups, with frequencies ranging from 66.1% to 78.5% found in former studies (Magerl et al., 1994; Viera et al., 2018).

Consecutively, type A encompasses nine categories that are subdivided into three groups based on morphological criteria. The first group, A1, represents impaction fractures to which osteoporotic people are most susceptible. The other categories of type A fractures are the A2 split fractures and the A3 burst fractures. Impaction fractures are characterized by the deformation of the vertebral body due to the compression of trabecular bone (Magerl et al., 1994). Lastly, type A.1 can be subdivided once more. Without a doubt, type A1.2, wedge impaction fractures, occur most abundantly. Compared to all other vertebral fractures classified as type A, wedge fractures occur twice to seven times more (Viera et al., 2018).

A.3 Current Surgical Procedures

Some of the most widely known first, second and third generation surgical procedures for an osteoporotic VCF were summed in chapter 2 section 2.3. Here, a further deliberation on these procedures is presented.

Vertebroplasty (VP) was the first performed surgical procedure for VCFs and was initially described in 1987 (Galibert, Deramond, Rosat, & Le, 1987). This procedure resulted in the stabilization of the vertebral column and pain relief by injecting bone cement into the fractured vertebra. No re-expansion of the vertebral height was achieved with this procedure. The bone cement consisted of polymethyl methacrylate, referred to as PMMA. In the lower thoracic and lumbar spines where most osteoporotic VCFs occur, the PMMA was often injected transpedicular, simultaneous in both pedicles (Han, Kim, Eun, & Chung, 2005). Figure A.3 gives a visual representation of the procedure.

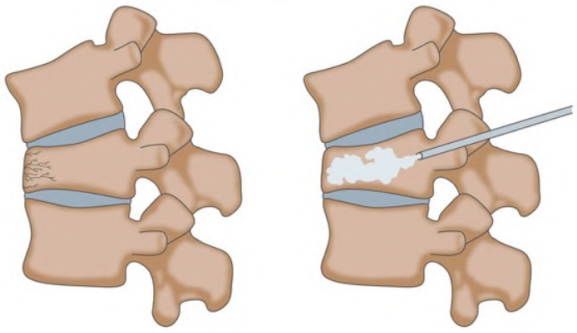

Figure A.3: Vertebroplasty (Cardiovascular and Interventional Radiological Society of Europe (CIRSE), n.d.)

In the second generation procedure, the balloon kyphoplasty (BKP), a first attempt regarding the prevention of spinal deformities was made. In addition to the VP, in this procedure an inflatable balloon is implemented that could create a cavity in the VB. Thereafter, the balloon is deflated and withdrawn and PMMA is injected.

Former studies have concluded that the VP and BKP procedures did not result in optimal outcomes. Regarding the biomechanical outcomes, distinct losses for height restoration and angle correction were evaluated. Firstly, the deflation of the balloon before cement injection mainly bore short-term responsibility for this phenomenon. Moreover, the KAVIAR trial showed an anterior height restoration for BKP of 15.1% at postop and 6.3% at follow-up of 12 months, clearly indicating a long-term loss of height (Dohm et al., 2014). For the kyphotic or lordotic angle, a correction of 21.9% postop and 13.2% at 12 months follow-up was found, also indicating the loss of angle correction over time (Dohm et al., 2014). Thus, the necessity for a procedure that could result in short-term and long-term optimal results arose.

Besides a proper height restoration and angle correction, a main goal of the third generation procedures was to minimize the pitfalls related to the injected PMMA, since this has shown to bring along several risks and complications. Principally, the PMMA altered the local stiffness of the vertebra since the strength of the PMMA is much higher compared to the trabecular bone. This led to an adjustment of the load distribution through the spine, resulting in adjacent VCFs (Berlemann, Ferguson, Nolte,& Heini, 2002). Furthermore, the PMMA disabled bone healing in the vertebral body due to its nonabsorbability and induced the risk of neural or vascular injury due to its exothermic reaction (Kim et al., 2007). Additionally, during the injection of the PMMA a limited quantity often leaked into the disc space. Eventually, this PMMA leakage could result in pulmonary embolism or neurological deficits, which might cause a severe risk to one's health (Upasani, Robertson, Lee, Tomlinson, & Mahar, 2010). The third generation procedures that tried to improve the outcomes of the VP and BKP procedures are described below and presented in figure A.4.

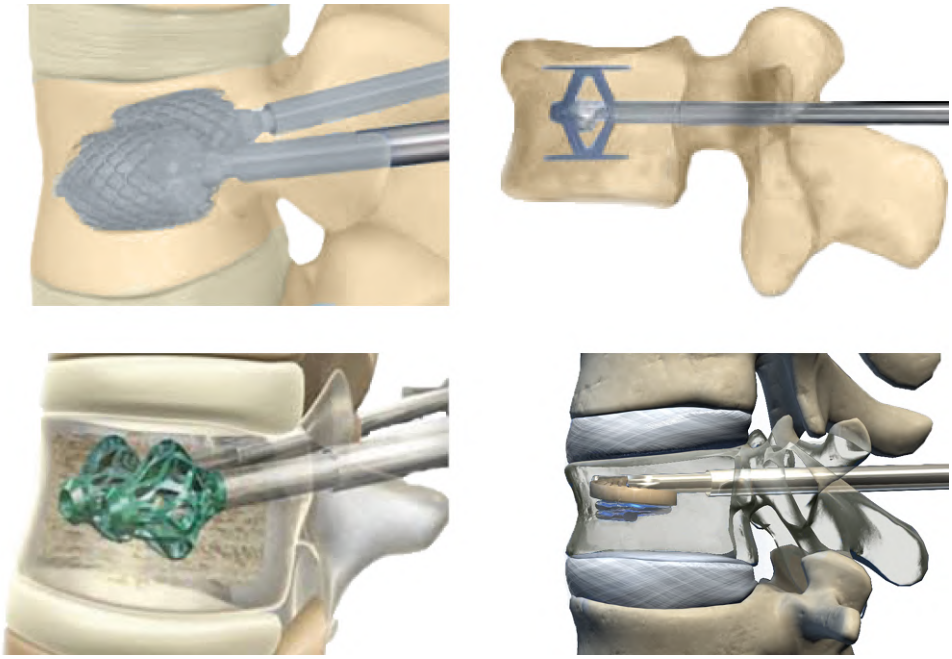

Figure A.4: Four of the most commonly studied third generation surgical procedures for an osteoporotic VCF; VBS (top left (Vanni et al., 2016)), SpineJack (top right (Le Pape, n.d.)), Osseofix (bottom left (Vanni et al., 2016)) and KIVA (bottom right (Benvenue Medical, 2019))

During the procedure of the Vertebral Body Stenting (VBS System) (Synthes, Solothurn, Switzerland), expandable titanium scaffolding structures are first inserted and expanded in the VB whereafter the PMMA is injected. So, in addition to the BKP two stents are present at the outer surface of the balloon and will remain in the VB. Thereby, a collapse of the cavity created by the balloons was tried to be avoided.

The SpineJack® (Vexim SA, Balma, France) procedure encompasses the insertion of two vertebral jacks that expand in craniocaudal direction. As for VBS, the remaining SpineJack implants are composed of a titanium alloy and the center of the implants are filled with PMMA after expansion.

The Osseofix® System (Alphatec Spine Inc., Carlsbad, CA, USA) is another procedure that is based on the insertion of two titanium implants. Unlike the two procedures described above, only a limited amount of PMMA needs to be inserted for these implants. While the central parts of the VBS and SpineJack are completely filled with PMMA, PMMA is only required on the outer surfaces of the Osseofix implants to ensure fixation.

The most unconventional procedure is the KIVA® VCF Treatment System (Benvenue Medical, Santa Clara, SA, USA). Firstly, the procedure only includes the insertion of a single implant. Secondly, the implant is made out of a polymer referred to as polyetheretherketone (PEEK) instead of a titanium alloy. Lastly, the implant is not expandable. Instead, it is a coiled implant that is inserted by a helical wedge-distraction effect. Though, one similarity is present among all described procedures, since KIVA is dependent on the insertion of PMMA simultaneously.

Appendix B

The embedding protocol

In this appendix, the protocol for the specimen preparation is explained. This appendix shows the preparatory steps before the actual testing of the vertebrae could start, which is elaborated on in appendix E. The specimen preparation is explained step-by-step for an individual vertebra.

B.1 Specimen Preparation

- Extract the vertebra from the cadaver torso
- Cut away all soft tissue from the vertebra
- Saw the vertebral arch so that the laminae, spinous process, inferior articular processes can be removed
- Saw through the upper part of the superior articular processes so that the superior endplate of the vertebral body exceeds the height of these processes
- Determine the center of the vertebra with a digital caliper and mark it
- Determine the centre of the mould ring in x- and y-direction and mark them
- Grease the mould bottom plate and the inferior part of the mould ring with Vaseline® (Unilever, London, UK)
- Attach the mould ring and bottom plate with four M3 screws and four M3 butterfly nuts
- Make the epoxy resin (Technovit®, Heraeus Kulzer, Wehrheim, Germany)
  - Fill two plastics cups with epoxy powder (Technovit® 3040 Powder, yellow) until the 12.5ml line is reached
  - Fill one plastic cup with epoxy liquid (Technovi® Universal Liquid) until the 12.5ml line is reached
  - Pore one cup of the epoxy powder in the cup with the epoxy liquid and start stirring thoroughly with a wooden spatula
  - Add the second cup of epoxy powder to the mixture and continue stirring for 40 seconds
  - Let the dough rest for 10-15 seconds
  - Stir for another 20 seconds
- Fill the mould with the epoxy mixture till half of the mould rings height is covered
- Place the isolated vertebra in the mould while aligning the centers of the vertebra and the mould ring
- Wait for 10 minutes before the epoxy resin is hardened
- Unscrew the mould ring from the mould bottom plate
- Carefully remove the ring from the bottom plate with a spatula

- Place the vertebra in the mechanical set-up
- Exert 50N on the mechanical set-up to ensure identical tightness
- Place the mechanical set-up in the μCT in the medium bore size
- Make a μCT scan to obtain the initial geometry of the vertebra

The mould ring and bottom plate are visible in figure B.1. Consecutively, in figure B.2 three epoxy embedded vertebrae are visible.

Figure B.1: The mould ring and bottom plate

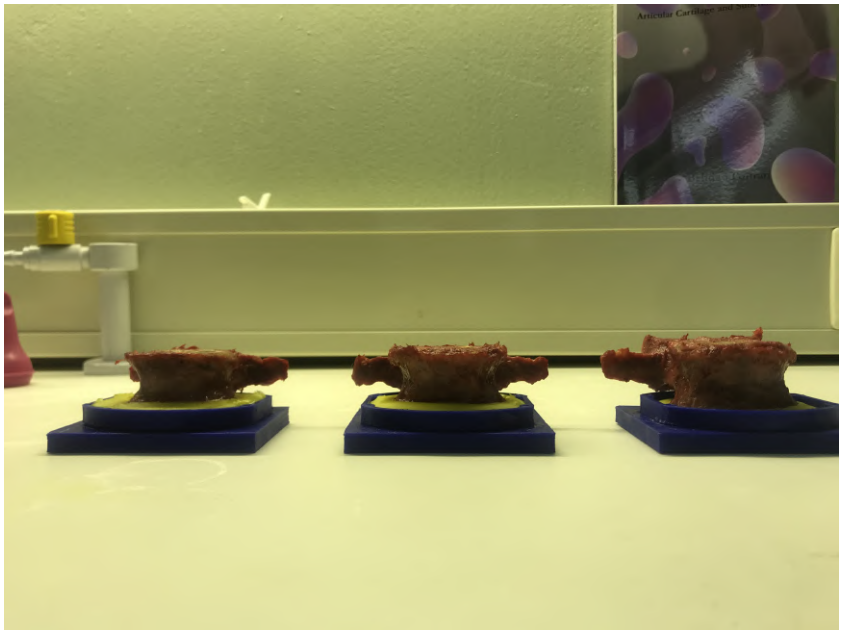

Figure B.2: Three vertebrae embedded in the epoxy resin (left to right: S1L2, S1L3, S1L4)

Appendix C

Technical drawings of the mechanical set-up

As was stated in chapter 5, all parts for the mechanical set-up were specifically designed and manufactured for the biomechanical tests that were performed. In the figures below, one can evaluate all the technical drawings of the individual parts. The parts are sequenced from superior to inferior in the mechanical set-up.

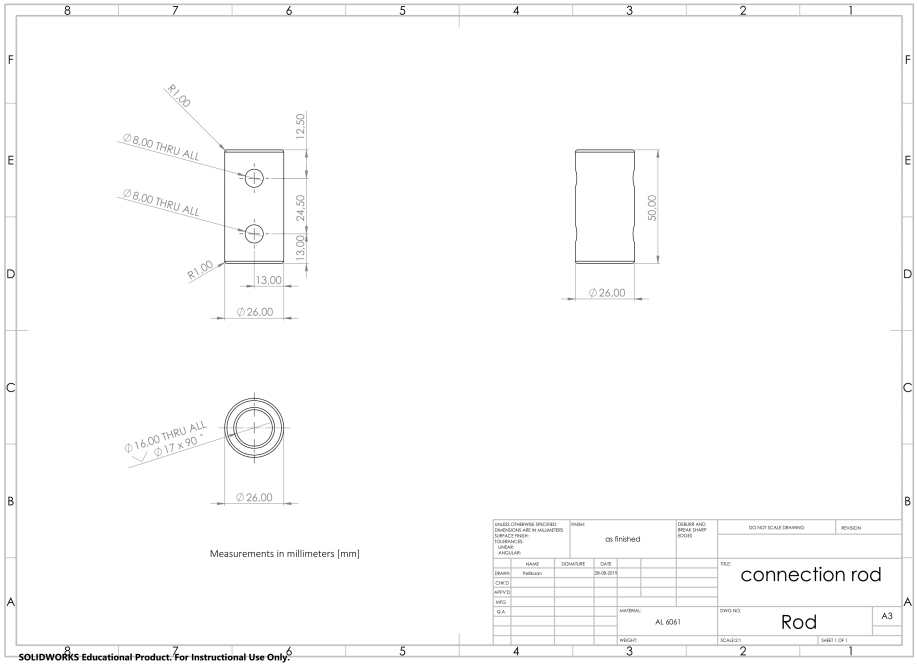

Figure C.1: The rod that connects to the mechanical test machine

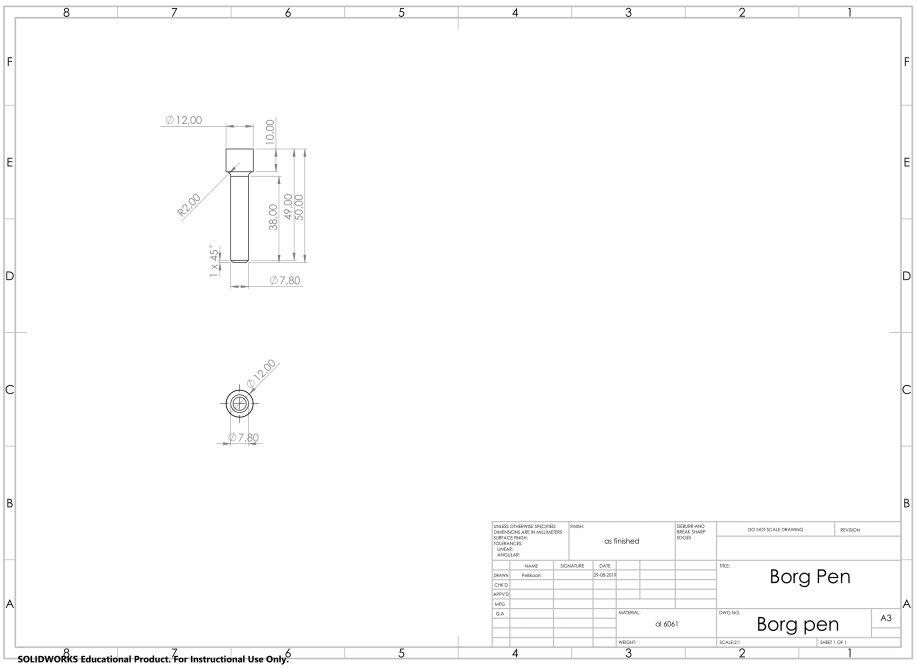

Figure C.2: The rod pin

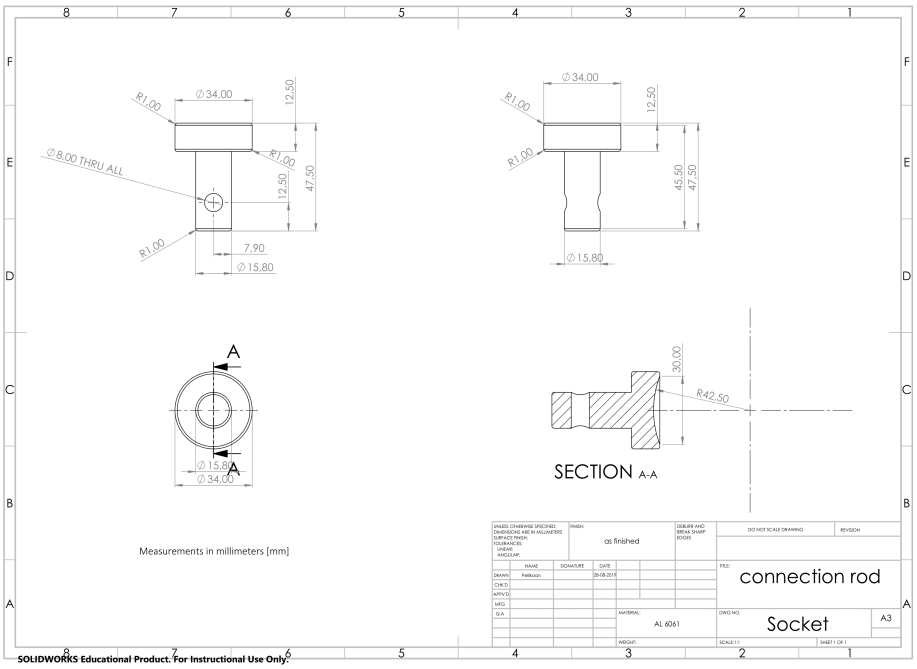

Figure C.3: The rod connector with a socket shaped end

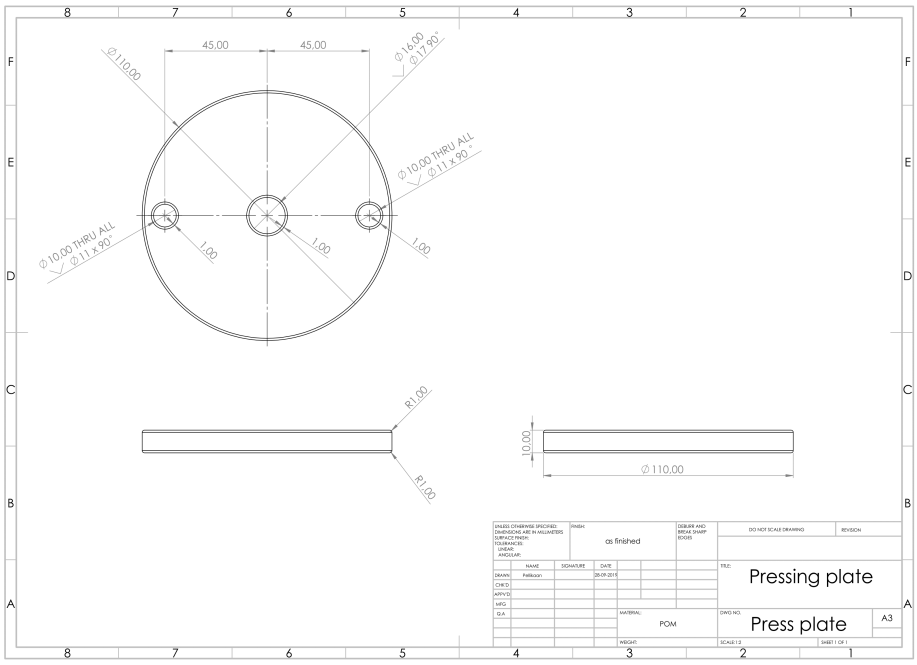

Figure C.4: The superior press plate

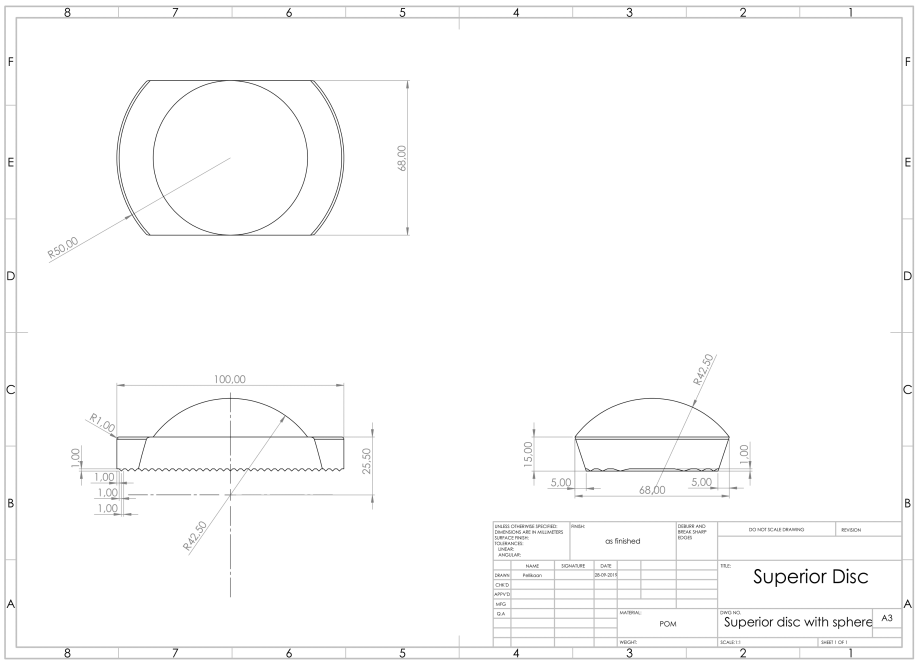

Figure C.5: The ribbed disc with the ball shaped top

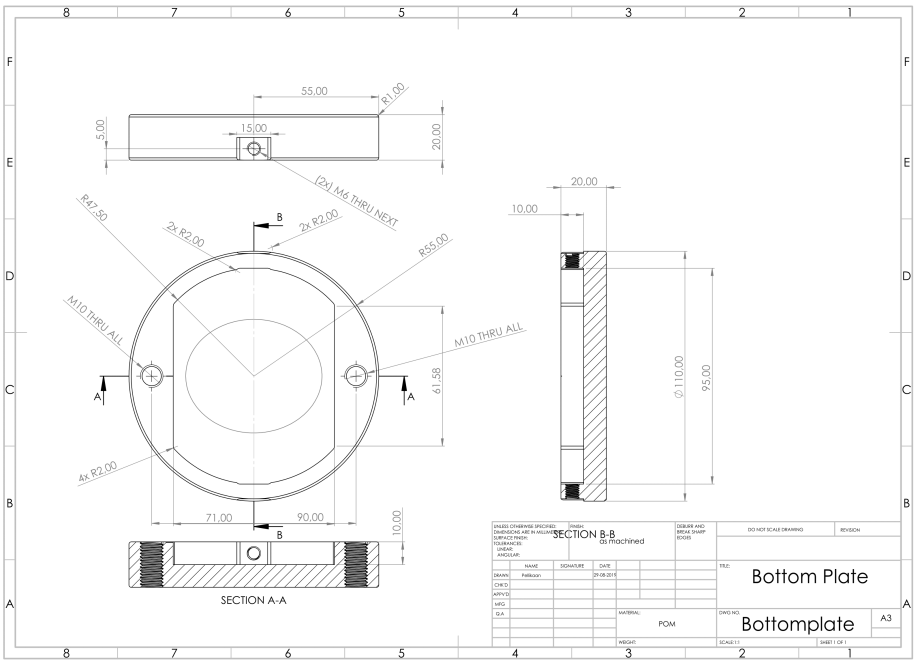

Figure C.6: The bottom disc that enabled variable loading positions

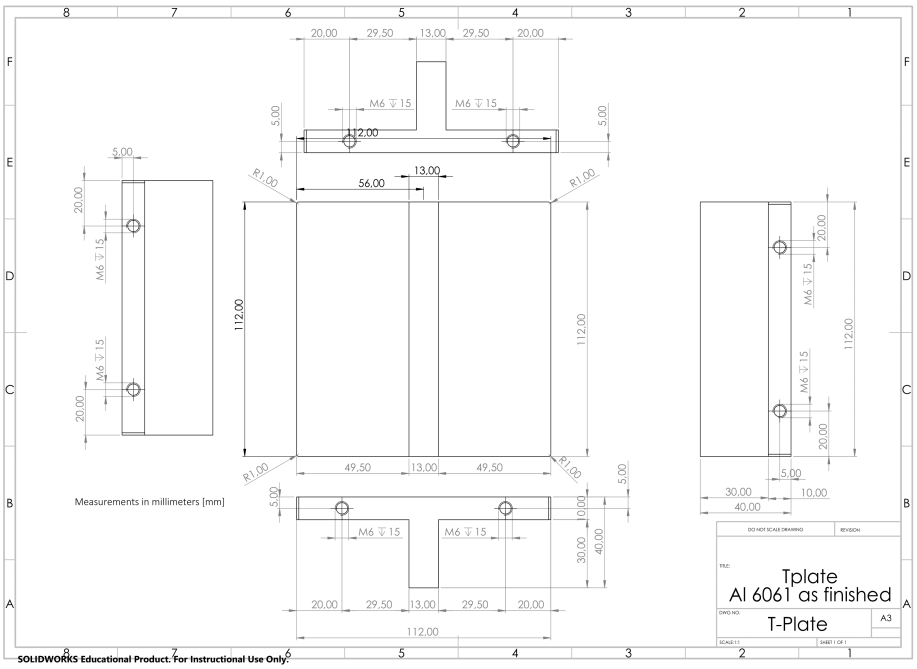

Figure C.7: The T-plate that is clamped by the testing machine on the inferior end

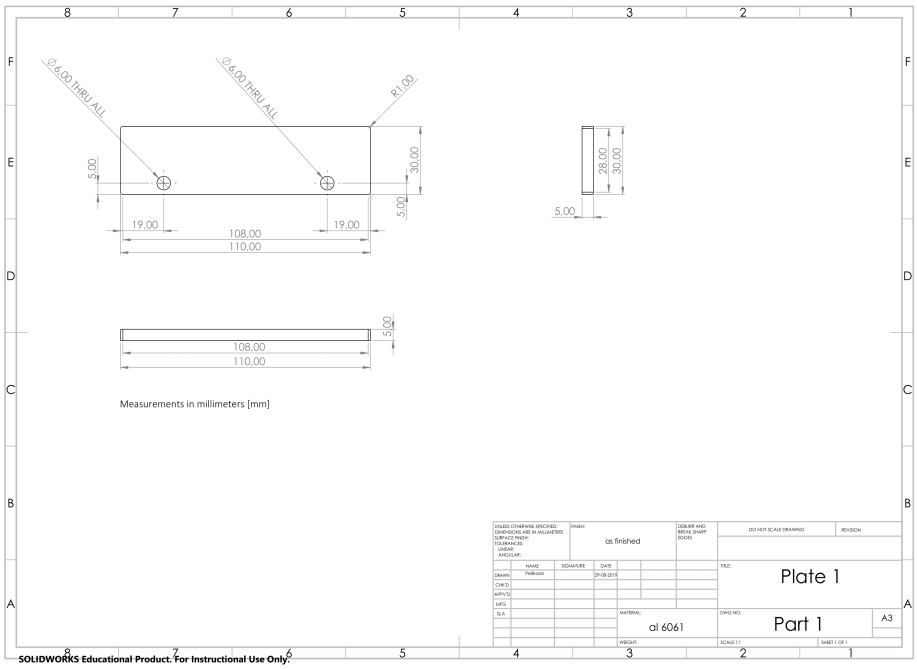

Figure C.8: Supporting plate for the lateral sides of the T-plate

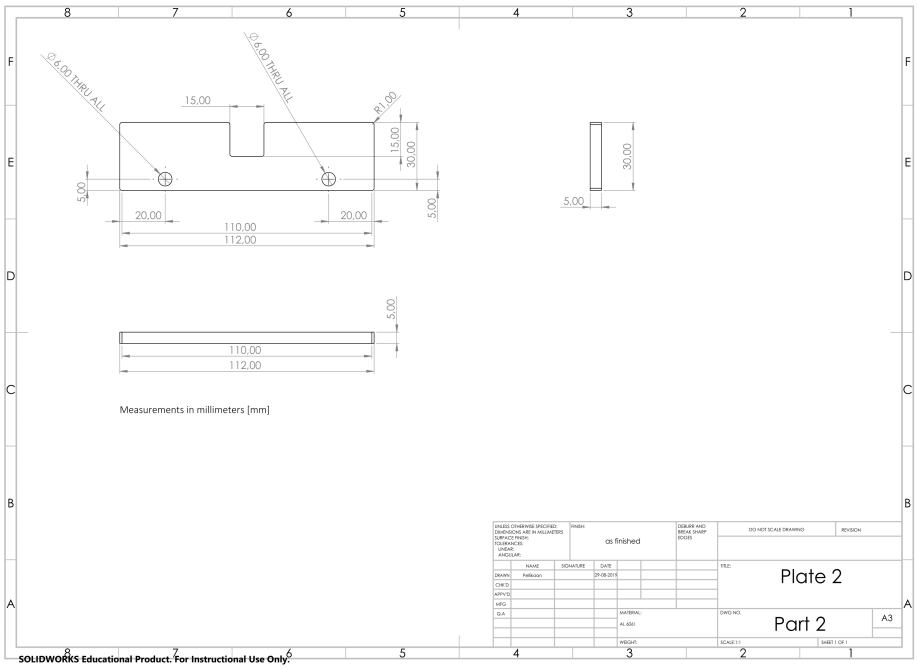

Figure C.9: Supporting plate for the anterior and posterior sides of the T-plate

Appendix D

Overview of study designs

In table D.1 the most important characteristics of the cadaveric studies that were implemented in my literature study are given. The characteristics that are described are the specimen characterization, the fracture generation, the preloading condition, the cyclic loading condition and finally the ultimate loading condition. The study design for the biomechanical tests during this project were mainly based on these findings in combination with supporting literature.

	Specimen Characterization	Fracture Generation	Preloading Condition	Cyclic Loading Condition	Ultimate Loading Condition
VBS					
Disch and Schmoelz (2014)	3-Segmental study on T12-L5	Eccentric loading, 20mm/min untill 50% reduction anteriorly	2.5Nm	3x 1000 cycles ranging from 50-250N, 50-450N and 50-650N at 0.5Hz	-
Rotter et al. (2010)	Isolated VB study on T11-L5	2mm/min until 40% reduction anteriorly at 5Hz	110N	10.000 cycles ranging from 200-2000N at 1 Hz	2mm/min until macroscopic failure
Wang et al. (2018)	Isolated VB study on T12-L5	5mm/min until 50% reduction anteriorly at 10Hz	-	10.000 cycles ranging from 300-3000N at 5Hz	5mm/min until macroscopic failure
Yimin, Zhi, ZhiWei, Wei, and Jha (2014)	3-Segmental study on T9-L5	5mm/min until 1.5cm reduction anteriorly	-	-	-
Spine Jack					
Kruger et al. (2013)	Isolated VB study T10-L3	Eccentric load on the anterior third, 1mm/min until 40% reduction anteriorly	100N	10.000 cycles ranging from 100-600N at 1Hz	-
Kruger et al. (2015)	Isolated VB study, T6-L5	Eccentric load on the anterior fourth, 1mm/min until 40% reduction anteriorly	100N	-	-
Rotter et al. (2015)	Isolated VB study, T11-L3	2mm/min until 40% reduction anteriorly at 5Hz	100N	10.000 cycles ranging from 200-600N at 1Hz	2mm/min until macroscopic failure
Osseofix					
Ghofrani et al. (2010)	Isolated VB study, T4-L5	0.5mm/s until 25% reduction anteriorly at 10Hz	-	Compression untill 25% reduction	-
Upasani et al. (2010)	Isolated VB study, T2-L5	0.5mm/s until 25% reduction anteriorly at 10Hz	-	Compression untill 25% reduction	-
KIVA					
Wilson et al. (2012)	3-Segmental study on T9-L3	Eccentric load on 15cm anterior, 1mm/s until 50% reduction anteriorly	100N	50.000 cycles ranging from 200-500N at 3Hz	-

Table D.1: Overview of the study designs from in vitro studies focused on current third generation procedures

Appendix E

The test protocol for the biomechanical tests

In this appendix, the test protocol for a single vertebra restored with the implant procedure and tested under normal cyclic loading is described stepwise. For clarification purposes, the steps have been subdivided into the three main operations during the tests; fracture generation, implant insertion and cyclic loading.

E.1 Fracture Generation

- Determine the anterior fourth of the vertebra
- Place the vertebra in the mechanical set-up so that the axial load is located on its anterior fourth
- Start the machine with a compressive speed of 2mm/min and let it run until the anterior vertebra height has decreased by 40% with the following script:

  1. Test Parameters:
     (a) Direction: Compression
     (b) Preload: 100N, 2mm/min
     (c) Height: Auto-measure with 3N, 30mm/min
     (d) Break: Not expected
     (e) Auto-Zero: on
     (f) Auto-Return: off
  2. Primary Script:
     (a) SetUpStage [[Height+[10mm]] * 0.4], [2.0mm/min]
     (b) Runstage
     (c) Result "Extension 40% Height Decrease", Extn

- Maintain the end load for 15 minutes
- Place the vertebra in the 3D-printed holder
- Place the holder in the testing machine with only the socket part attached
- Put a compressive load of 50N on the vertebra
- Tighten the screws of the holder so that compressive load drops to 0N
- Transport the vertebra to the μCT
- Make a μCT to obtain the geometry of the vertebra

E.2 Implant Insertion

- Place the vertebra in the 3D-printed holder with the posterior part of the vertebra pointed upwards
- Access the vertebra through both pedicles with two osteo introducers with a trocar and a diamond shaped tip
- Insert the introducer until the anterior wall of the vertebral body is reached
- Take the introducer out of the vertebra
- Insert the bone drill and clear the path
- Extract the bone drill
- Insert both implants as far anterior as feasible
- Rotate the holder so that the superior part of the vertebra points upwards
- Loosen the screws of the 3D-printed holder
- Simultaneously open the implants with a screw driver by twisting it counterclockwise
- Extract the screwing tool when the height is visibly restored or when the maximum height expansion is reached
- Place the holder in the testing machine with only the socket part attached
- Put a compressive load of 50N on the vertebra
- Tighten the screws of the holder so that compressive load drops to 0N
- Transport the vertebra to the μCT
- Make a μCT to obtain the internal structure and the geometry of the vertebra

In figure E.1, the bone access tools that were used are visible.

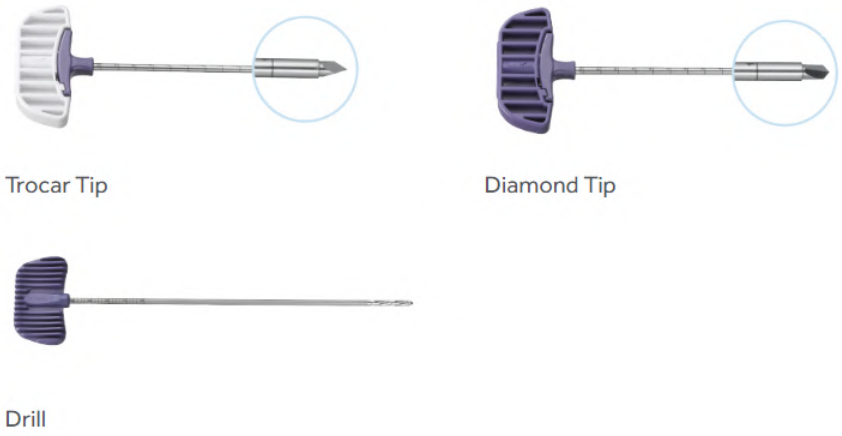

Figure E.1: Bone access tools: two osteo introducers with a trocar and diamond shaped tip and the bone drill (Medtronic, n.d.)

E.3 Cyclic Loading

- Determine the center of the vertebra
- Place the vertebra in the mechanical set-up so that the axial load is located on its center
- Start the machine with cyclic loading of 10.000 cycles at 0.5Hz and a compression oscillates between 100N to 600N with the following script:

  1. Test Parameters:
     (a) Direction: Compression
     (b) Preload: 100N, 2mm/min
     (c) Height: Auto-Measure with 3N, 30mm/min
     (d) Break: Not Expected
     (e) Auto-Zero: On
     (f) Auto-Return: On
  2. Primary Script:
     (a) For i=1 to 10000
     (b) Progress "Cyclic numbers" & i
     (c) Stage [600N], [2.0mm/s]
     (d) if [Extn > [Height * 0.6]] then exit for
     (e) Stage [100N], [2.0mm/s]
     (f) next
     (g) Result "Extn", ExtnAtMax

- Place the vertebra in the 3D-printed holder
- Place the holder in the testing machine with only the socket part attached
- Put a compressive load of 50N on the vertebra
- Tighten the screws of the holder so that compressive load drops to 0N
- Transport the vertebra to the μCT
- Make a μCT to obtain the internal structure and the geometry of the vertebra

The 3D-printed holder that was compressed with 50N after fracture generation, implant insertion and cyclic loading was printed in PLA. The holder encompasses a ball-and-socket joint similar to the mechanical set-up to ensure axial compression. In figure E.2, a visible representation of the holder is given.

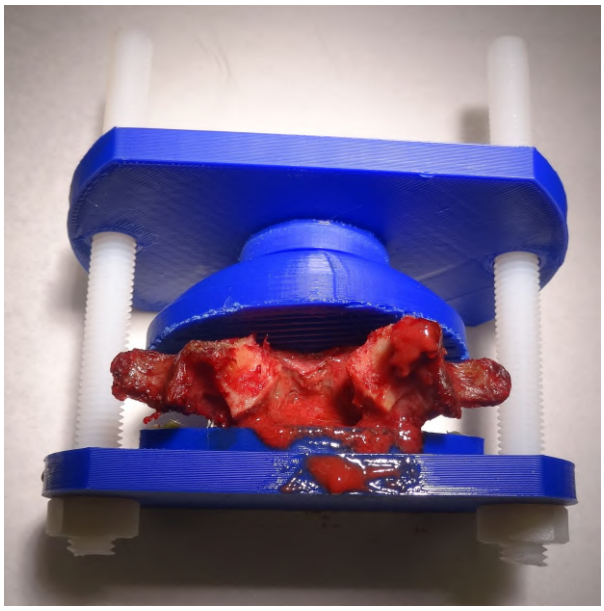

Figure E.2: The 3D-printed holder with the posterior part of the vertebral body pointed upwards

Appendix F

The initial dimensions of all vertebrae

Here the initial dimensions of all vertebrae are given. In table F.1, F.2 and F.3 the dimensions for specimen 1, 2 and 3 are given respectively. The negative kyphotic angles presented in the last column indicate a lordotic angle of that specific vertebra.

Specimen 1 Characteristics

	Height A, C, P (mm)	Width S, C, I (mm)	Depth S, C, I (mm)	Pedicle Heights R, L (mm)	Transverse Pedicle Diameters R, L (mm)	Kyphotic Angle (°)
T8	15.4	30.0	26.1	8.0	3.3	14.0
	15.7	27.1	25.3	7.8	2.8	
	20.1	30.5	26.1			
T9	18.2	30.2	25.9	7.7	4.0	5.9
	17.2	28.4	25.3	9.2	3.7	
	20.7	30.2	27.1			
T10	19.4	33.3	26.5	9.5	4.5	4.3
	17.8	30.6	26.2	8.7	3.8	
	21.3	36.6	27.4			
T11	19.7	34.9	27.8	11.1	6.2	2.4
	18.4	31.8	25.2	11.1	6.0	
	22.1	37.3	27.7			
T12	22.2	36.6	27.7	12.7	9.4	2.8
	19.5	31.4	25.8	12.4	8.9	
	23.5	38.8	26.8			
L1	25.2	37.5	26.8	13.5	6.4	1.8
	20.9	33.2	25.8	13.8	6.6	
	25.3	42.6	28.1			
L2	26.6	41.2	27.4	11.4	6.5	-3.6
	21.3	35.7	25.3	11.3	6.2	
	27.1	48.0	29.4			
L3	27.7	45.3	31.5	11.1	6.5	-2.1
	22.5	37.7	27.3	11.8	6.6	
	26.0	48.1	29.8			
L4	28.0	44.4	30.4	12.2	8.2	-2.3
	23.1	39.7	28.6	12.9	8.4	
	25.5	49.3	29.9			

Table F.1: The initial dimensions of specimen 1

Specimen 2 Characteristics

	Height A, C, P (mm)	Width S, C, I (mm)	Depth S, C, I (mm)	Pedicle Heights R, L (mm)	Transverse Pedicle Diameters R, L (mm)	Kyphotic Angle (°)
L1	28.7 25.6 33.4	52.9 40.4 55.1	40.3 32.5 36.6	18.4 18.6	9.3 9.2	4.5
L2	31.2 23.8 32.0	56.0 40.7 54.4	39.1 34.6 38.4	15.4 15.2	7.9 9.0	-0.7
L3	30.5 24.4 29.0	54.2 55.1 43.8	41.6 37.2 42.5	14.8 13.8	10.8 11.4	-1.5
L4	31.2 23.4 28.1	58.4 45.1 58.5	42.7 35.3 40.4	15.4 14.4	12.9 12.6	-7.2
L5	29.3 19.4 28.1	58.8 49.7 60.5	41.7 35.8 39.8	12.4 12.4	19.2 16.7	-5.4

Table E.2: The initial dimensions of specimen 2

Specimen 3 Characteristics

	Height A, C, P (mm)	Width S, C, I (mm)	Depth S, C, I (mm)	Pedicle Heights R, L (mm)	Transverse Pedicle Diameters R, L (mm)	Kyphotic Angle (°)
T8	14.2	36.6	36.7	10.2	4.2	10.1
	14.5	32.4	33.6	11.4	3.7	
	20.0	37.5	34.0			
T9	22.5	38.5	34.1	12.7	6.7	4.7
	20.9	34.2	33.2	12.4	6.5	
	24.9	42.6	36.0			
T10	24.1	42.0	36.0	16.0	6.6	5.1
	22.1	34.9	34.3	16.1	6.5	
	26.3	42.9	36.7			
T11	25.8	41.5	35.0	17.3	9.6	12.3
	24.6	37.2	32.1	15.7	10.5	
	29.0	42.6	33.9			
T12	18.4	45.8	38.4	18.6	8.8	12.5
	12.3	42.5	34.6	18.5	8.3	
	28.4	47.6	36.3			
L1	30.2	46.9	36.7	16.9	6.0	3.6
	25.5	36.8	35.3	10.8	8.1	
	30.2	50.3	37.7			
L2	30.5	50.5	44.0	12.7	10.9	-0.8
	25.6	43.4	37.6	15.2	10.2	
	30.9	62.3	41.9			
L3	30.2	50.6	38.7	14.8	8.0	-0.5
	26.6	40.8	36.0	13.8	7.2	
	30.3	53.9	40.4			
L4	26.6	63.6	42.6	12.0	14.7	0.8
	22.1	45.9	37.0	15.2	14.0	
	26.9	58.6	39.7			

Table F.3: The initial dimensions of specimen 3

Appendix G

The excluded vertebrae

In this appendix, the excluded vertebrae are discussed. While their results could not be included in the main study outcomes, these vertebrae have shown some remarkable events. Therefore, the vertebrae S1T8, S1T11, S1L2, S2L2, S2L4, S3T12 and S3L4 and their failures are discussed per test stage here. The vertebrae S1T8, S1T11 and S3T12 belonged to the implant group tested under normal loading, while S2L2 belonged to the BKP group and finally the vertebrae S1L2, S2L4 and S3L4 belonged to the implant group tested under high loading.

G.1 Fracture Generation

During the fracture generation no abnormal or remarkable events happened. In figure G.1 the load-displacement curves for the vertebrae can be observed and in table G.1 the results for the stiffness are given.

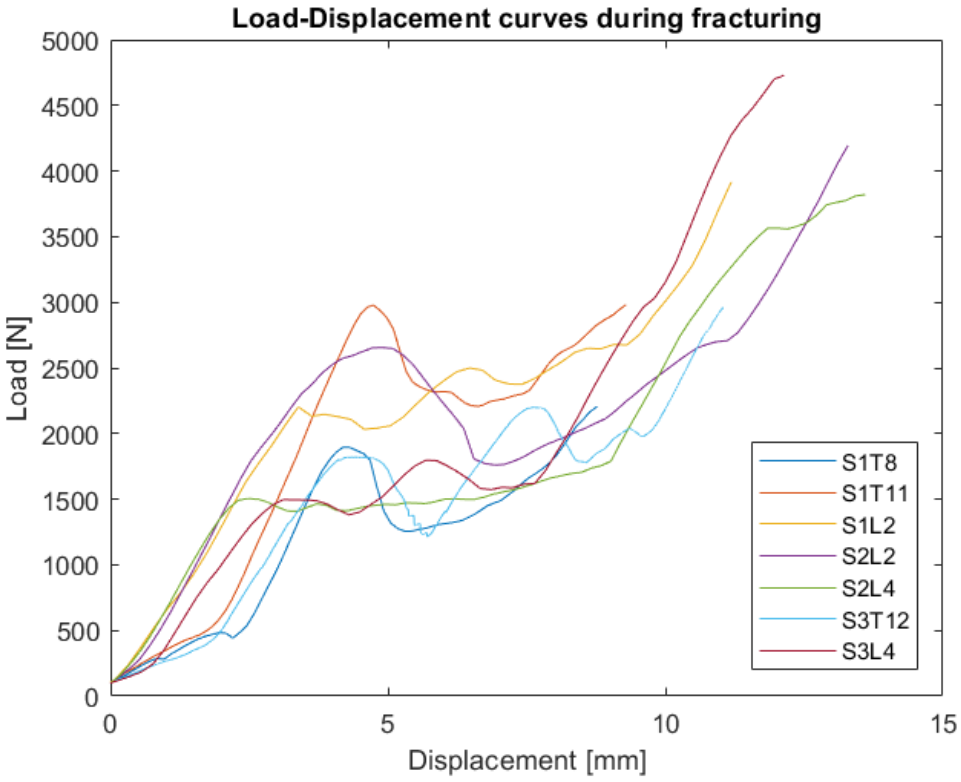

Figure G.1: The load-displacement curves during the fracture generation for the excluded vertebrae

Overview of the stiffnesses observed during fracture generation for the exluded vertebrae	Stiffness (N/mm)
S1T8	734
S1T11	841
S1L2	621
S2L2	541
S2L4	565
S3T12	575
S3L4	532

Table G.1: the stiffnesses observed from the fracture generation for the excluded vertebrae

G.2 Vertebral Restoration

The first failures could be evaluated during this test stage. In S1L2 the bigger implants with a diameter of 6mm were inserted. However, when the implants were expanded, the superior endplate was lifted and partially detached from the rest of the vertebra. This was a failure moderately due to the lack of visual feedback during the restoration. Besides, no feedback on the progress of the expansion was given by the surgical equipment. Lastly, as the implant's length was relatively large for the size of this vertebra, the posterior ends of the implants were fixed in the pedicles. Thereby, the implant's angle could have been further increased anteriorly. As a consequence of these incidents, it was unable to perform any further tests on S1L2. Additionally, no height measurements were performed as the outcomes would have been inequitable. In figure G.2 images after the restoration for S1L2 can be found.

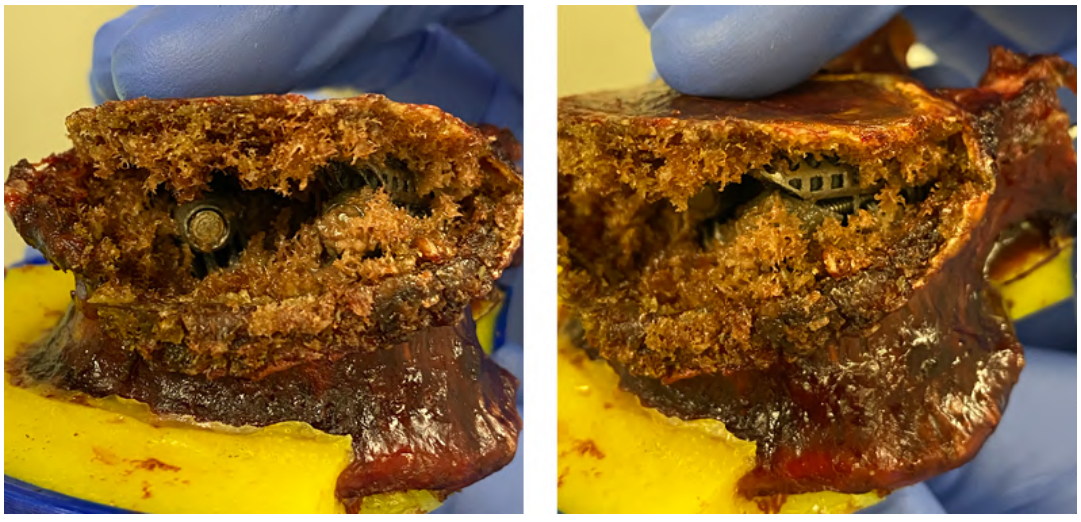

Figure G.2: S1L2 after vertebral restoration

S2L2 was the first vertebrae to perform the BKP procedure on. Presumably, as this exact procedure and its equipment were new for the orthopaedic surgeon, a lack of experience led to the failure of the vertebral restoration. Hardly any height restoration was observed during the restoration. Later, the μCT scans showed that the balloons were not expanded inside the vertebral body. Thereby, the procedure that was applied to this vertebra looked more like a vertebroplasty than a balloon kyphoplasty.

For S3T12 implants without surface treatment were inserted. Presumably, this could create more fixation with the trabecular bone in the vertebral body as their surfaces were coarser. Nonetheless, as a result of the coarse surface, the implants were stuck in the pedicles and could not be pushed through. Moreover, the implants could not be extracted from the pedicles, thus no other implants could be inserted. Thereby, S3T12 needed to be excluded from further testing.

During the restoration of S3L4 a peculiar sound was observed. The μCT showed the cause of this sound; one of the implants was broken during the expansion. In figure G.3 one can detect the broken implant inside the vertebral body. As a result, less height restoration was realised. In table G.2 the anterior height after restoration and cyclic loading are given for S1T8, S1T11, S2L2, S2L4 and S3L4.

Overview of the results for the anterior height restoration (the initial height equals 100%) for the excluded vertebrae

	S1T8	S1T11	S2L2	S2L4	S3L4
Restored anterior height (%)	111.5	97.7	84.4	95.8	90.6
Cyclic anterior height (%)	91.3	91.7	83.4	60.7	72.8

Table G.2: An overview of the restored and cyclic anterior heights for the excluded vertebrae

G.3 Cyclic Loading

Although S2L2 and S3L4 showed an event of failure during the vertebral restoration, they were still tested in the cyclic loading test according to their initial test group protocol. Thus, S2L2 was tested for loads ranging between 100N and 600N at 0.5Hz while S3L4 was tested for loads ranging between 100N and 1000N at 1Hz. From table G.2 it could be concluded that the outcomes between the restored and cyclic stage for S2L2 were in line with the outcomes for the BKP group in chapter 6 as only a minor height reduction was observed after cyclic loading. However, the restored height of 84.4% was lower compared to average for the BKP group. Obviously, this was a result of the failure during balloon expansion.

On the other hand, S3L4 showed less impressive outcomes in comparison to the implant group under high loading. For this vertebrae, a decrease of height of 17.8% was observed when comparing the restored and cyclic anterior outcomes. As a result of the broken implant, less support was given to the vertebra and more deformation was observed. Figure G.3 very clearly shows the result of the broken implant. Nevertheless, the restored height itself was merely lower than the mean restored anterior height that was found for this group.

The cyclic test for S1T8 stopped after approximately 25 minutes as a result of the break condition that was implemented in the test script; the test had to stop when the height of the vertebra was decreased by more than 60%. An evaluation of the μCT images led to the source of this height decrease. As one can observe in G.4, the left implant was severely tilted.

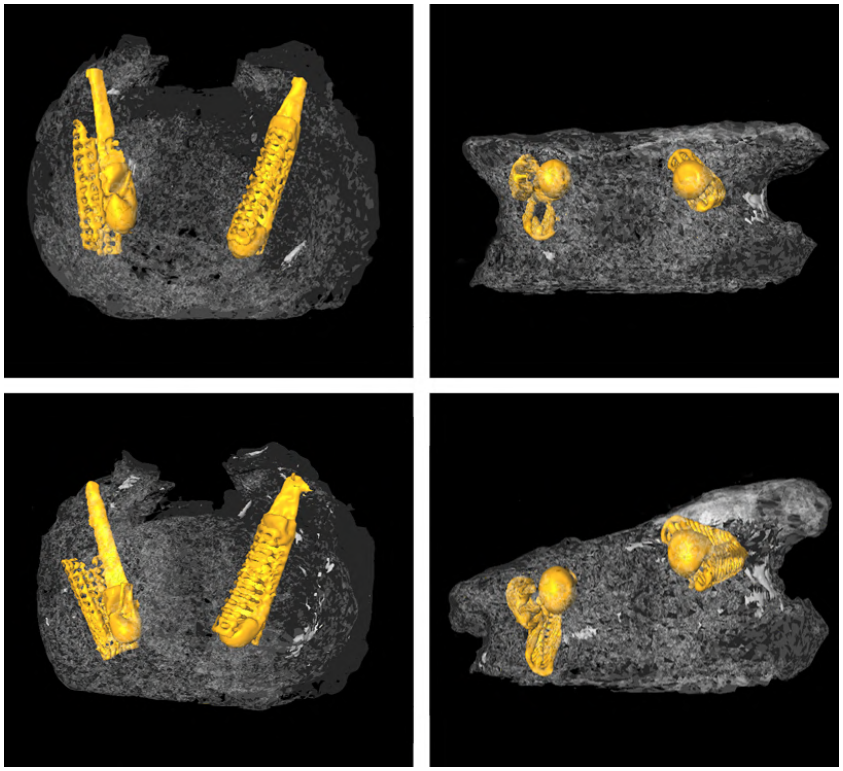

Figure G.3: The graphical results for S3L4 after restoration and cyclic loading. First row; restored (top view), restored (side view). Second row: cyclic (top view), cyclic (side view).

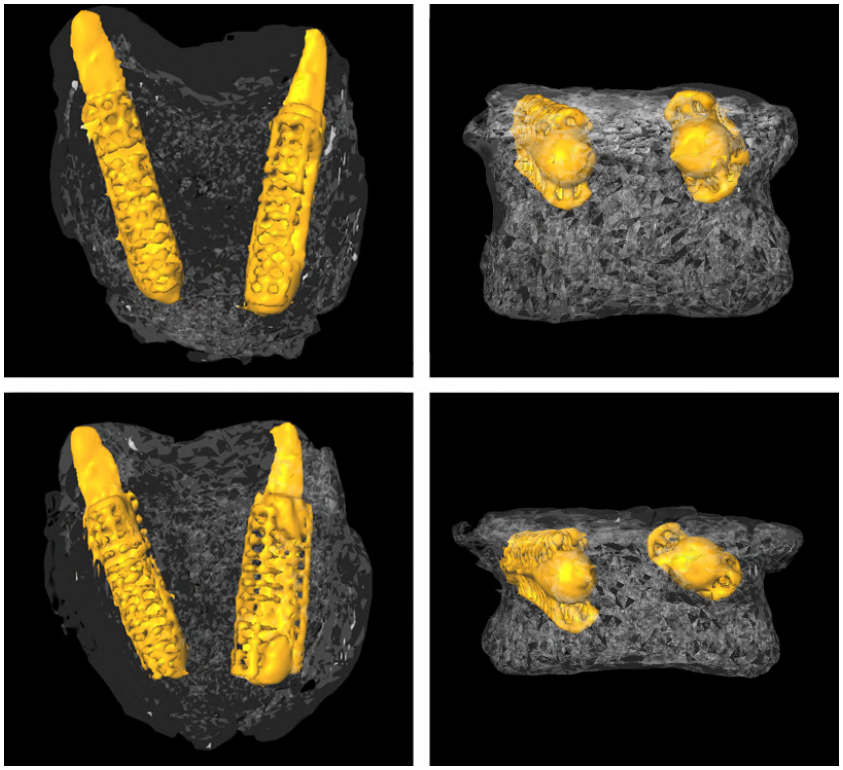

Figure G.4: The graphical results for S1T8 after restoration and cyclic loading. First row; restored (top view), restored (side view). Second row: cyclic (top view), cyclic (side view).

For S1T11, no termination of the cyclic test was seen. However when analysing the μCT images, an identical situation as the one described above was observed. As in S1T8, in S1T11 the left implant was critically tilted. Besides, the right implant showed a considerable implant rotation after cyclic loading. In figure G.5 a visible representation is given. For S1T8 and S1T11, the left implants had initial rotations of 21.0° and 21.5° respectively that further developed to 54.1° and 58.7° during the cyclic tests. Thereby, it could be concluded that an initial implant rotational angle above 20° could increase the chance of failures. In the test groups discussed in chapter 6, only one other implant with an initial rotation angle above 20° was observed that did not fail.

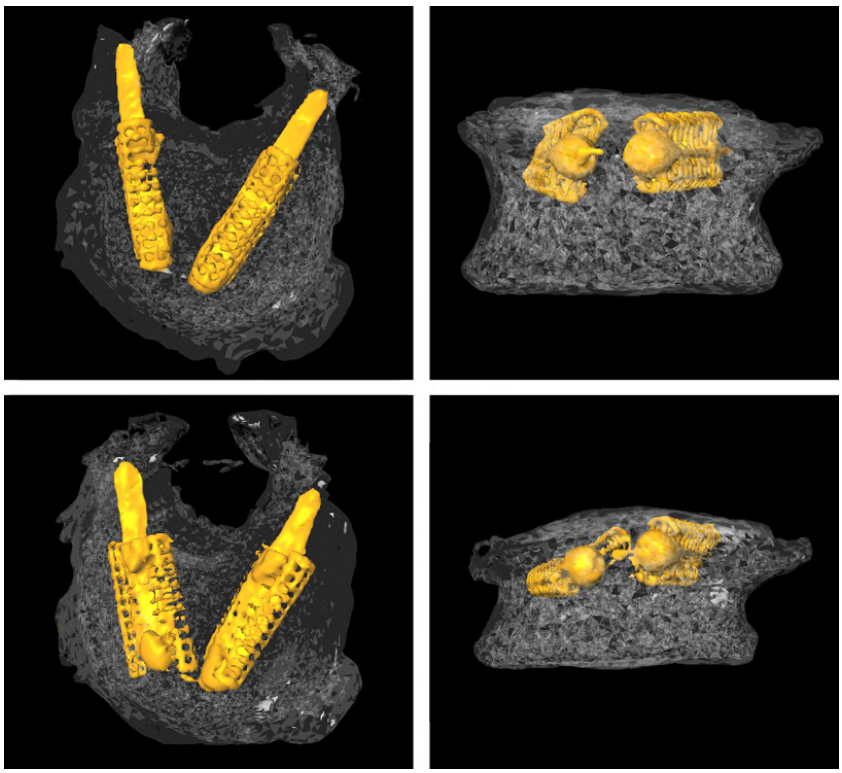

Figure G.5: The graphical results for S1T11 after restoration and cyclic loading. First row; restored (top view), restored (side view). Second row: cyclic (top view), cyclic (side view).

Finally, S2L4 needs to be discussed. Initially, no deviating or abnormal circumstances were observed for this vertebra after evaluation of the heights during restoration and cyclic loading. However, when better evaluating the μCT scans, a failure was detected. In figure G.6 one could see S2L4 after restoration and after cyclic loading. During the cyclic loading, the right implant was pushed in the inferior direction which resulted in contact with the left implant. Eventually, this led to a broken left implant. Although the results for this vertebra did not deviate much from the ones shown in table 6.4.

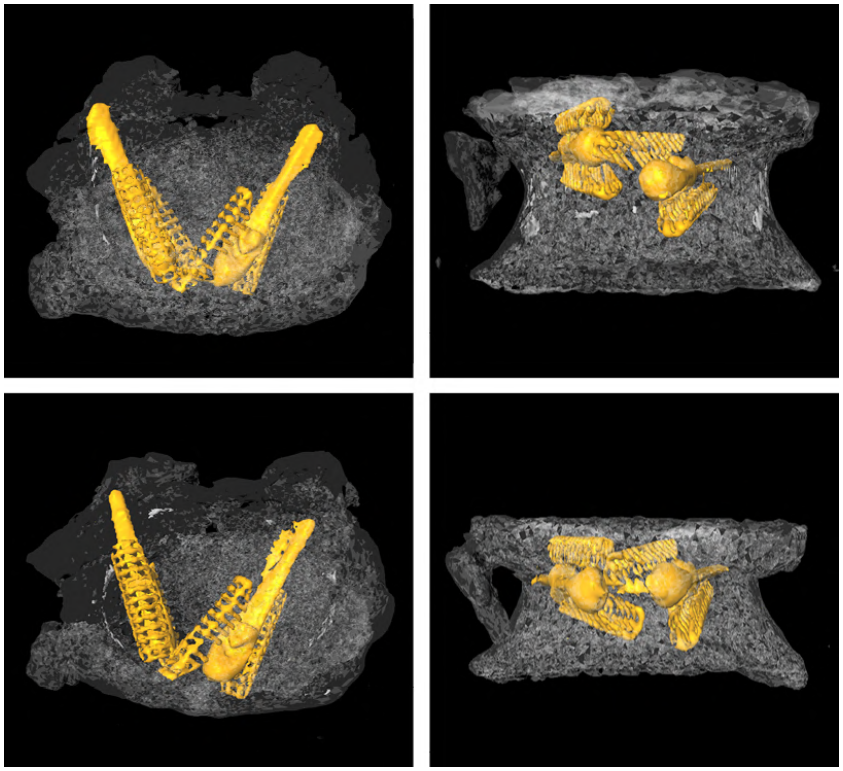

Figure G.6: The graphical results for S2L4 after restoration and cyclic loading. First row; restored (top view), restored (side view). Second row: cyclic (top view), cyclic (side view).

Figure G.3, G.4, G.5 and G.6 were obtained by the MeVisLab network that is visible in figure G.7. As one can see, this network is split into two branches after the ImageResample module; the left branch results in the representation of the vertebrae while the right branch results in the depiction of the implants. By applying different ISO values to the image, different components were extracted or vanished. Eventually, the diffuse, ambient and specular colors were determined in the SoWemRenderer modules. Furthermore, the face alpha, i.e. the transparency, and the face shininess were selected. As the implants were seen as the most important component to visualize, they were most accentuated. For the remaining vertebral structures, a lower transparency and shininess was chosen.

G.4 Conclusion

In conclusion, the failures that were observed were partially related to the inexperience of the researchers. Furthermore, the fact that no visual guiding or feedback on the tools were available contributed to these failures. In particular the initial implant rotation showed to increase the risk of failure. Furthermore, the lack of visual guidance during the vertebral restoration was the reason for one implant to break during the expansion.

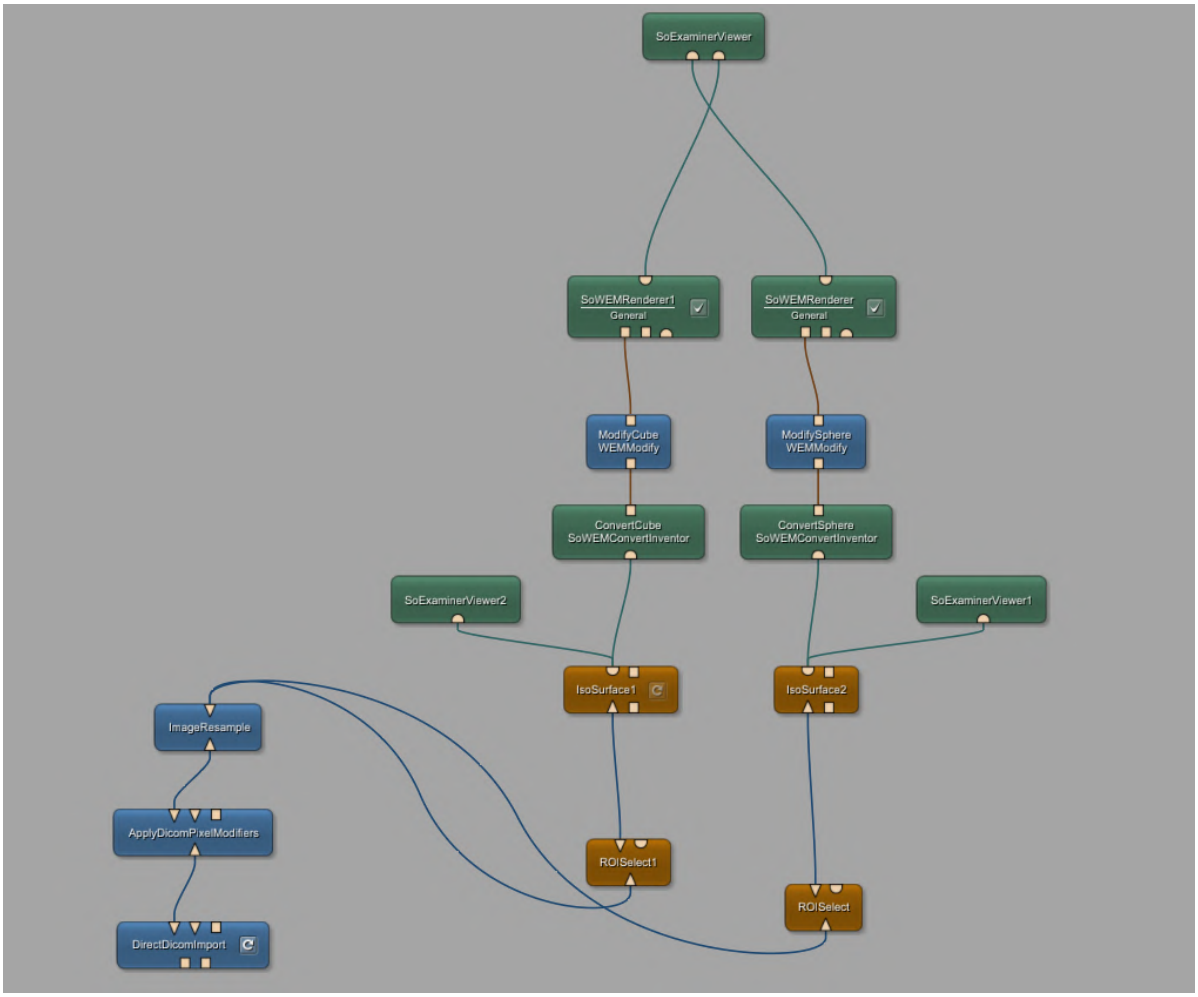

Figure G.7: The MeVisLab network